Fluid Flow Modeling of Resin Transfer Molding for Composite Material Wind Turbine Blade Structures

Douglas S. Cairns and Scott M. Rossell

Approved for public release; further dissemination unlimited.

⊞ Sandia National Laboratories

FLUID FLOW MODELING OF RESIN TRANSFER MOLDING FOR COMPOSITE MATERIAL WIND TURBINE BLADE STRUCTURES

Principal Investigator: Douglas S. Cairns
Written by: Scott M. Rossell

Department of Chemical Engineering
Montana State University-Bozeman
Bozeman, Montana

ABSTRACT

Resin transfer molding (RTM) is a closed mold process for making composite materials. It has the potential to produce parts more cost effectively than hand lay-up or other methods. However, fluid flow tends to be unpredictable and parts the size of a wind turbine blade are difficult to engineer without some predictive method for resin flow.

There were five goals of this study. The first was to determine permeabilities for three fabrics commonly used for RTM over a useful range of fiber volume fractions. Next, relations to estimate permeabilities in mixed fabric lay-ups were evaluated. Flow in blade substructures was analyzed and compared to predictions. Flow in a full-scale blade was predicted and substructure results were used to validate the accuracy of a full-scale blade prediction.

TABLE OF CONTENTS

LIST OF FIGURES

9

11

LIST OF TABLES

FULL ABSTRACT

Resin transfer molding (RTM) is a closed mold process for making composite materials. It has the potential to produce parts more cost effectively than hand lay-up or other methods. However, fluid flow tends to be unpredictable and parts the size of a wind turbine blade are difficult to engineer without some predictive method for resin flow.

There were five goals of this study. The first was to determine permeabilities for three fabrics commonly used for RTM over a useful range of fiber volume fractions. Next, relations to estimate permeabilities in mixed fabric lay-ups were evaluated. Flow in blade substructures was to be analyzed and compared to predictions. Flow in a full-scale blade was to be predicted and substructure results were to be used to validate the accuracy of a full-scale blade prediction.

Permeabilities were calculated for three fabrics (A130, DB120 and D155) in the fiber volume fraction range of 0.27 to 0.47. In addition, relationships were determined for each fabric over the given range of fiber volume fractions.

Two estimation methods were used to predict flow. One method was based on the relative thickness of glass in the fabrics and the other was based on the thickness of fabric layers at a given clamping pressure. The clamping pressure method was able to accurately predict the flow front shapes of a lay-up, but tended to under predict permeabilities. The relative thickness method did not capture the proper flow front shapes and under predicted permeabilities as well.

Liquid Injection Modeling Simulation (LIMS) was used to predict flow in the substructural models. Substructures in which flow was analyzed include a thick flanged T-section and a steel root insert. Filling times were well predicted in the T-section, but flow front shapes were not exact due to preferential flow in the mold. The steel root insert section was not well predicted due to the complex lay-up and a significant amount of interlaminar flow.

Two full blade simulations were created. One was an end injection and the other consisted of 6 injection ports in three stations. Ports were located at the flange on the low and high pressure sides of the blade at each station. Filling times were reduced by a factor of 10 using the 3 stage injection instead of injection from an end.

Based on results from the substructure experiments, the blade filling times are overpredicted. Due to the large scale of the blade, interlaminar flow problems should be negligible so flow front shapes should be accurately predicted.

CHAPTER 1

INTRODUCTION

Advanced composite materials offer an exciting and diverse alternative to traditional materials. Their high strength and stiffness-to-weight ratios combined with a wide range of design options have allowed them to be a popular material in performance-driven areas such as aerospace and sporting goods industries. In addition, they can provide a competitive, low-cost solution in piping, storage tank, and marine applications.[1,2] Another application where advanced composites are gaining popularity is the wind industry. E-glass reinforced polyester, vinyl-ester and epoxy composites are the materials of choice for producing wind turbine blades. These composites allow designers to make lighter more efficient blades at an affordable price.

Wind energy is a clean, renewable source of energy. Despite the potential benefits of wind energy, its cost per kilowatt-hour remains high enough to limit its growth in the United States. One area where wind energy can see a cost reduction is in the manufacturing of wind turbine blades. Currently most composite wind turbine blades are manufactured by the hand lay-up process. The blade for the AOC 15/50 wind turbine is one example.[3] Resin transfer molding (RTM) offers the potential of making lighter, more efficient blades while at the same time lowering production costs of the blades.[4] [5] A typical blade geometry and structure are illustrated in Figure 1.[3]
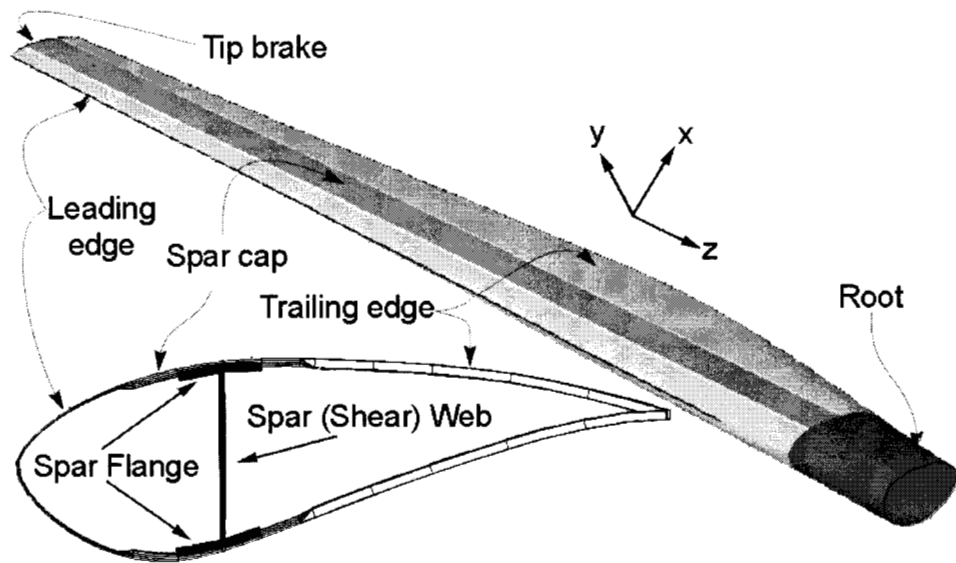
Figure 1. AOC 15/50 blade and cross section (length is approximately 8 m).[3]

Motivation

Hand lay-up involves manufacturing by the sequential addition of layers of reinforcement and resin matrix in an open mold. It allows for the manufacture of a wide range of geometries and requires low initial investment. Despite these advantages, hand lay-up is not well suited to large-scale production due to the fact that it is very labor intensive and requires long cycle times. In addition, it is not easy to make hollow structures with the hand lay-up process. Therefore, a blade is usually manufactured in pieces and secondarily bonded together, Figure 2. The hand lay-up process uses a one-sided mold, which adds complications to the manufacturing process. For example, parts tend to vary significantly in thickness and only have only one finished surface. The unfinished surface requires additional time to condition for bonding, Figure 3, and poor manufacturing tolerances may result in thick and/or thin bond lines, Figure 4. Another

limitation of hand lay-up, is that fiber volume fractions are generally under 35%[4]. Since the fibers bear the majority of the load in a composite, the presence of excess resin just adds weight. A weight savings of 6.3 kg, 10% of the AOC 15/50 blade weight, would be achieved if the skin thickness could be compressed by one millimeter.[4]
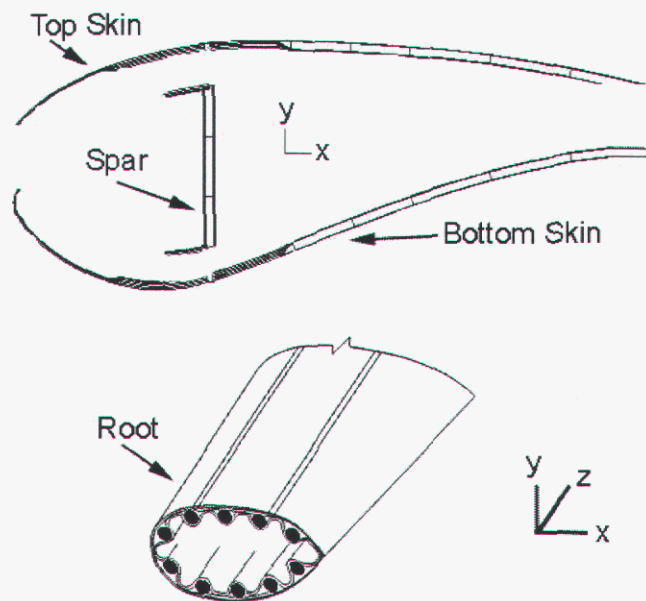
Figure 2. Components of the AOC 15/50 wind turbine blade.
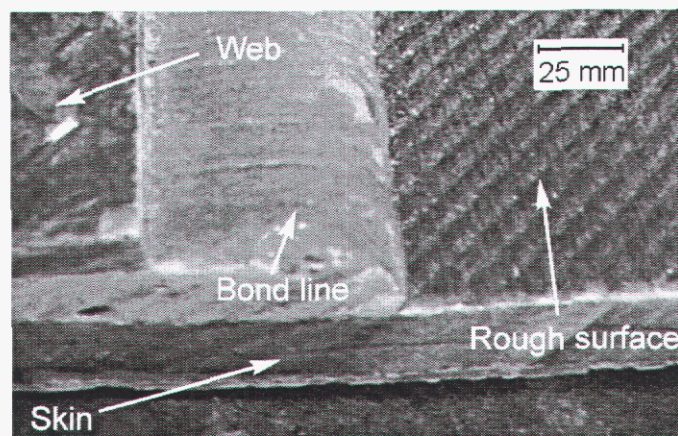
Figure 3. Rough inside surface of a wind turbine blade.
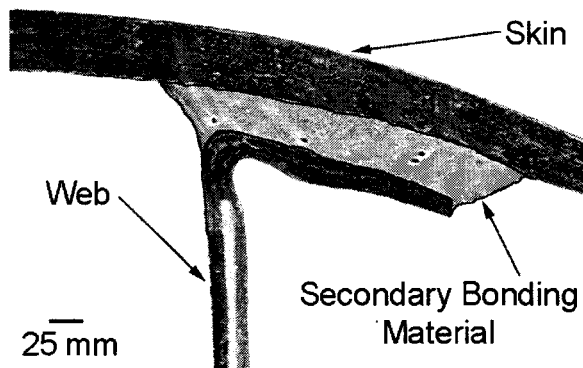
Figure 4. Thick bond line in a wind turbine blade

Resin Transfer Molding (RTM) offers numerous advantages over hand lay-up.[4] Parts can be produced more rapidly with less labor expense. In addition, it is possible to more easily produce hollow parts with RTM since all fiber layers are placed into a two-sided mold before resin is added. This reduces the labor required to make a part. Also, the two-sided mold produces parts with tighter dimensional tolerances, higher fiber volume fractions and a smooth surface finish on all surfaces. RTM also eliminates excess resin and thick bond lines. Thus, even if the blade is molded in parts the weight is lowered and parts are much easier to condition for secondary bonding.

Fabricating RTM molds are much more expensive to make than ones for hand lay-up, thus hindering their development. Multiple injection ports may be necessary for parts on the scale of wind turbine blades to keep injection times under the gel time of the resin. This complicates flow patterns and may result in a mold that traps air, creating dry spots, or ones that fill incompletely. Currently, mold design is more of an art than a science; the odds that the initial layout of injection ports will have problems appear to be high. Since molds are very costly, accurate prediction of resin flow in the mold is

desirable. There has been a great deal of research in flow modeling for RTM. However, much of the research has not addressed the types of fiber reinforcements that are of interest for wind turbine blades, or has involved micro-flow models that would not be practical to model parts the size of a blade.

Objective and Approach

The objective of this research was to compare experimental resin flow modeling results for small-scale substructural components of the AOC 15/50 blade with predictions from generalized flow modeling software. Models were refined to better predict the resin flow observed in the substructural components. The models were then applied to predict the flow in larger, full-scale blades. Specific project goals were as follows:

1) Experimentally determine permeabilities for reinforcing fabrics of interest (A130, D155 and DB120) at different fiber volume fractions

2) Determine the accuracy with which permeabilities for individual fabrics can be used to predict permabilities for mixed and single fabric lay-ups.

3) Simulate flow in blade substructures using permeability data as input for flow prediction modeling software Liquid Injection Modeling Simulation (LIMS) and compare the flow predictions with experimental data.

4) Use LIMS to predict resin flow in a wind turbine blade

5) Use substructure prediction versus experimental correlations to assess the accuracy of a full-scale blade injection

Organization of Report

In Chapter 2, fluid flow theory is described as it relates to modeling flow of the RTM process. Several modeling methods are also discussed. In Chapter 3, experimental procedures are discussed and a test matrix is presented. In Chapter 4, all experimental

21

results are presented. In Chapter 5, predictions are compared with experimental results for resin flow in various geometries, including the full size AOC 15/50 blade. In chapter 6, the conclusions from this study are presented as well as a list of items that should be included in future studies.

CHAPTER 2

BACKGROUND

Composite Materials

Composite materials, by definition, are made from combining two or more different materials. These materials can be as simple as straw and clay, or as complex as carbon fiber and epoxy resin. A typical composite material consists of strong, light fibers held in-place by a polymeric matrix material, Figure 5. E-glass fibers in polyester, vinyl-ester or epoxy resin are currently the composite materials of choice for wind turbine blades because of their strength and stiffness to weight ratios, environmental resistance, and low cost.[6, 7]
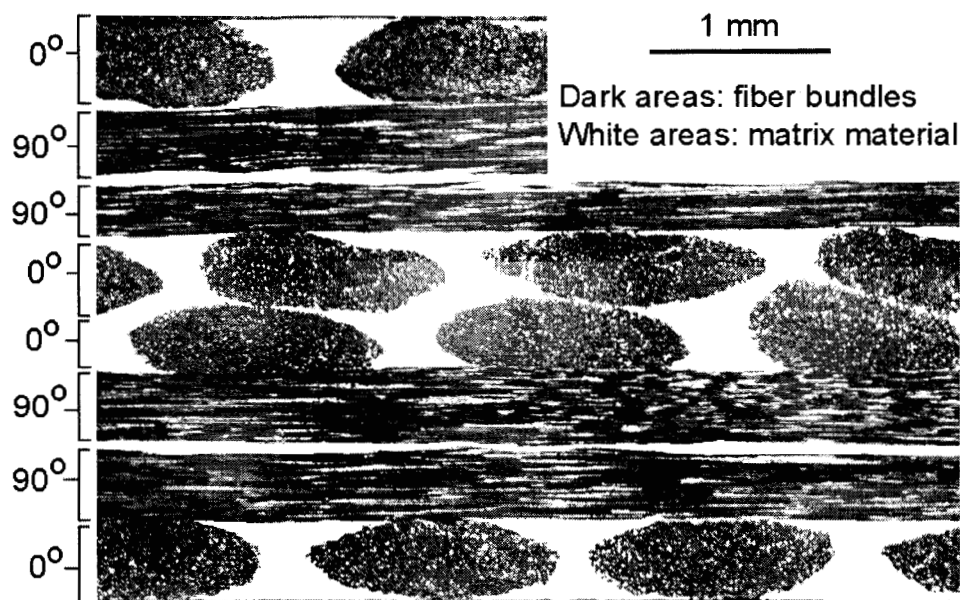
Figure 5. Cross section of a [0/90$_2$/0]s composite.

Material Properties

Mechanical properties for polyester and E-glass as well as their composites are given in Table 1. Properties of 6061-T6 aluminum are listed as a reference. One can see in Table 1 that the E-glass fibers are considerably stronger than the polyester matrix material. The fibers serve as the primary load bearing material in the composite. The role of the matrix is to hold the composite together. It also protects the fibers from the environment and helps distribute loads between fibers. Generally, the composite with the higher volume fraction of glass fibers will be stronger if all other things are equal. Also, the strength of a composite is highly dependent on the orientation of the fibers to the direction of load. The composites are much stronger in the fiber direction, Table 1. This allows designers to optimize the weight of a structure by reinforcing it in the directions of anticipated load.

Table 1. Tensile properties of aluminum, E-glass, polyester resin, and E-glass, polyester composites.

Material	Tensile Strength (MPa)	Elastic Modulus (GPa)	Specific Gravity	Strength to Weight Ratio $(10^3$ m) [*]	Modulus to Weight Ratio $(10^6$ m) [*]
6061-T6 Aluminum [**]	310	68.9	2.70	11.7	2.60
E-glass fibers [**]	3450	72.4	2.54	139	2.91
Polyester Resin [3]	54.1	3.18	1.16	4.76	0.280
E-glass/polyester $[0]_8$ [#]	868	36.3	1.78	49.7	2.08
E-glass/polyester $[90]_8$ [#]	33.8	8.76	1.78	1.94	0.502

[*] Calculated by dividing the property by its specific weight (density*gravitational acceleration).

[**] Properities from Reference.[2]

[#] Properties from the DOE/MSU database.[8] Unidirectional composites with A130 fabric 45% fiber volume tested in the 0° and 90° directions relative to the fiber axis.

$[0]_8$ refers to eight fabric layers in the 0° direction.

Resin Systems

Common resin systems used in advanced composites include polyesters, vinyl-esters, epoxies and thermoplastics. Epoxy resin systems tend to be the most versatile, but are expensive and have environmental concerns associated with them. Thermoplastic resin systems are the toughest of the resin systems, but they are highly viscous and are not suited to processing by either hand lay-up or RTM. Polyester and vinyl-ester resins have low viscosities, are more benign environmentally than epoxies and tend to be the least expensive. Epoxies, vinyl-esters and polyesters are all commonly used in wind turbine blade manufacture.

Generally, resin systems are processed as liquids. Resin systems cure by either forming cross-linked polymer chains, thermosets, or by making very long, entangled polymer chains, thermoplastics.[9] Epoxy, polyester and vinyl-ester resins fall into the thermoset category. The cure time of a resin system is very important to both RTM and hand lay-up. Resin systems have to remain liquid long enough to fill the mold and properly wet out the fibers. The working time of a resin is referred to as the gel time. Gel times of fifteen minutes to one hour are common for most systems used for both RTM and hand lay-up.

Fiber Reinforcements

As stated earlier, fibers bear the majority of the load in a composite. Since cost is a major driving factor in manufacturing wind turbine blades, E-glass fibers are used. Fibers used for this study were manufactured by Owens Corning and come pre-coated with a silane coupling agent. The silane provides an environmentally resistant bonding

interface so the matrix material bonds with the glass fibers and promotes wetting of the resin at the fiber surface.

Fibers used for RTM and hand lay-up generally come in a textile form. First, groups of fibers are bundled together, commonly called fiber tows. Then bundles are stitched or woven to make a fabric. Fabrics may consist of randomly oriented fibers, unidirectional fibers or several differently oriented fiber layers stitched together. Fibers may be orientated in either the weft, or warp direction of the fabric roll, Figure 6. The most common orientations of fibers are $0°$, $\pm45°$ and $90°$. Many fabrics consist of several layers stitched together. Weaves of $0°$ and $90°$ fibers are also common. While popular in non-structural applications, random fiber mats are generally used in blades only to hold the main fibers in place during handling.
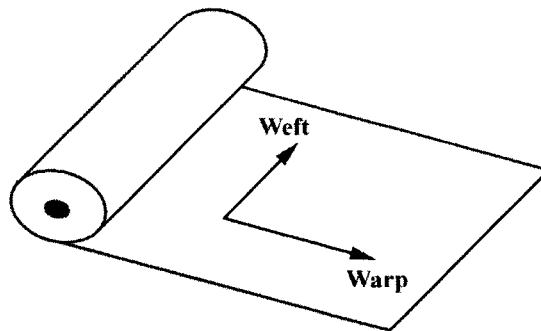
Figure 6. Schematic of the axis relative to a roll of fabric.

Composite Manufacturing

In order to make a composite material, the resin system needs to be combined with the fiber reinforcement. Since the orientation of the fibers is critical to the properties, it is essential that the manufacturing process properly align the fibers. In

addition, a good process will leave parts with a high, uniform fiber volume fraction, allow rapid production of a large volume of parts economically and have repeatable dimensional tolerances. The following section describes hand lay-up, the most common process for manufacturing wind turbine blades, and RTM, a potential process for improving blade manufacturing.

Hand Lay-up

Hand lay-up is an open mold process. Fabric layers are laid one at a time onto a one-sided mold. Resin is applied to each layer by pouring or spraying, and pressed through the thickness with a roller. A squeegee is used to remove excess resin, and then another layer is added. This process is repeated until all reinforcement layers have been placed.

Because hand lay-up only requires simple tools and one mold surface, it is inexpensive to start up. Unfortunately, it also requires a large amount of labor and high cycle times to produce parts. In addition, the quality of parts manufactured from hand lay-up tends to be inferior to parts produced by other processing methods.

The fiber placement and impregnation process results in a considerable amount of fabric handling which may displace fibers. Part thickness depends on the amount of resin added and is highly variable. High fiber volume fractions are not possible since there is not another mold face to compress the part. In addition, molds with steep sides may pose difficulty if the resin viscosity is too low, and hollow parts are difficult to produce with good dimensional tolerances.[4, 10] Another limitation is that parts are only finished on the mold side. Finally, since hand lay-up is an open mold process, a considerable amount of

volatiles are released from the resin during processing.

The shortcomings of hand lay-up result in unnecessary blade weight as well as extra time processing and assembling blade parts, and exposure of workers to volatile resin components. Each of these areas can be improved by RTM.

RTM

RTM is a closed mold process. First, dry reinforcing fibers are placed in a two-sided mold. The mold is then sealed, and at this time, it is common to pull a vacuum. A vacuum helps eliminate void formation during injection since the resin does not need to push air out of the mold. The resin is then mixed to initiate curing and injected under pressure. For a diagram of a typical RTM injection see Figure 7.
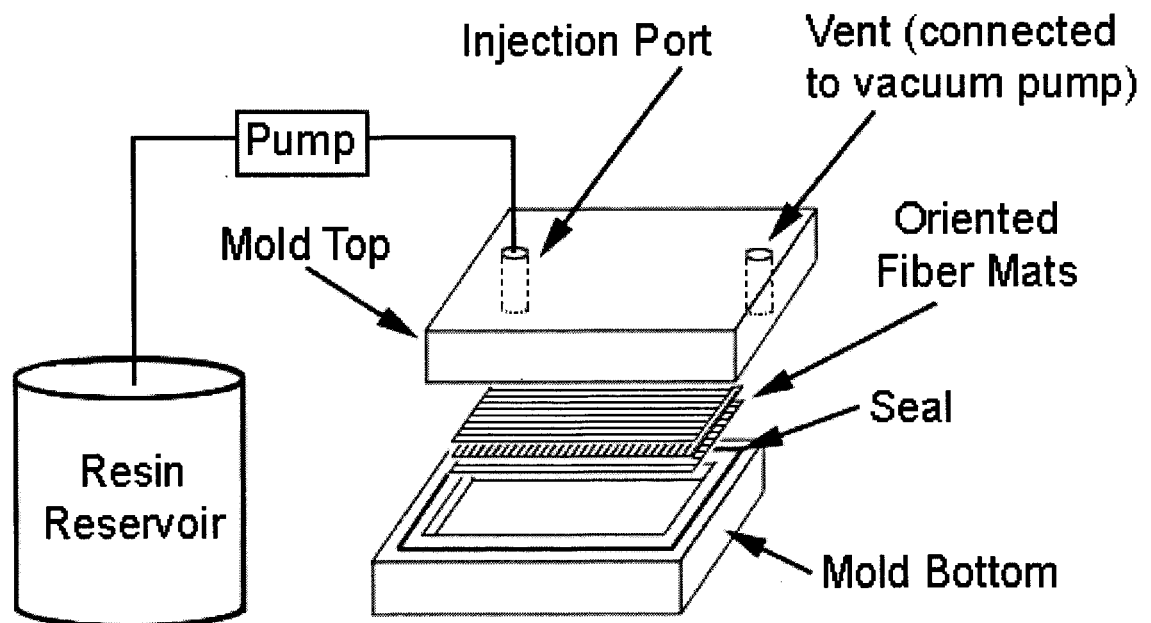
Figure 7. Diagram of a simple RTM injection setup.

Resin viscosity is critical to the RTM process. Injection times are limited and the fiber mats have a very low permeability. If pressures get too high, the fibers will be moved by the resin, commonly called fiber wash. Low viscosities decrease injection times and lower the risk of fiber wash. It is possible to process resins with viscosities up to 1000 cP. In practice, however, most RTM resin systems have viscosities less than 500 cP, with ideal resin viscosities in the 100 to 200 cP range.[11]

The closed mold of RTM offers several advantages over hand lay-up. Parts have tighter tolerances, they are finished on both sides, and higher fiber volume fractions are possible. In addition, the reinforcing fiber layers may be preformed so they can be laid into the mold in one piece, offering considerable time savings. Even without preforming the fabric, RTM offers a timesaving over hand lay-up in the production of complex parts.[4, 11] In addition, the closed mold prevents volatiles from escaping during processing. The principal drawback to RTM is the start-up cost. RTM requires expensive injection equipment, and RTM molds are expensive to produce. Most mold design and particularly the number and locations of injection and vent ports, is done by trial and error, and currently it is more of an art than a science. Accurate predictions of resin flow are necessary in order to properly locate injection and vent ports.

Flow Theory

Prediction of the flow of resin through different mold geometries first requires an understanding of the fiber mats inside the mold and the processing parameters. Flow through fibrous preforms tends to be complicated to model. Since the flow is anisotropic, models must include layer orientation and stacking order as well as the fiber packing

density. This section first details the geometric considerations of orientated fiber mats, and then presents typical methods for describing fluid flow through fibrous media.

Preform Geometry

In order to select an appropriate equation for flow modeling, one must first have a firm understanding of the micro and macro-geometric details of the reinforcement. There are multiple length scales in a typical composite, see Figure 8. There are the microscopic spaces between individual fibers in a fiber tow, spaces on the order of a few millimeters between fiber tows, and there is the macro geometry of the entire mold.
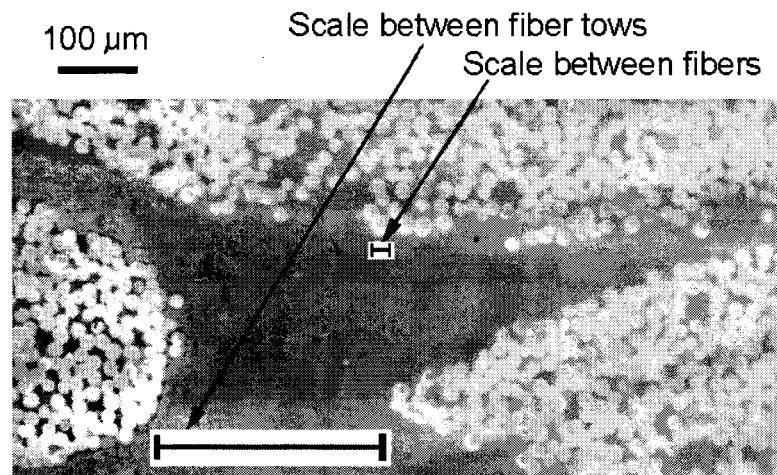
Figure 8. Multiple length scales for flow.

The smallest micro-geometry exists within the fiber tows as shown in Figure 9. Typical tows consist of 500 to 3000 fibers grouped together.[12] Their permeability is highly anisotropic, with permeabilities being much higher in the direction of the fibers. The next level of micro geometry would be the spaces between fiber tows. Finally, there is the macro geometry of the fabric. Fiber tows are typically formatted into a textile form for ease of handling since placing fiber tows one at a time into a mold would be

30

100 μm
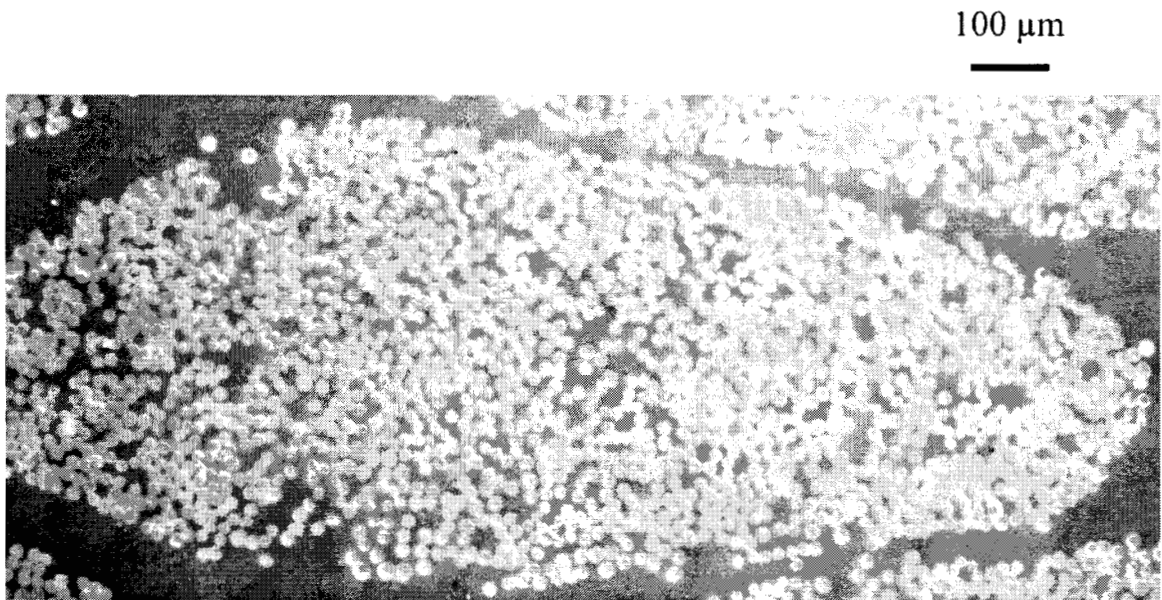
Figure 9. D155 fiber bundle.

impractical. Three common fabrics are D155, A130 and DB120, produced by Owens

Corning Fabrics. The D155 fabric consists of unidirectional fiber tows stitched together,

the A130 fabric consists of unidirectional tows woven over a small glass strand and the

DB120 fabric consists of tows stitched together at a ±45° angle relative to the fabric, see

Figure 10. In addition, tows may be woven over each other in a 0-90° pattern (woven

roving) or tows woven in a satin weave pattern.[2] Fiber mats also come in random mat

form and three-dimensional weave patterns, but these are not used widely in blades. The

final complication to fiber preform geometry comes when fiber mats are stacked on top

of one another in differing orientations and compressed when the mold is closed.

Obviously there are numerous ways to incorporate these geometric complexities

into a flow model. Some of the most common approaches are described below.

| A130 | D155 | DB120 |
| (worp unidirectional) | (weft unidirectional) | (stitched $\pm 45°$) |

2 cm
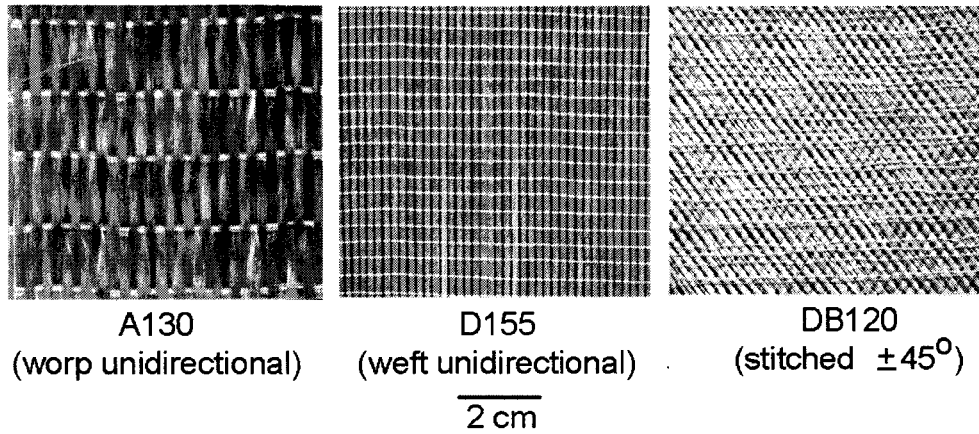
Figure 10. Common fabrics used for RTM and hand lay-up.

General Flow

The basic equations for flow of the liquid resin through the spaces in the mats are described in this section. Generally, resin systems are modeled as Newtonian fluids with constant density and viscosity so the Navier-Stokes equation is valid.

1)
$$\rho \frac{Du}{Dt} = -\nabla P + \mu \nabla^2 u + \rho g = \nabla P + \mu \nabla^2 u$$

where ρ is the density, u is the velocity of the fluid, t is time, P is the pressure, μ is the viscosity of resin and g is the acceleration due to gravity[13].

The generalized Navier-Stokes equation may be further simplified by eliminating non-linear momentum effects contained in the material derivative. Flow rates in RTM are slow enough that these effects do not arise.[11] The resulting flow type is described as Stokes flow.

2)
$$0 = -\nabla P + \mu \nabla^2 u$$

The analytical solution of this equation is limited, however. In order to evaluate the Stokes equation, it is necessary to define fluid velocities or fluxes at the boundaries.

Since the resin is flowing through a very complex geometry, evaluating this equation

with its boundary condition would be prohibitively complex. Therefore either the

geometry must be greatly simplified, or a different set of field equations must be

developed.

Darcy's Law

The most widely used equation for describing flow through RTM molds is

Darcy's equation for flow through porous media[11], a further simplification of Equation 2,

3)
$$u_i = -\left(\frac{K_{ij}}{\mu}\right) \cdot (\nabla P_i)$$

where u_i is the volume average velocity of the fluid, K_{ij} is the permeability tensor for the

preform, μ is the viscosity of the resin and P is the pressure in the resin. It is important to

note that K_{ij} is a second order, symmetric tensor. If one were to expand the equation for

three-dimensional flow it would read as follows:

4)
$$\begin{Bmatrix} u_x \\ u_y \\ u_z \end{Bmatrix} = -\frac{1}{\mu} \begin{pmatrix} K_{xx} & K_{xy} & K_{xz} \\ K_{yx} & K_{yy} & K_{yz} \\ K_{zx} & K_{zy} & K_{zz} \end{pmatrix} \begin{Bmatrix} \partial P / \partial x \\ \partial P / \partial y \\ \partial P / \partial z \end{Bmatrix}$$

Darcy's law eliminates the need to evaluate complicated boundary equations that arise if

Stokes flow is used, but it requires the evaluation of the permeability tensor. Calculation

of permeabilities is critical to modeling associated with RTM and will be discussed in a

later section.

Darcy's law has its limitations, which will be discussed, but in nearly all cases it

will apply to flow in RTM molds.[11] First, fluid flows need to be within a "seepage"

velocity range. In order for the flow to be within this range, the Reynolds number, Equation 5, must be inversely proportional to the friction factor, Equation 6, of the medium[14].

$$5) \qquad\qquad N_{\text{Re}} = \frac{q\rho\delta}{\mu}$$

$$6) \qquad\qquad \lambda = \frac{2\delta\Delta P}{q^2\rho}$$

where N_{Re} is the Reynolds number, q is the scalar "filter velocity" of the fluid, λ is the friction factor, ΔP is a one-dimensional pressure drop and δ is a diameter associated to the flow channels of the preform. A common assumption is that if N_{Re} is one or less then it is in range of Darcy's law.[11]

Another limitation of Darcy's law is that permeabilities for gases in a porous medium are higher than those observed for liquids. It has been determined that as the channel diameter approaches the mean free molecular path of the gas, Darcy's law breaks down.[15] This can create a problem taking into account pushing air out of a mold that is not under vacuum.

Also, variations from Darcy's law have been observed around packed tubes; the variations were determined to be caused by a boundary effect.[14] Flows were found to increase with distance from the center of the tube, and then drop significantly, approximately one tube diameter from the wall[16].

Finally, fluids modeled by Darcy's law must obey the assumptions used to formulate the Navier-Stokes equation. Namely, fluids must have a constant density and viscosity and must obey Newtonian behavior.

Permeability Determination

In order to solve Darcy's law, one needs to calculate permeabilities. This topic has been an area of much research in other fields as well as research that directly applies to RTM. In fact, permeability data have been deemed important enough to the manufacture of composites that research has been sponsored by the National Institute of Standards, NIST, to develop a database of fabric permeabilities.[17, 18] Additional work has been done to define a standard reference fabric to assist in the measurement of permeability.[19]

Various methods for calculating permeability exist. Both numerical and experimental models will be discussed in the following section. When modeling flow, it is common to assume that it occurs in two dimensions since the thickness of parts is typically small when compared to the other dimensions. Therefore, the calculation methods detailed below are only for flow in the principal directions of the fabric unless otherwise noted. This reduces the size of K_{ij} in Equation 4 to a 2-D tensor with three independent terms.

Numerical Calculation Methods

There are two common ways to calculate permeability values numerically. Boundary conditions may be defined over a unit cell and the Stokes equation solved, or hydraulic radius theory may be used to estimate the permeability. The two approaches are briefly discussed below.

The first approach requires an idealized unit cell. The unit cell must be representative of the geometry of the fabric being modeled in order to be of practical use.

There have been numerous studies in this area.[20,21,22,23,24,25] One study was able to evaluate a unit cell for a woven fabric.[20] This was also extended to cover permeabilities for multi-layer preforms. Evaluating permeabilities this way requires a considerable amount of time to develop the models, and they contain considerable simplifications of the fabric geometry. The advantage of this method is it requires no experimental data and can be quite accurate if the fabric geometry is simple to model.

The Kozeny-Carman equation is a second common method to estimate permeabilities. The Kozeny-Carman equation (hydraulic radius theory), Equation 7, is based on taking a volume averaged flow through a porous medium formed from constant diameter fibers with uniform spacing with a certain volume fraction of connected void space or connected porosity, on flow channels.

7)
$$u = \frac{R^2 \varepsilon^3}{c(1-\varepsilon)^2} \cdot \frac{\Delta P}{\mu}$$

where u is the volume average velocity, R is the radius of a fiber, ε is the porosity, and c is a shape factor. The shape factor or tortuosity, c, relating to fibers is dependant on the arrangement of fibers as well as their packing density.[26]

The Kozeny-Carman equation is derived from the flow through multiple capillary tubes which is described by the Hagen-Poiseuille equation[26]. The Kozeny-Carman equation is related to Darcy's law through Equation 8.

8)
$$K = \frac{R^2}{c} \cdot \frac{(1-v_f)^3}{v_f^2}$$

where K is the permeability constant and v_f is the fiber volume fraction.[27] Therefore, if the arrangement of fibers is known, the permeabilities may be calculated directly.

However, that requires knowing the exact geometry of the fiber structure. So, in practice, the constants are evaluated experimentally.

The Kozeny-Carman equation works well for isotropic porous media and in cases of one-dimensional flow, but it has been found to break down in anisotropic fluid flow.[22,23] Obviously, this would be of little use in composites since the oriented fibers create an anisotropic medium. However, it is possible to modify the Kozeny-Carmen equation for flow transverse to the fibers.[27] In Reference 27 the author used separate relations for flow parallel and perpendicular to the fibers, and then estimated shape factors. This approach is limited in its use because it requires fibers that are regularly aligned, and experimental work is also required. Therefore the preferred method of determining permeabilities is experimental.

Experimental Methods

There are several methods that one may use to experimentally determine permeabilities. The two main classes of experiments are saturated and unsaturated. In saturated flow experiments, the mold (with dry fiber preplaced) is filled until it is completely saturated with a fluid before measuring flow rates. This approach requires separate experiments for fabrics orientated at three differing angles in order to calculate the permeability tensor. Saturated flow experiments accurately characterize permeabilities, but they require multiple experiments to calculate the permeability tensor. If one performs an unsaturated experiment with a central injection port, it is possible to calculate permeabilities with only one experiment as flow may be tracked in both x, y directions at the same time.[28,29]

A generalized flow front for an unsaturated radial flow experiment is shown in Figure 11, where R_o is the radius of hole cut into the fabric, R_1 and R_2 are the radii in the major and minor flow directions of the fabric and θ is the angle between the fabric coordinate system and global x and y coordinates. By substitution of Darcy's law into
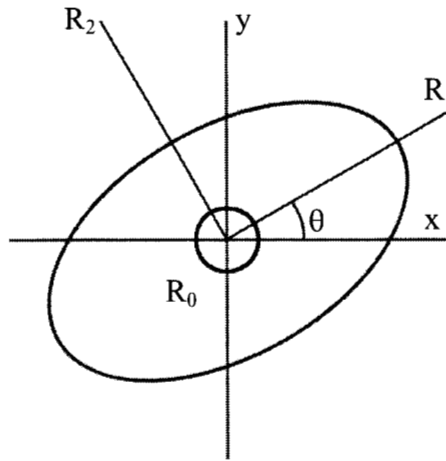
Figure 11. Generalized flow for an anisotropic medium with an injection port of radius R_0 centered at (0,0).

the continuity equation, Equation 9, the following expression, Equation 10, is obtained.

9) $$\nabla \cdot u = 0$$

10) $$\nabla \cdot (k \cdot \nabla p) = 0$$

If Equation 10 is to be solved for permeabilities, experiments must then be run at a constant pressure or constant flow rate. The constant pressure method is detailed below. Information on calculating permeabilities from constant flow rate experiments as well as saturated flow is detailed by Lai.[29]

First the location of the flow front must be defined by Equation 11

11)
$$u_{flow} = \left(\frac{dx}{dt}\right)_{flow} = \left(\frac{u}{\varepsilon}\right)_{flow}$$

where u_{flow} is the volume averaged velocity of the fluid. If the flow experiment is performed in the coordinates of the fabric, θ will be zero, eliminating the coupling terms in the permeability tensor, leaving the following to be solved

12)
$$K_x \frac{\partial^2 p}{\partial x^2} + K_y \frac{\partial^2 p}{\partial y^2} = 0$$

In order to solve Equation 12, it must first be transformed into an "equivalent isotropic system" (EIS)[30]. The relevant relationships between a point (x,y) and its equivalent in EIS coordinates (x_e, y_e) are

13)
$$R_{xo,e} = \left(\frac{K_y}{K_x}\right)^{1/4} R_{xo} ; \quad R_y = \left(\frac{K_y}{K_x}\right)^{1/2} R_x ; \quad R_{xe} = \left(\frac{K_y}{K_x}\right)^{1/4} R_x ; \quad K_e = \left(K_x K_y\right)^{1/2}$$

where R_x is the radius of the flow front in the x direction, R_y is the radius of the flow front in the y direction and R_{xo} is radius of the hole in the fabric. Substitution of these parameters into Equation 12 leaves a Laplace equation. Solving this equation for the geometry described earlier gives the following relationship for a volume averaged flow velocity:[31]

14)
$$u_{flow} = \left(\frac{R_{xe}}{R_{xo,e}}\right)^2 \left[2 \cdot \ln\left(\frac{R_{xe}}{R_{xo,e}}\right) - 1\right] + 1 = \frac{4 K_e \Delta P}{\varepsilon \mu R_{xo,e}^2} t$$

Proper substitutions with Equations 13 and 14 yield the following two equations:

15)
$$\left(\frac{R_x}{R_{xo}}\right)^2 \left[2 \cdot \ln\left(\frac{R_x}{R_{xo}}\right) - 1\right] + 1 = \frac{K_x 4 \Delta P}{\varepsilon \mu R_{xo}^2} t$$

39

16)
$$R_y^2 = \frac{R_x^2}{K_x} K_y$$

Equations 15 and 16 follow linear behavior along principal directions of permeability. The slopes will be K_x and K_y if the known constants are grouped with their respective independent variables.

Sources of Error

There are several factors to be considered when preparing permeability experiments. First, it is of utmost importance that pressure induced mold deflections are kept to a minimum. Mold deflections will create a part with non-uniform thickness that can alter preform geometry enough to invalidate the experiments. Two-dimensional unsaturated flow experiments are most susceptible to this type of error since larger molds with more surface area, and thus more out-of-plane loads are generated on the mold.

Capillary pressure is another source of error that needs to be taken into account for unsaturated flow experiments. Under certain conditions capillary forces may be significant relative to the overall pressure drop of the mold. If so, ΔP of the mold is described by Equation 17,

17)
$$\Delta P = P_{in} - P_{out} - P_{cap}$$

where ΔP is the pressure drop across the mold, P_{in} is the pressure at the injection port, P_{out} is the pressure at the vent and P_{cap} is capillary pressure.

Capillary pressure is defined by Equation 18,

18)
$$P_{cap} = \frac{\gamma \cos \theta}{\delta}$$

where γ is the surface tension of the fluid, θ is the contact angle between the resin and the fibers and δ is the equivalent diameter of the pores.

It has been observed that this method tends to overpredict capillary pressure in fibrous preforms.[29,32, 33] An alternate method of calculating capillary pressure has been proposed, Equation 19, based on the Kozeny-Carman equation:[32]

$$19) \qquad P_{cap} = \sqrt{\frac{c}{c_{ideal}}} \cdot \frac{2\gamma \cos\theta}{r_c}$$

where c is a shape factor based on Kozeny theory, c_{ideal} is a correction factor for flow through an idealized porous media and r_c is given by Equation 20

$$20) \qquad r_c = 2r \frac{\sqrt{\varepsilon/\pi}}{\left(1 - \sqrt{\varepsilon}\right)}$$

where r is the radius of an individual fiber and ε is the porosity. This set of equations takes into account both parallel and serial nonuniformities that are specific to RTM molds. In addition, they include experimentally determined values for c for a variety of fabric structures.

Another problem that can arise during one-dimensional flow experiments is preferential flow. This happens when the fabric is not properly fitted to the mold, leaving areas of high permeability at the borders, also know as race tracking. If a saturated flow experiment is run on a mold that exhibits race tracking, it will not measure the true permeability of the reinforcement.

<center>Modeling Theory</center>

Fluid flow in RTM molds is very complex. One complication involves the treatment of multiphase fluid flow. Prior to injection there is air, or void space if a vacuum is drawn, and solid fibers. During injection there are multiple flow areas with resin and fibers in one region and fibers and air or void space in another. Often times a transition region exists between the two where air and resin coexist in varying concentrations. Another complication involves dealing with the multiple length scales present in the fiber preform.

A model that includes all the geometric complexities of the porous medium inside the mold would be overwhelming for a reasonable sized mold, let alone take into account the multi-phase flow regions. Thus it is common to make several assumptions when evaluating flow through RTM molds.

There are two common approaches. The first approach is to combine porous media theory with more generalized flow models such as Stokes flow to take into account micro-geometric effects. This approach is referred to as micro-modeling. Another approach is to use porous media theory and apply it to the entire mold, macro-flow. Micro-flow models can take into account complex geometry regions of a mold, while macro-flow models can consider larger, more complex molds.

Micro Modeling Schemes

Micro flow models are important in determining flow in detailed regions of composites as well as providing a basic understanding of flow in an RTM mold. One such micro-model was developed at MSU.[25,34]

<center>42</center>

MSU Micro Model

The model separates flow into two regions, channels and fiber tows. Channel permeabilities in all three directions are calculated from general flow equations. Permeabilities along the length of fiber tows are calculated experimentally and permeabilities transverse to the fiber bundles are calculated using the Kozeny-Carmen equation, Equation 7, for estimating permeabilities.

Different cells corresponding to either fibers or channels are then stacked according to the preform geometry, Figure 12. Flow through the cells is solved using the Gauss-Seidel difference scheme.[35] The Gauss-Seidel method was chosen because pressure at given cells needs to be calculated for every time step in order to advance flow fronts, and other finite difference methods would not be able to solve for flow in a reasonable amount of time.
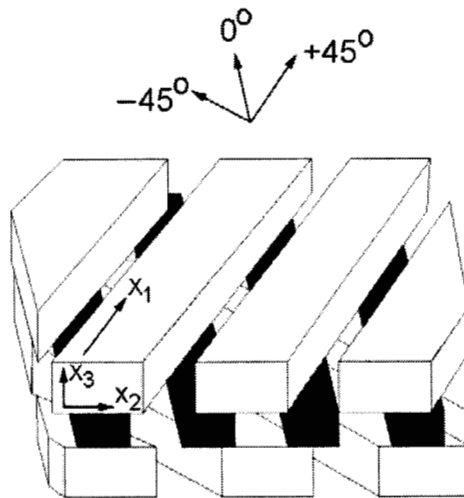
Figure 12. Stacking sequence for a [+45/0/-45] lay-up. Fibers are the solid regions and channels are void spaces between fibers.[34]

As one may imagine, computing flow through a model with cells on the order of tow size for an entire mold would be very time consuming. However, the model was able to predict detailed flow characteristics and took into account flow in individual fabric layers.

Macro-Flow Modeling Schemes

Macro-flow models consider flow through a fiber preform by grouping all layers of reinforcement and giving them a single permeability. While this method cannot predict flow details without corrections, it makes computations simple enough that large parts with multiple injection ports may be modeled. One such modeling program is Liquid Injection Molding Software (LIMS) developed by the University of Delaware's Center for Composite Materials.[11,36]

LIMS

LIMS calculates flow through RTM molds using a finite element/boundary method. The boundary between saturated flow and empty preform is modeled using the fill factor method, where each node is given a fill factor between zero and one. This takes care of conservation of mass problems that may occur. LIMS uses 2-D linear elements for its calculations, so flow through the thickness of elements in not taken into account. However, the program does accurately model flow in three-dimensional regions such as curves or T-intersections.

LIMS has several features that set it apart from other flow modeling programs. It accepts meshed finite element models from PATRAN so the user may create models with

complex shapes with relatively little effort. Once the model is meshed and exported, LIMS then reads the file and prepares it for modeling. One may then add injection ports, vent ports, and assign permeabilities to ranges of elements. In addition, LIMS includes its own scripting language. Scripts allow the user to turn on or off gates at any time during an injection as well as control their flow rate or pressure over time. Scripts also allow the user to record nodal data such as flow history, pressure or fill factor over the course of an injection.

Another advantage of LIMS is that it does not require a powerful computer. It will preform simple analysis on a 486 PC in a matter of minutes.

Flow Phenomena (Sources for Modeling Error)

All the areas that may cause inaccurate measurements in permeability calculations also apply to full-scale models. Namely, race tracking, mold deflection and capillary pressures all may contribute to modeling errors. In addition, certain model geometries create regions of high permeability in a model. One of theses geometric details is shown in Figure 13. As one can see, fabric going from the skin of the T-section to the web leaves a void area that allows locally high flow. Since LIMS and most other RTM fluid flow models assume thin-shell characteristics, preforms that have a significant amount of through-thickness flow will not be modeled correctly. Finally, errors may result if unsaturated flow regions are significant. Typically, the filling process will consist of two main regions, saturated flow and empty preform. However, there is a transition region of unsaturated flow between the two where resin and void space coexist, see Figure 14. In this region, the main flow channels are wet-out, but flow has not completely saturated the

fiber bundles. If this region is large, the part will appear full, but there will still be

regions with a significant amount of void space.
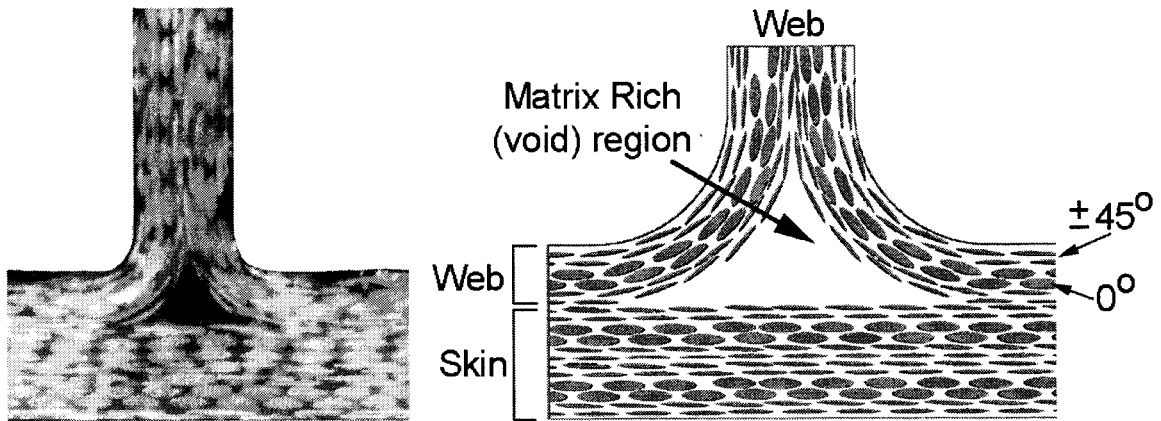
Figure 13. Photograph showing a void area in a T-section.
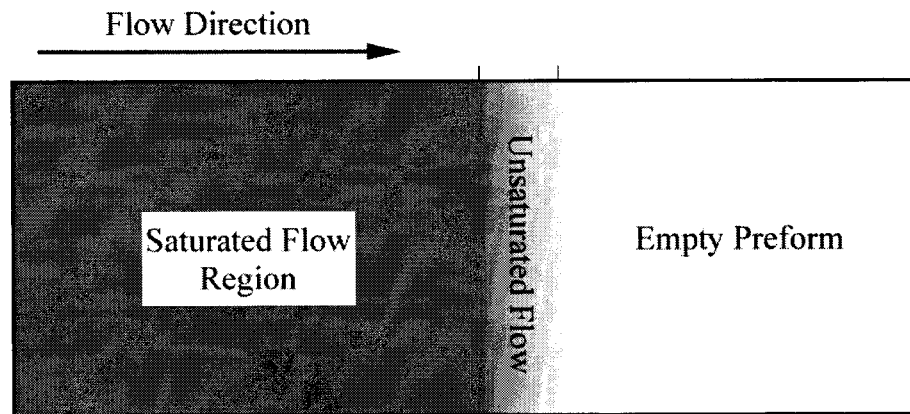
Figure 14. Three regions of flow in an RTM mold.

CHAPTER 3

EXPERIMENTAL METHODS AND PROCEDURES

Materials and Process Equipment

Widely used components in the manufacture of wind turbine blades are a polyester resin system and E-glass reinforcement material. Materials for this study are representative of the cost and strength of materials used in the wind industry. Injection equipment was selected to give accurate injection data, and allow for visual inspection of flow fronts while at the same time producing parts with close tolerances.

E-glass fiber reinforcement

Fabric selection was based on the following criteria. Fabrics needed to have similar architecture and price range to those currently used to make wind turbine blades. They needed to be easy to handle, able to be processed under RTM conditions, and have sufficient structural properties to compete with current industrial fabrics. Four continuous strand fabrics were selected and are summarized in Table 2.

Table 2. Summary of E-glass fabric reinforcement material used.

Manufacturer	Fabric Designation	Strand orientation to roll	Architecture	Ply Angle(s)
Owens-Corning Fabrics	A130	warp	woven	0°
	D155	weft	stitched	0°
	DB120	±45	stitched double biased	±45°
	CDB200	warp & ±45	stitched triple biased	0/±45°

The first fabric, Knytex A130, is representative of what is currently used in the manufacture of wind turbine blades for 0° reinforcement. It is composed of fibers in the warp direction so it is suited to making large parts such as wind turbine blades. One can see from Figure 15 that, the A130's are woven over a 90° glass bead. The bead is coated with a thermoplastic material to allow for ease of handling. Unfortunately the thermoplastic material interferes with resin bonding, and also limits flow through the thickness of the material. Furthermore, the weaving of the fabric compromises the compressive strength of the A130's since the fiber bundles are out of plane relative to the loading direction.[8] Despite this weakness, the A130 fabric has been sited as the best option currently available for blade manufacture,[5] and is used in the skin and spar sections of the MSU AOC 15/50 blade design.
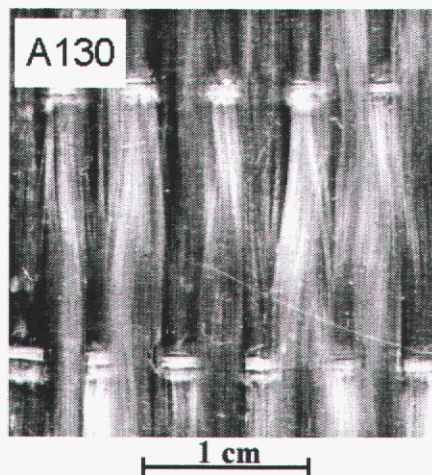
Figure 15. A130 Fabric.

The D155 fabric, Figure 16, consists of fiber bundles stitched together. It is one of the best performing unidirectional E-glass fabrics currently available,[5,8] since the fibers

are not bent like those in the A130 material and the compressive strength is notably

higher. In addition, it wets out better than A130s in both the hand lay-up and RTM. The

drawback of this material is that the 0° fibers are orientated in the weft direction of the

roll, Figure 6. This limits part size to the width of the roll they come on, currently 1.27

meters. The smaller size of the root in the AOC 15/50 blade allows use of this material.

1 cm
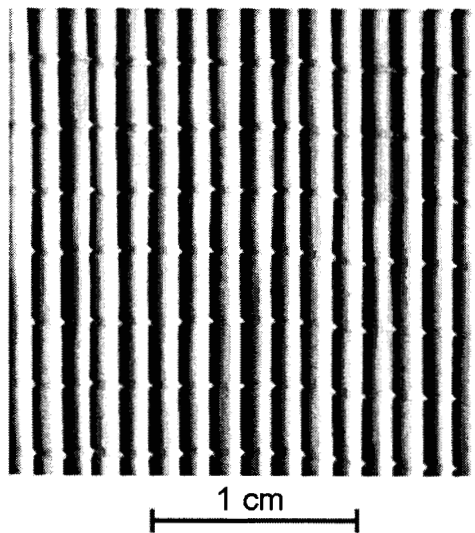
Figure 16. D155 Fabric

As mentioned earlier, composites are very weak perpendicular to the fibers, so all

structural applications need reinforcement in other directions. The DB120 fabric, see

Figure 17, is used for this purpose. It consists of two layers of fabric stitched together in

the ±45° directions, relative to the warp direction of the roll. This eliminates the need for

cutting unidirectional fabric at angles and splicing it together. Also, having both the ±45°

layers together eliminates the need for cutting and handling two layers of fabric and

makes it easier to produce symmetric lay-ups. Like most double biased fabrics, the

individual plies tend to have poor orientation control. Variations in roll tensioning, fabric
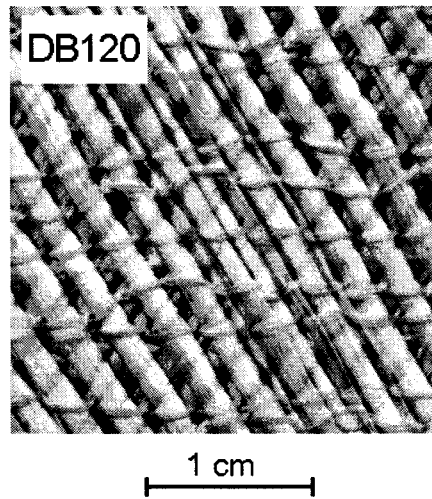
Figure 17. DB120 Fabric

handling and processing typically result in variations of individual +45° and -45° by 5°.[12]

The final fabric is the CDB200 tri-axial material. It consists of three layers of fabric stitched together in a 0/±45° orientation, see Figure 18. It was used solely as filler material in the steel insert section of the MSU blade since it has good material properties and its thickness allows rapid build up of the fiber volume in thick areas.

Front   Back
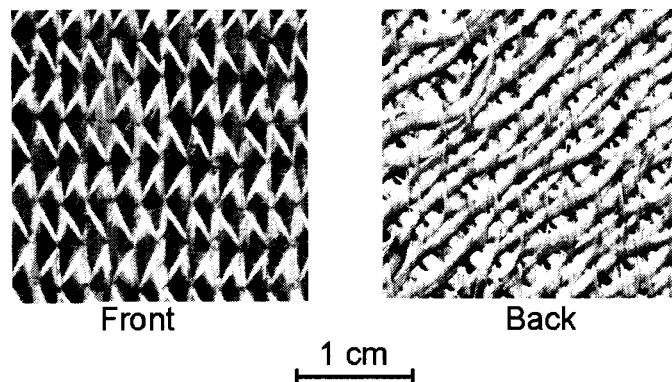
Figure 18. 0° and ±45° sides of CDB200 fabric.

Resin System

All flow experiments were conducted with an unsaturated polyester resin system made by Interplastic Corporation, CoRezyn 63-AX-051. The resin was catalyzed with 1% by volume of methyl ethyl ketone peroxide, Lupersol DDM-9 MEKP. The overall matrix system is comparable in cost and strength to matrix materials used in industrial wind turbine blade manufacture. In addition it has a relatively low viscosity, 150 cP at 25 °C, and a room temperature cure. This eliminates the need for heated molds and expensive injection equipment. Other useful properties of this resin system are that it is a Newtonian fluid,[10] the viscosity stays constant until gelation and when mixed with 1% of catalyst it will have a gelation time of around an hour. While injection times this long are generally avoided in industry, they are necessary to get accurate permeability data.

Injection Equipment

All flow experiments were conducted under constant pressure so a pressure pot system was ideal. The pressure pot was made from 0.645 cm thick, 20.3 cm diameter steel pipe welded to steel plate, see Figure 19. A 0.318 cm rubber gasket was placed between the lid and the pot in order to produce an airtight seal when the pressure pot was bolted together. A 15 kg/cm^2 regulator controlled the compressed air coming into the pressure pot. In order to get an accurate pressure in the pressure pot, an Omega Engineering 103 kPa test gauge with 0.345 kPa. gradations was connected. Standard air hose, and hose clamps were used to connect the pressure regulator and the test gauge to the pressure pot. Parker Presto-Lok® fittings along with 6.4 mm polyethylene tubes were used to transfer the resin from the pot to the mold.
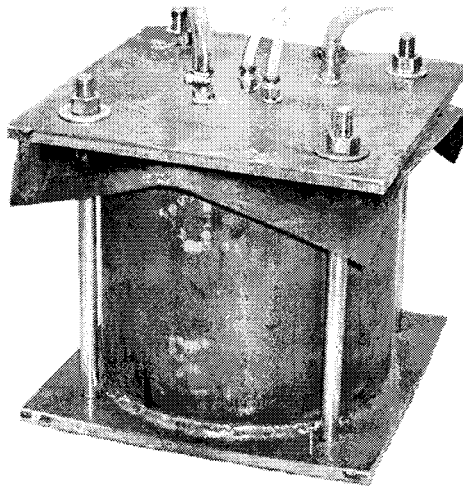
Figure 19. Pressure pot.

Molds

Three different RTM molds were used in the flow experiments. These molds

include a 510 mm by 810 mm by 3 mm thick flat plate, a thick flanged T-section mold,

and a steel root stud insert mold. A clear view of the flow fronts was of utmost

importance, so whenever possible transparent mold faces were used. In addition, molds

were designed to keep deflection to a minimum while they were under pressure.

Flat plate mold   The flat plate mold shown in Figure 20 was used for the

majority of the experiments. It was designed to produce parts roughly 3.18 mm thick by

510 by 810 mm. The base of the mold was made from 25.4 mm thick aluminum. A 3.18

by 510 by 810 mm cavity was machined into the base. In addition, there was a grove

machined into it to accommodate a 4.78 mm silicone O-ring. Seven 8.33 mm

injection/vent ports were drilled in the base as well. One port was located at each of the

four corners of the 510x810 mm cavity, and the fifth port was located at the center. For

the top plate, two pieces of 6.37 mm thick tempered glass were placed on top of the

aluminum base. They were clamped flush to the surface of the aluminum, compressing
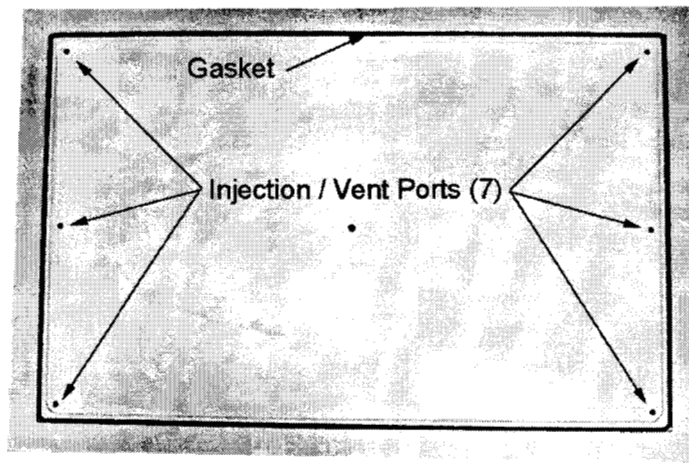
Figure 20. Flat plate mold.

the O-ring and making an airtight seal. Fifteen centimeter C-clamps were used to clamp

the glass plates to the aluminum. Four pieces of 50 by 50 by 6.1 mm hollow structural

steel (HSS) stiffeners were placed between the glass and the C-clamps to distribute the

clamping pressures and help keep glass deflections to a minimum. The HSS was located

at each end of the plate and the other two were located 102 mm from the central injection

port, one on each side.

Thick Flanged T-section Mold   T-section experiments were performed with a

thick flanged T-mold. This model gets this name because it produces T-sections with a

thick flange (Figure 21). Not only does this mold demonstrate flow at an intersection, but

its multiple thicknesses add additional complexity to the modeling of this part. The mold

consists of two L-shaped pieces of 25.4 mm thick aluminum. A 10.6 mm deep cavity is

machined into the skin part of the mold to account for the flange, along with a 2.98 mm

groove for a gasket, Figure 22. The skin's thickness comes from a combination of a 6.34

by 6.34 mm. gasket and a 0.58 mm spacer. The web surface has a 2.06 mm cavity

machined into each half, and a 1.60 mm silicone gasket provides the remaining thickness

for the web.
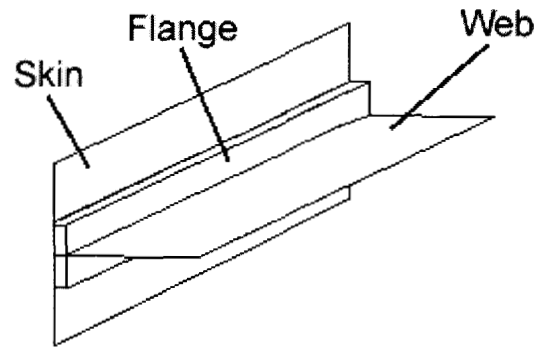
Section	Length (mm)	Width (mm)	Thickness (mm)
Skin	546	183	2.91
Web	546	115	5.29
Flange	546	98.8	10.1

Figure 21. Schematic of thick flanged T section and its dimensions.

In order to see what is happening in the web section of the mold, one of the aluminum pieces on the web was replaced with a clear polycarbonate (PVC) part, Figure 22. A 6.02 mm thick piece of clear PVC was used as the molding surface because it is unaffected by the polyester resin, and a 20.26 mm thick piece of polycarbonate was bonded to the PVC to build up the thickness to a level that was sufficient to control the deflection of this mold surface.
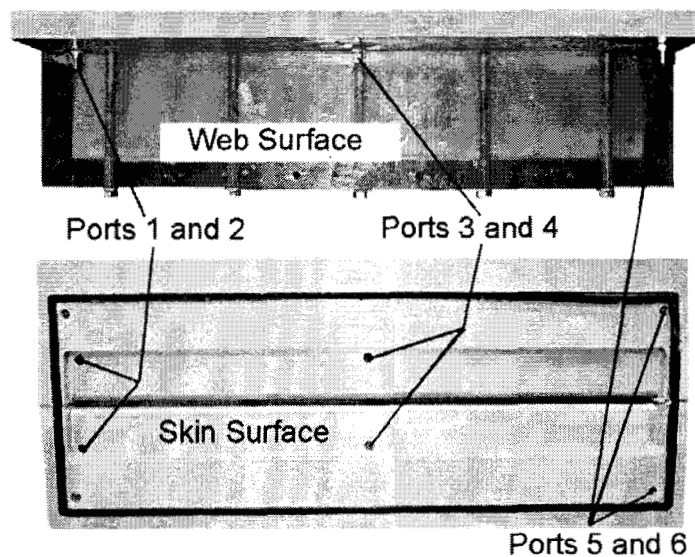
Figure 22. T-section mold.

Steel Root Insert Mold

The AOC 15/50 blade is attached to the wind turbine rotor with 10 bolts, as detailed in Figure 2. The bolts engage a steel root stud which transfers the stress from the blade to the rotor. The steel root stud insert mold shown in Figure 23, has composite molding surfaces reinforced by steel tubing. It is easier and less expensive to construct complex shaped molds from composites, and this method produces molds that are much more manageable than one machined from aluminum or steel. The injection port is located in the center of the mold on the skin surface. There are four additional vent ports. Silicone and neoprene gaskets are used to seal the mold. The silicone gasket is used to define the edges of the part because it is relatively inert to resin systems and provides a finished edge. The neoprene gasket is on the outside and helps provide an airtight seal. The mold is closed using four heavy-duty toggle clamps. Headwaters Composites Inc. in Three Forks, MT manufactured the mold for MSU under funding from the DOE EPSCoR program. Parts produced by the mold are approximately 635 mm long by 203 mm wide. At the thickest point, the part is 50 mm thick, including the steel insert. The thickness drops off to a minimum of 10 mm at the end of the part.

Imaging Equipment

To record flow front locations, a camera mounted on a tripod was used. Cameras used include a 35 mm Olympus, a Fuji DX-9 digital camera and an AGFA CL 50 digital camera. In order to get digitized images of the photos, the 10.2 by 15.1 cm prints were scanned at a resolution of 300 dpi with an Envisions ENV6100 color scanner.
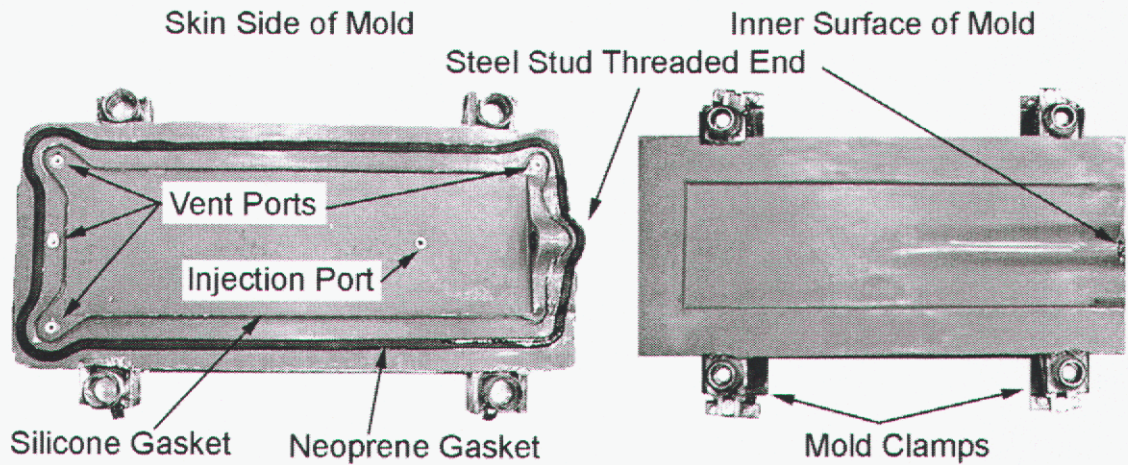
Figure 23. Skin and inner-surface halves of the steel insert mold.

Resin and Fabric Characterization

Motivation

The following experimental determinations are essential to permeability experiments. Resin viscosity is a required parameter in Darcy's law and surface tension is necessary to estimate capillary forces in a flow experiment. Fabric characteristics of interest include fiber volume fraction and the stacking sequence. Fiber volume fraction is a required parameter in Darcy's law, and the stacking sequence of different fabrics at a given 'clamping pressure' can help one estimate layer by layer fiber volume fractions for a composite containing different fabrics. Methods for determining these parameters are given below.

Resin Viscosity

Since constant viscosity is an underlying assumption in Darcy's law, it was of interest to evaluate the viscosity relative to cure time. In addition, viscosities of glycerol-water solutions were evaluated to determine if the testing procedure was yielding accurate results. Values for the viscosity for glycerol-water solutions are known[37] and provide a similar range to typical RTM resins.

Viscosities were determined experimentally using a capillary rheometer designed to ASTM Standard D3835-79 and shown in Figure 24. The dimensions of the rheometer can be found in Table 3. Resin was loaded to the top of the barrel. Then the piston was
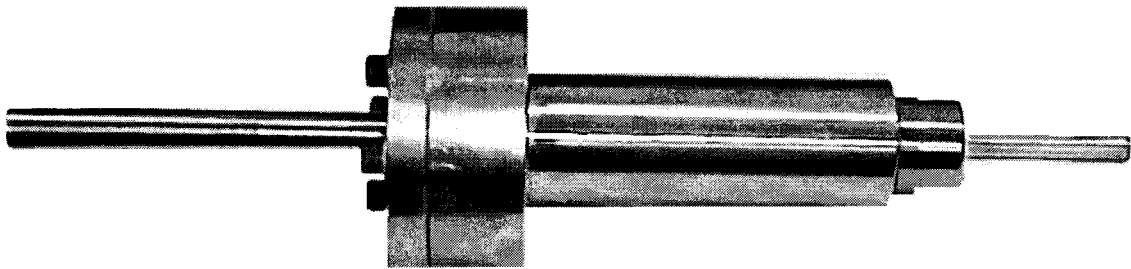
Figure 24. Capillary rheometer.

Table 3. Rheometer dimensions.

r_{cap} (m)	7.30 e-4
L_{cap} (m)	84.4 e-3
r_{barrel} (m)	6.35 e-3
m_{rod} (kg)	0.1522

carefully inserted and allowed to drop about 1.25 cm before test information was recorded. The resin was pushed through the capillary by the weight of the piston and the time it took the piston to travel a preset distance was recorded. The viscosity of the resin was determined from the following

21)
$$\mu = \frac{F r_{cap} t}{8 r_{bar}^2 L V}$$

where F is the force being applied to the resin, r_{cap} is the inner radius of the capillary, t is the time it takes for the piston to travel a given distance, r_{bar} is the radius of the barrel, L is the length of the capillary, and V is the volume of fluid displaced.

The piston was cleaned after each experiment with acetone and allowed to air dry, otherwise the piston would tend to stick to the walls of the test cylinder, yielding erroneous results.

Another characteristic of interest is the extent to which the resin is a Newtonian fluid. The capillary rheometer used for the viscosity tests may also be used to test the shear stress and shear rate of a resin. Tests on this particular resin were performed by Hedley[10] and it was determined that Newtonian behavior was followed under the conditions of an RTM injection. A detailed list of viscosity related experiments carried out in this study is shown in Table 4.

Surface tension

Surface tension of the resin is necessary to estimate the capillary effects during mold filling. Surface tension was measured/determined for uncatalyzed as well as catalyzed resin at varying times. In addition, the surface tension of glycerol was measured in order to insure that the method was producing accurate results.

Table 4. Viscosity Experiments.

fluid	temp. (°C)	time after cure (s)	number of tests
94% by weight Glycerol/Water	22	na	7
90% by weight Glycerol/Water	22	na	9
Uncatalyzed Resin	22	na	8
Uncatalyzed Resin vac. 15 min	22	na	6
Uncatalyzed Resin	24	na	3
Catalyzed Resin	24	258, 582, 862, 1312, 1644, 2175, 2618, 2837, 3353	one for each time interval

Surface tension was determined by following the procedure in Reference 38. Drops of resin were allowed to drip off the end of a capillary tube of known diameter. The diameter of the capillary was not the parameter of interest, but rather the diameter of the surface that the drop was forming on. The surface needed to be level and the edges rounded in order to give accurate results. Weight per drop was then measured. The following relationship was used to relate average drop weight to surface tension.[38]

22)
$$\gamma = \frac{mg}{2\pi r} \cdot \frac{1}{f\left(r/\sqrt[3]{V}\right)}$$

where γ is surface tension, m is the average weight per drop, g is the gravitational constant, r is the radius of the surface the drop is forming on and $f\left(r/\sqrt[3]{V}\right)$ is a correlation based on r and the volume of a drop, V, given in Reference 38.

Capillary Pressure

Capillary pressures were determined from surface tension values via Equation 19 and the method detailed in Reference 32. Values for c were taken from Reference 32 in order to estimate the maximum capillary pressures for both transverse and longitudinal

fluid flow.

Experiment Designation Scheme

All fabric related experiments followed the following the designations: XYnn-m.

X refers to the experiment type either S or M. S means an experiment has only one fabric type with all plies orientated in the same direction. A value of M indicates that the lay-up contains either multiple fabrics or one fabric orientated in several directions.

Y refers to the major fabric type present in the lay-up. Possible values include A for A130 fabric, B for DB120 fabric or D for D155 fabric.

The next term, nn, refers to the number of plies for a S type experiment, or the lay-up for a M type experiment. Current mixed lay-up designations include: $01 = [0/90_2/0]s$, $02 = [(90/0)_2]s$, $03 = [0/90/0/\overline{90}]s$, $04 = [0/\pm45_2/0]s$ and $05 = [0/\pm45_2/90]s$

Finally, m refers to the trial number for a given experiment, if more than one identical experiment has been performed. A list of tests are given in Table 5. Composites made from all three fabrics as well as a combination of the fabrics were tested.

Fiber Volume Fraction

Fiber volume fraction is another important parameter to evaluate. Two methods were used to characterize fiber volume fractions. The first method was by fiber burn-off, and the other was an empirical method based on the relative thickness of the fabric, number of plies and the composite thickness. Fiber volume burn-off tests were then compared with the empirical method to check for agreement.

Fiber Burn Off

Fiber burn-off tests were conducted by placing a composite of known dimensions in an oven at 550°C according to ASTM D2584. Burn-off times depended on the size of the composite and the amount of matrix material that needed to be removed. Samples were taken out of the oven after there were no visible carbon deposits on the glass fibers. The remaining glass fibers were then weighed and their volume was obtained from the density of glass, 2.56 g/cm³. The volume of glass was then divided by the original composite volume yielding a fiber volume fraction.

Relative Thickness The objective of the relative thickness method was to get a "relative ply thickness" for each of the fabrics used in this study. Then fiber volume fractions may be estimated by simply knowing the lay-up and the number plies of each fabric in the composite. This method is preferred since burn-off tests take a considerable amount of time.

Table 5. Burn off tests.

Test Name	Lay-up	Fabric Layers in lay-up		
		A130	DB120	D155
SA08-1	$[0_8]$	8	0	0
MA01-1	$[0/90_2/0]_S$	8	0	0
MA02-1	$[(90/0)_2]_S$	8	0	0
MA03-1	$[90/0/90/\bar{0}]_S$	7	0	0
MA01-2	$[0/90_2/0]_S$	8	0	0
MAB01-1	$[0/\pm45_2/0]_S$	4	4	0
MAB02-1	$[0/\pm45_2/90]_S$	4	4	0
SB07-1	$[0_7]$	0	7	0
SB08-1	$[0_8]$	0	8	0
SD01-1	$[0/90_2/0]_S$	0	0	8
SD02-1	$[(90/0)_2]_S$	0	0	8

The relative thickness method involved calculating the thickness of a ply of fabric as if it were solid glass. This was done by putting a sample of known area into an oven at 550° C to remove the binder material and stitching. For this study square samples of approximately 30.5 cm a side were cut. After the sample cooled, it was weighed. Once again the volume of the glass in the fabric may be calculated from its mass and density. Then, by dividing the glass volume of the fabric by its area a relative thickness for an individual layer was obtained. Three fabric samples for each fabric type were taken from different locations in the fabric rolls. Also, the amount of stitching or binder material was calculated from each fabric by subtracting the weight of the fabric before the burn off test from its weight after the test.

Fiber Stacking and Compressibility

Knowing how different fabric layers stack as well as pack together can offer valuable insight into flow through multi-layer composite preforms. Each of the three fabrics were evaluated as well as eleven different lay-ups using these fabrics (Table 6).

A servo-electric screw machine, Instron 4206, was used to compress the fabrics and measure the thickness. A Labview data acquisition box was used to record the displacement and load values off of the Instron. The first set of tests was to measure the natural stacking thickness of the lay-up. The desired lay-up was placed on a 11.4 by 15.2 by 2.5 cm steel plate. Then a thin fiberglass plate was placed on top of the lay-up to evenly distribute the force applied by the Instron. The Instron then compressed the fabric until a load of approximately 8.4 N was achieved.

Table 6. Fabric stacking and compression test matrix.

Test	Fabrics	Lay-Up	Motivation
SA06	A130	0_6	Find natural stacking height and compression for each fabric and determine if surface interactions have any effect by using lay-ups of differing thicknesses.
SA09	A130	0_9	
SB07	DB120	0_7	
SB12	DB120	0_{12}	
SD06	D155	0_6	
SD09	D155	0_9	
MA01	A130	$[0/90_2/0]_S$	Test compaction of 0° and 90° degree layers compared with unidirectional lay-ups.
MD01	D155		
MA02	A130	$[(90/0)_2]_S$	Compare different stacking order on compression
MD02	D155		
MA03	A130	$[90/0/90/\bar{0}]_S$	Determine whether 0° and 90° intersections stack and compress differently.
MD03	D155		
MA04	A130/DB120	$[0/\pm45_2/0]_S$	Compare how two different fabrics stack and compress.
MD04	D155DB120		
MA05	A130/DB120	$[0/\pm45_2/90]_S$	Determine whether there is a difference when there are 90° layers at the center.
MD05	D155DB120		
MB05	DB120	0/90/0/90/0	Determine whether orientation of DB120 fabric matters.

The displacement accounting for the thickness of the fiberglass plate was then recorded at this pressure. A similar procedure was followed for the compaction tests, but the fiberglass plate was replaced with two 11.5 by 15.0 by 2.5 cm. steel plates, Figure 25. The Instron compressed the fabrics at a rate of 0.127 cm per minute until a load of approximately 53 kN was reached. This information was then used to find compaction relative to clamping pressure. In this test loads were high enough that displacements in the test fixture and the Instron machine were significant sources of error. In order to compensate for this, the compression tests were run with just the test fixture in the machine. That way the displacement at a given load could be subtracted from the fabric compression tests so that only the displacement due to fabric compression was determined.
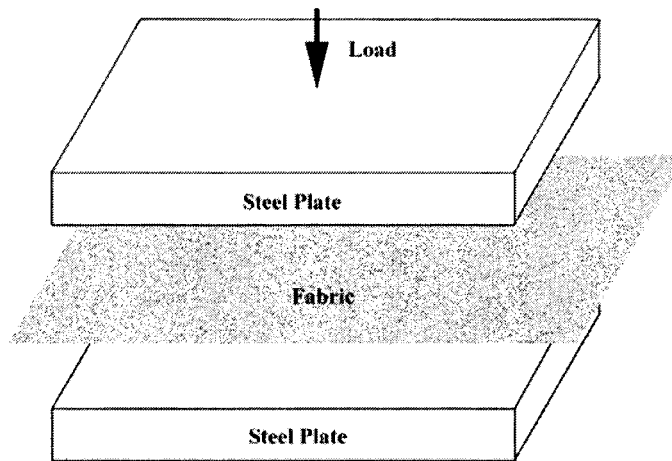
Figure 25. Fabric compression diagram.

Permeability

Motivation and Test Matrix

The first part of the project was to determine permeabilities of each fabric used. Since permeability varies greatly with fiber volume fraction,[39,40] it was necessary to find permeability values over a range of fiber volume fractions. Fiber volume fractions were changed by placing varying amounts of fabric into a mold of constant thickness. Table 7 lists the tests that were performed. It was desired to determine the repeatability of these experiments, so three experiments were run on the eight-layer A130 laminate. It was the most difficult of the three fabrics to process so the valiance of these experiments should be a worst case scenario.

Experimental Methods

All permeability experiments used the unsaturated radial flow method for calculating the permeability of the fabrics. This method has been proven to be accurate and requires only one experiment to determine the permeability of a given fabric.[41]

Table 7. Permeability test matrix.

Fabric	Test Name	Lay-up	Motivation
A130	SA06-1	$[0_6]$	Define permeability over a range of fiber volume fractions.
	SA07-1	$[0_7]$	
	SA08-1	$[0_8]$	Find maximum variability in permeability measurements.
	SA08-2	$[0_8]$	
	SA08-3	$[0_8]$	
	SA09-1	$[0_9]$	
DB120	SB07-1	$[0_7]$	Define permeability over a range of fiber volume fractions.
	SB08-1	$[0_8]$	
	SB10-1	$[0_{10}]$	
	SB12-1	$[0_{12}]$	
D155	SD05-1	$[0_5]$	Define permeability over a range of fiber volume fractions.
	SD06-1	$[0_6]$	
	SD08-1	$[0_8]$	
	SD09-1	$[0_9]$	

Accurate cutting of the fabric and minimal handling is necessary when one is calculating permeabilities. Fabric was cut using a rigid, premanufactured template for the given mold. Fibers were cut with a 45 mm hand roller cutter (Eastman ST-810). Then a 6.35 mm hole was punched at the center, and the fabric was then carefully placed in the mold. The injection port was aligned with the hole in the fabric to allow the resin to permeate all layers simultaneously. Special care had to be taken with the DB120 fabrics to avoid displacing the fibers from their ±45° orientations.

Prior to placing fabric in the mold, all surfaces that come into contact with the resin were coated with a mold release (Freekote 700-NC). After the fabric was placed and aligned, the glass plates were placed on top of the mold and the four steel stiffeners were used along with C-clamps to secure the two surfaces. Two steel stiffeners were placed 12 cm from the injection port and the other two were placed at the ends of the mold. Special care was taken when clamping the two surfaces to make sure that the glass plates and the aluminum surface were flush and the o-ring was properly compressed. The

stiffeners help distribute the clamping pressure and also stiffens the glass plates to minimize deflection.

The polyester was catalyzed with 1% of MEKP by volume. This low catalyst amount allowed for the extended injection times required. It was possible to use the resin for an hour before it began to gel. Processing times, however, were limited to less than 40 minutes.

The setup for the permeability experiments is shown in Figure 26. The pressure pot is hooked up to a compressed air source with a pressure regulator. Pressure in the pot is monitored through the test gauge attached to the pot and was kept within a range of ± 0.345 kPa. A timer was started when the resin first entered the mold. Flow front location was tracked with a camera set up on a tripod directly above the central injection port, and the zoom was adjusted to display the entire mold. It was desired to get about ten images per experiment, and the pressure was adjusted so that flow fronts did not reach the edge of the mold for at least twenty minutes.

Mixed Fabric

Motivation and Test Matrix

Flow though mixed-fabric preforms was the next set of experiments performed. This geometry is representative of several sections of the AOC 15/50 blade, Figure 27, the combinations are representative of those used in other wind turbine blades. The materials tested are listed in Table 8. The first series of these tests were with the unidirectional fabrics orientated in the 0° and 90° directions. Three lay-ups were chosen: $[0/90_2/0]$s,
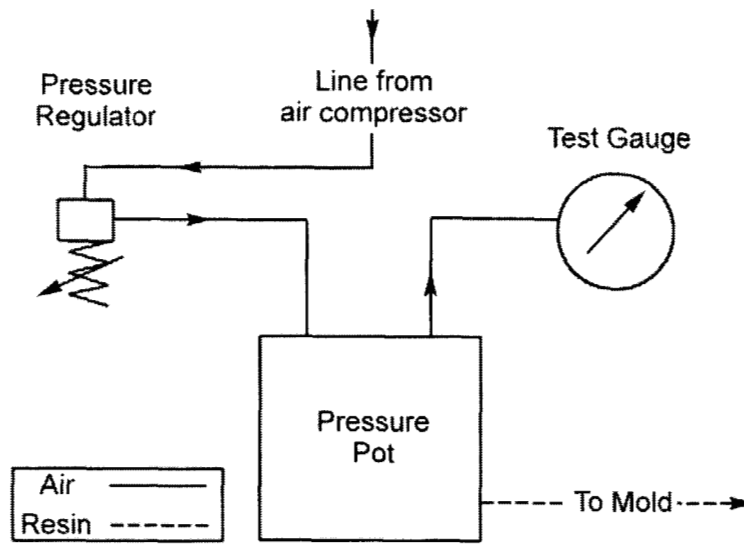
Figure 26. Diagram of experimental permeability setup.

$[(90/0)_2]$ and $[90/0/90/\overline{0}]$s. The first two experiments were to determine the effect of stacking order on the unidirectional plies as well as to determine if plies at the surface of the mold had different permeabilities than other plies. The third lay-up has a different stacking arrangement as well as a different fiber volume fraction since the middle ply is not repeated, this is denoted by the bar over the last ply in the symmetric lay-up.
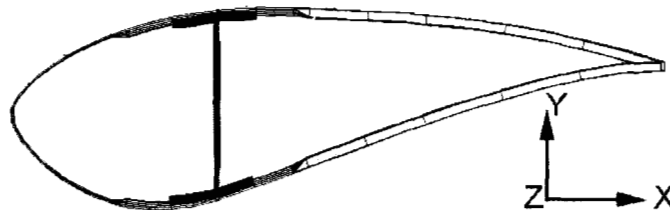
Figure 27. Regions of the AOC 15/50 that may be modeled by a flat plate geometry.

The next set of experiments involved mixing fabrics with differing thicknesses and permeabilities. Both the A130 and the D155 fabrics were thicker than the DB120's. The first of these lay-ups was $[0/\pm45_2/0]$s. Then this lay-up was compared with a $[0/\pm45_2/90]$s lay-up to see if one could take into account the addition of the 90° plies.

Table 8. Mixed fabric test matrix.

Test	Zero Degree Fabric	Lay-up	Motivation
MA01-1	A130	$[0/90_2/0]$s	Test predictability of multi-directional lay-ups form single ply permeability data.
MA01-2	A130		
MD01-1	D155		
MA02-1	A130	$[(90/0)_2]$s	Find if stacking order is a significant factor.
MD02-1	D155		
MA03-1	A130	$[90/0/90/\overline{0}]$s	Determine the effect of fiber volume fraction as well as stacking order.
MA03-2	A130		
MD03-1	D155		
MA04-1	A130	$[0/\pm45_2/0]$s	Determine how well multi fabric permeabilities can be predicted
MD04-1	D155		
MA05-1	A130	$[0/\pm45_2/90]$s	Determine if the addition of the 90° plies can be properly predicted.
MD05-2	D155		

Predictive Methods

It would be desirable to predict the permeability of any given lay-up from the permeabilities of the component fabrics and the thickness of the part. These methods assume that flow only occurs in the plane of the fabric, so it will not take into account interlaminar flow.

The first method determines a single fiber volume fraction for the entire lay-up. That is used to determine the permeability of all the individual component layers. The permeability is calculated by[39]

23)
$$K = \sum_{i=1}^{n} x_i k(v_f)_i$$

where K is the permeability of the entire lay-up, i is the number of layers, x is the thickness fraction of a given layer and k is the permeability of an individual layer which is a function of its fiber volume fraction v_f. The thickness fraction of a given layer is calculated from relative thickness data, and the permeability of a given layer is calculated from the fiber volume fraction of the entire composite. This method was found to work well for lay-ups whose thickness was small compared with the other dimensions of the part, and when permeability did not vary greatly between layers.[39]

The second method follows the same equation, but x, k and v_f values for each layer are calculated from clamping pressure data. Using this method, different fabric layers can have different fiber volume fractions instead of using a smeared fiber volume fraction for the entire lay-up.

Experimental Procedures

The flat plate mold was used for the mixed fabric experiments. In addition, all procedures that were followed for the permeability experiments were followed for the mixed fabric experiments.

T-Section

Motivation and Test Matrix

The T-section flow experiments represent the skin-web intersection in the AOC 15/50 blade, see Figure 28. A130 fabric was used as the unidirectional material for these
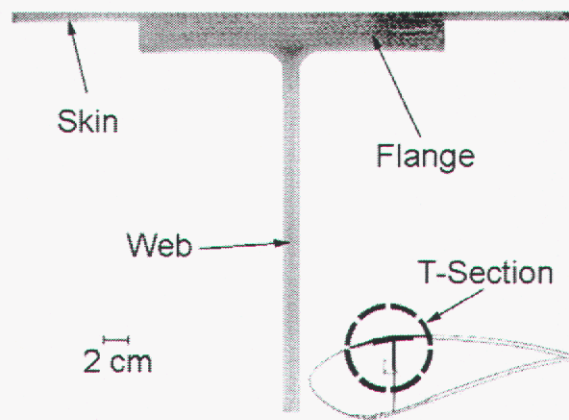
Figure 28. T-section part and how it relates to the AOC 15/50.

experiments and DB120 fabric was used for the ±45 layers. A130 fabric was chosen

because it is what is used in the AOC 15/50 design for the skin, the web and the flange.

The T-section mold offers several interesting features. First, it is a three-dimensional

geometry and the intersection between the plane of the skin and the plane of the web

must be taken into account. Next, the mold has three different thickness regions.

Two injections methods were chosen for the T-mold. The first method was a center

injection from two symmetrical ports located on the web side of the flange. The next

method was an end injection with two symmetrical injection ports located on the web

side of the flange, see Figure 29. From these two injections one should be able to

determine the effects of the thick flange region as well as any effects due to gravity that

may be present.

Experimental Methods

The same pressure pot system was used for the T-section experiments, except two

injection lines were run from the pot. Special care needed to be taken when closing up

the mold. Since the mold consists of three pieces, it must be certain that the two

L-shaped halves had to be exactly aligned to prevent leaking. Also, the skin and web
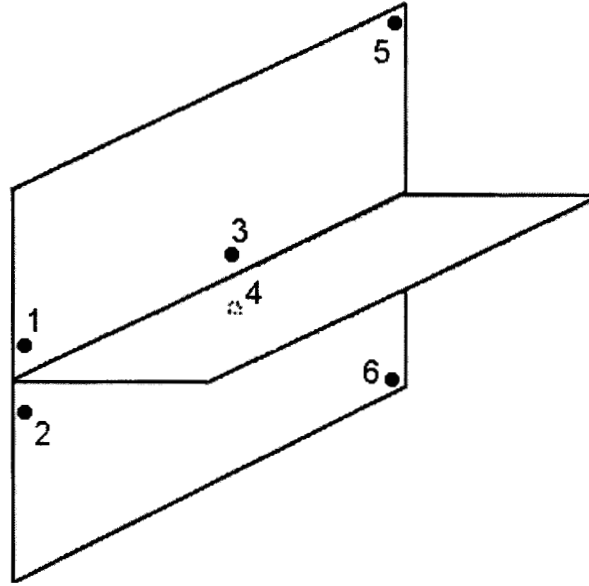
Figure 29. Port locations on the thick flanged T-mold.

sections use gaskets instead of O-rings, so clamping thickness of the mold must be carefully monitored to insure that there is a uniform thickness through the part.

A preliminary injection was performed with the D155 fabric as the unidirectional material. In order to simplify modeling and injection, lay-ups for the three sections (web, flange and skin) were chosen to give a constant fiber volume fraction throughout the part (Table 9). One camera was setup above the web on a tripod. The other was fixed at the level of the web surface. Once again the timer was started when resin first impregnated the mold. A timer was used to record the time of the images and also to assist in taking simultaneous images at both the web and the flange surfaces.

Table 9. Properties of T-section components.

	Web	Skin	Flange
D155 Lay-up	$[\pm45_2/0_2/\pm45_2]s$	$[\pm45_2/0]s$	$[\pm45/0_2/\pm45/0_2/\pm45]s$
A130 Lay-up	$[\pm45_2/0_2/\pm45_2]s$	$[0/\pm45/0]s$	$[\pm45_2/0_2/\pm45_2/0_2/\pm45_2]s$
Thickness TA01 (mm)	5.32	2.83	12.83
Fiber Volume fraction TA01	0.342	0.346	0.316
Thickness TD01 (mm)	5.15	2.94	12.81
Fiber Volume fraction TD01	0.273	0.334	0.271
Thickness TA02 (mm)	5.30	2.95	13.10
Fiber Volume fraction TA02	0.343	0.331	0.310

<u>Root Insert Section</u>

The root insert mold was selected because it represents a geometry present in the root of the AOC 15/50 wind turbine blade, see Figure 30. In addition, the lay-up of the mold was quite complex compared with those of the flat plates and the T-section, so three-dimensional filling details may be observed. Injections were performed from the skin side of the mold, and vent ports were located at the four corners. It was desired to get flow front shape as well as filling time for this mold. Since the insert mold was opaque, a partial injection was stopped at 160 s to get an estimate of the initial filling pattern in the mold. Also, a full injection was done and the time was recorded when resin reached each of the vent ports.
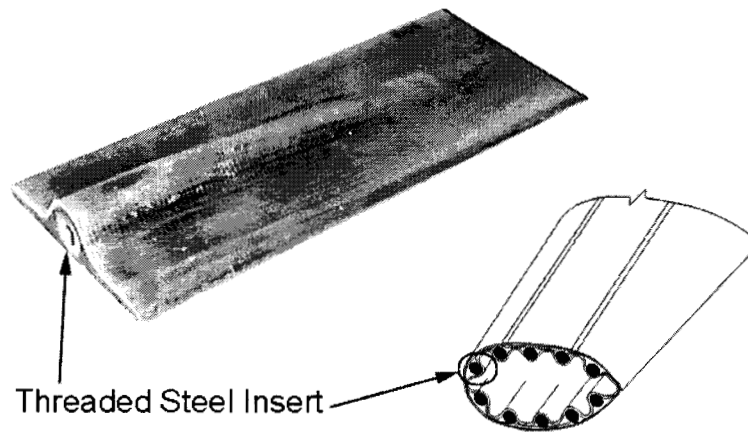
Figure 30. Steel insert part and how it relates to the AOC 15/50 blade.

Experimental Procedures

The lay-up for the root mold was much more complex than the other two molds. Figure 31 contains a photograph of half of the root lay-up. The lay-up for the skin surface is $[\pm45/0_2/\pm45]$s and the lay-up for the inner surface is $[\pm45/0/\pm45/0_2/\pm45]$s. In addition, three different sections of fabric were added around the steel insert to provide a constant fiber volume content.[4] First, there were two darts made from D155 fabric which consisted of a piece of 305 by 356 mm D155 fabric cut at a 45° angle and rolled into a dart. Next, four strips of CBD200 warp triaxial fabric were added between the dart and the skin surface. The strips were 51 mm in width and ranged in length from 229 to 305 mm. Finally, eight layers of the CBD200 fabric were layered under the tip of the insert. These plies were cut into a trapezoidal shape 191 mm in length and tapering from 76.2 to 25.4 mm along the length. All tri-axial plies were placed to avoid multiple ply-drops at the same location.

The injection setup for the steel insert experiments was the same as for the previous experiments minus the imaging equipment. The injection ports were located at the middle of the insert on the skin side with vent ports at the four corners.
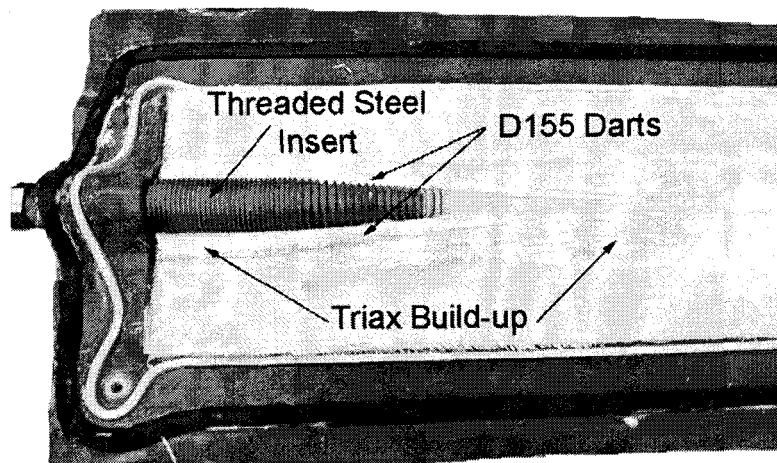
Figure 31. Lay-up of the skin side of the insert mold.

CHAPTER 4

EXPERIMENTAL RESULTS

The experimental results obtained in the study are presented in this chapter. First, the results of the resin and fabric characterization experiments are presented. Then, permeability results for single and mixed fabric lay-ups are presented and compared with estimates of the permeability of mixed fabrics based on single fabric data. Finally, resin flow results for the thick-flanged T and the steel root insert geometries are presented.

Resin and Fabric Characterization

Viscosity

Viscosity tests are summarized in Table 10 and Figure 32. The first set of viscosity tests were completed to determine if the rheometer was giving accurate readings. Viscosities of glycerol/water solutions were calculated for concentrations of 90 weight percent glycerol. Literature values for the viscosity are 234.6 mPa·s at 20° C and 163.6 mPa·s at 25° C.[37] The viscosity was experimentally calculated to be 188 and 186 mPa·s at 22° C, which was acceptable for a linear interpretation of the literature values of 192 mPa·s at 22° C. This shows that the rheometer is functioning properly in the range of the resin viscosity.

Table 10. Viscosity Results.

fluid	temp. (°C)	Average viscosity (mPas)	Standard deviation	number of tests
90% by weight Glycerol/Water	22	187	2.5	9
Uncatalyzed Resin	22	195	2.0	8
Uncatalyzed Resin vac. 15 min	22	203	3.0	6
Catalyzed Resin	24	266	2.1	1 test each for 9 time intervals
Uncatalyzed Resin (one year later)	24	267	9.0	3
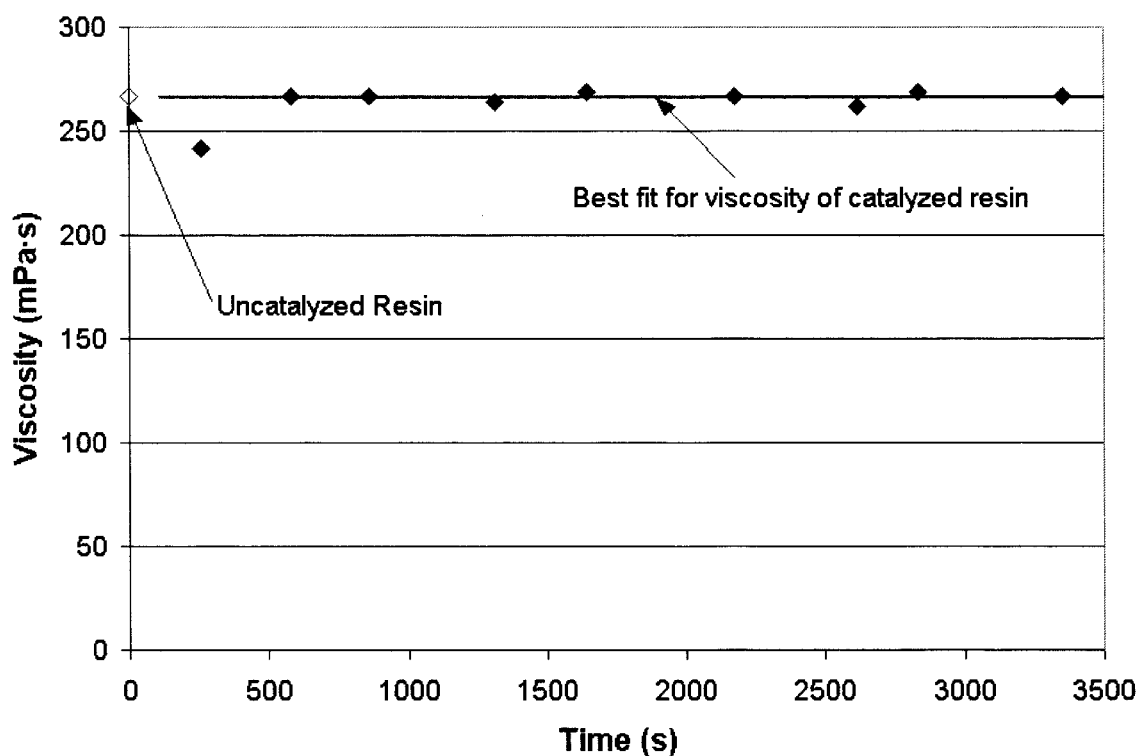
Figure 32. Viscosity of catalyzed CoRezyn 63-AX-051 with time. The average value for the uncatalyzed resin is shown at time equal to 0.

The resin system used has a limited shelf life since it was chemically promoted prior to storage. Polymer chains cross-link over time even without adding the catalyst. This leads to an increase in viscosity with time, so it is important to keep the resin stored in a cool place. The first set of viscosity tests on the resin were to determine if pulling a vacuum had an effect on the viscosity. Vacuum assisted RTM is a common practice so it was of interest to see if the viscosity of the resin would increase, since the vacuum tends to liberate extra styrene from the resin. The viscosity of the resin was evaluated to be 195 mPa·s and the viscosity of the resin under vacuum was 203 mPa·s. While a slight increase is shown when the resin is under vacuum, it is not much greater than the variations in permeability measurements.

Next, it was of interest to see if the viscosity of the resin changed when the catalyst was added. Experiments with the catalyzed resin were done a year after the original experiments on the uncatalyzed resin. At first it appeared as though there was a significant change, since the uncatalyzed resin was originally measured at 195 mPa·s, and the first data point for the catalyzed resin came out at 242 mPa·s with the remainder of the viscosities were near 267 mPa·s, as shown in Figure 32.

Experiments were then done on the batch of uncatalyzed resin that was used for the catalyzed resin experiment. The viscosity of the uncatalyzed resin turned out to be 267 mPa·s. The rheometer was then rechecked with the 90% glycerol solution, and it gave the same results as obtained one year earlier. Therefore, it was concluded that the uncatalyzed resin had increased in viscosity from 195 to 267 mPa·s over the 13-month time span and the original data point (242) of the catalyzed resin was reached in error.

The rheometer had been flushed with acetone prior to the catalyzed resin experiments, and the acetone may not have been completely removed thereby causing that first data point (242) to appear to have a lower viscosity.

The potential viscosity increase for the uncatalyzed resin is, therefore, on the order of 72 mPa·s (195 to 267) over 13 months of storage. This increase in may lead one to believe that the viscosity of resin used in the flow experiments is not accurately represented by the initial value of 195 mPa·s. However, resin used for the flow experiments was taken out of a 55-gallon drum and stored in 5-gallon buckets in a freezer until a new bucket was needed. This minimized the amount of time the resin had to react since the 5-gallon buckets were at room temperature for a maximum of four weeks before they were used. The resin with the 72 mPa·s increase in viscosity had been at room temperature for the entire 13 month period.

Surface Tension

Results of the surface tension experiments are summarized in Table 11. Surface tension results were first done on glycerol in order to see if the experimental apparatus was giving accurate results. The calculated surface tension of 6.50×10^{-2} N/m compared well with the literature value of 6.34×10^{-2} N/m at 20°C.[38] The surface tension varied slightly with cure, but this was due more to experimental variability than a significant increase in surface tension.

Table 11. Surface tension results.

substance	surface tension (N/m)	number of tests	Constants used for surface tension calculations	
glycerol	6.50×10^{-2}	5	radius (cm)	0.377
uncatalyzed resin	2.92×10^{-2}	20	ρ of glycerol $(g/cm^3)^{42}$	1.22 @ 22°C
cat. resin (741s)*	2.76×10^{-2}	5		
cat. resin (931s)*	3.29×10^{-2}	5	ρ of resin $(g/cm^3)^8$	1.14
cat. resin (1055s)*	3.15×10^{-2}	5		
cat. resin (1278s) *	3.02×10^{-2}	5		
* time after catalyst added				

Capillary Pressure

The surface tension results were used to estimate capillary pressures inside the mold using the method discussed earlier, and detailed by Skartsis.[32] Capillary pressure results are summarized in Table 12. Capillary pressures were estimated for both parallel and serial fiber arrangements. Parallel arrangements were for flow along the length direction of the fibers while serial capillary pressures were for flow transverse to the fibers. Constants were evaluated in order to give the most conservative values, which represent the highest capillary pressures. As one can see, capillary pressure along the length of the fibers was so low that it should not be a factor. Serial flow, however, was close to the order of experimental pressure variation. This may be responsible for small errors in flow predictions, but most likely it will be overshadowed by more significant sources of error.

Table 12. Capillary pressure.

Capillary pressure results		Constants used in capillary pressure calculations[32]	
P_{cap}-parallel	0.802 kPa	k_{trans}	1.20
		k_{par}	17.8
P_{cap}-serial	3.08 kPa	ε	0.55
		r_{fiber}	8.0e-6 m

Fiber Volume Fraction

Results from the relative thickness values experiments are shown in Table 13. As one can see, both the A130 fabric and the D155 fabric had considerably more glass fibers in them per unit volume than the DB120's, even though the DB120 fabric consists of two plies stitched together. The DB120's have the largest percent of non-structural material in them, 4.8%. This was not surprising since two plies were stitched together. The A130 fabric contained the next highest amount of non-structural material, 2.4%. It was the only one of the three fabrics that had a thermoplastic binder coated glass bead holding the tows together instead of stitching. Finally, the D155's had the lowest weight percent of non-structural material with 1.9%.

Table 13. Relative thickness and fabric composition results. Results are an average of three tests performed on each fabric type.

fabric	weight fraction stitching (s) or binder (b)	standard deviation	relative thickness (cm)	standard deviation
A130	0.0244-b	0.00182	0.0174	0.000260
DB120	0.0483-s	0.00184	0.0140	0.000452
D155	0.0194-s	0.00240	0.0209	0.000419

Fiber burn-off tests of various laminates were compared with predicted fiber contents in Figure 33. The relative thickness method predictions correlate well with

experimental data. Error bars of ±0.01 are plotted for the burn-off tests. They are given

by ASTM D2584 for a 5 g sample.
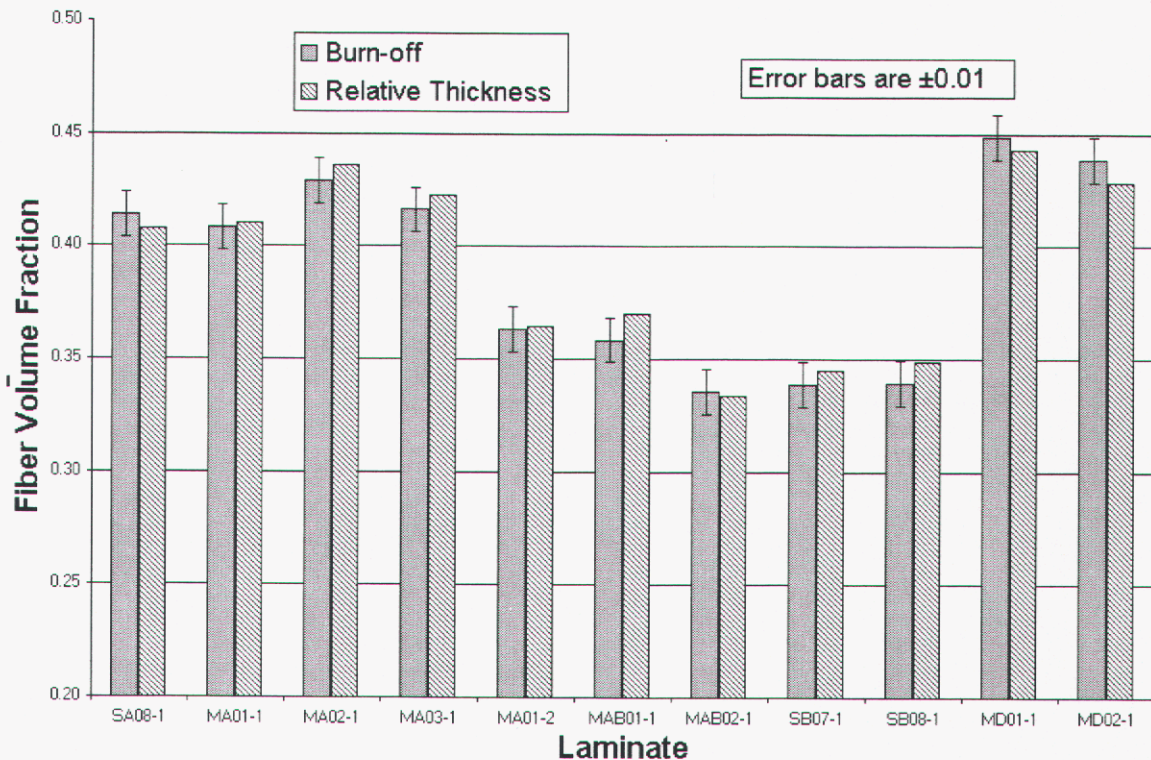
Figure 33. Comparison of relative thickness method prediction with experimental burn-off results.

Fabric Stacking and Compressibility

Since deflections were measured by piston movement, the first step in evaluating

the compression of the fabric layers was to determine the excess deflection related to the

compression apparatus and compression in the machine. To evaluate this, the

compression apparatus without fabric was placed in the Instron 8872 and the apparatus

and loaded. The loading test was repeated three times to determine if the displacements

were repeatable, see Figure 34. The results were repeatable to within the tolerances of

the machine (0.025 mm). The first run resulted in a step pattern because the sampling

rate was faster than the accuracy of the displacement measurements. Therefore, there

were several load values for each increment of 0.025 mm. The third run was used in the

fixture displacement calculations.
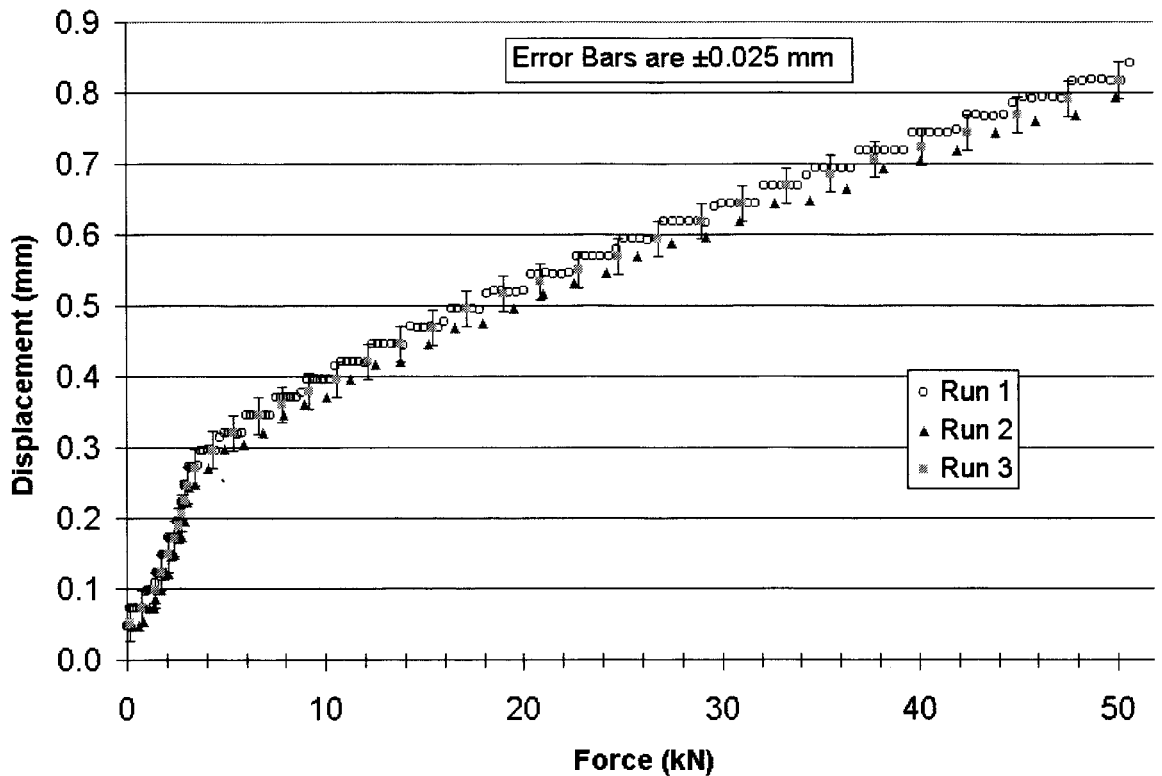
Figure 34. Displacement of fabric compression test fixture without fabric as a function of load. Error bars are placed on Run 3.

Fabric thickness was found by subtracting out the deflection of the compression

apparatus. Fixture deflection at a given load was found by linear interpolation from the

third run of the fixture compression tests. If a load was past the range of the third run, a

linear extrapolation from the last five data points was used. A plot of the compression

results for unidirectional, single fabric lay-ups are shown in Figure 35. Fiber volume
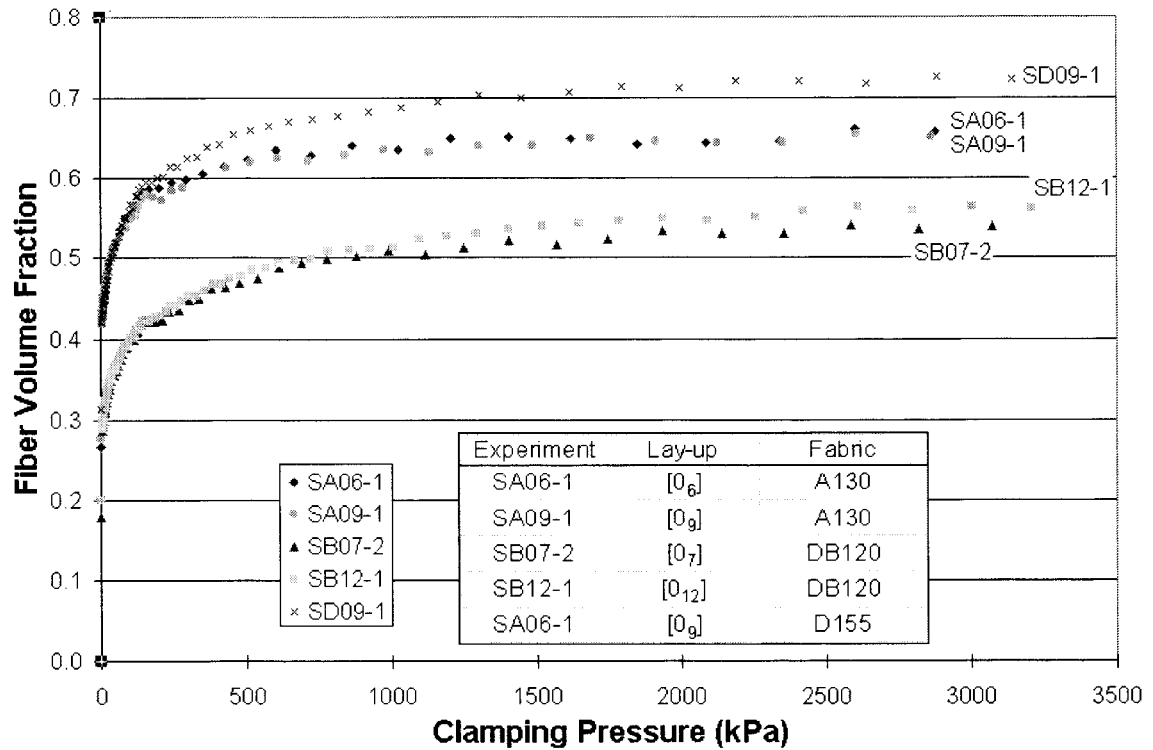
Figure 35. Compressibility of unidirectional A130, DB120 and D155 fabrics.

fractions were calculated by using relative ply thickness data and the thickness of the given lay-up. Clamping pressures were calculated assuming a uniform load across the area of the steel plates, 0.115 m by 0.150 m.

All fabrics followed a similar trend. The fabrics compressed rapidly for the first 150 kPa. Then, a large increase in clamping pressure was required for a small increase in fiber volume fraction. Finally, the fabric asymptotically approached a maximum fiber volume fraction. The D155 fabric and A130 fabrics followed a similar compression curve until the 150 kPa clamping pressure range. The A130 fabric leveled off at about 0.67 fiber volume fraction, while the D155 fabric was able to achieve a maximum fiber volume fraction around 0.73. The DB120 followed a similar trend but consistently had a

fiber volume fraction of at least 0.10 lower than either of the unidirectional fabrics. It approached a maximum fiber volume fraction of 0.56. The low fiber volume fractions of the DB120 fabric are most likely due to the large spacing between fiber tows, and the large amount of stitching required to bind the two plies together.

Next, three cross-plied lay-ups were compared with a unidirectional lay-up to determine the effect of ply stacking. The following lay-ups were used for both the D155 and the A130 fabrics: $[0/90_2/0]s$ Mx01 series, $[(90/0)_2]s$ Mx02 series and $[90/0/90/\overline{0}]s$ Mx03. Results from the A130 and D155 fabrics are shown in Figure 36 and Figure 37 respectively.

As one can see from Figure 36, the A130 fabric had a slight tendency to nest if fabric layers were aligned. The unidirectional lay-up, as expected, had the highest fiber volume fraction per clamping pressure followed by the MA01 lay-up which had the second most aligned plies. The MA02 and MA03 lay-ups had the lowest fiber volume fraction per clamping pressure. After 800 kPa, the A130 fabrics deviated from their original, relative stacking thickness, and the MA01 lay-up achieved the highest fiber volume fraction at a given clamping pressure. A possible cause for this may be that the A130 fabric layers did not nest well at higher pressures because of their woven architecture. Another cause may simply be experimental error due to the fact that the thinner lay-ups include a greater error.
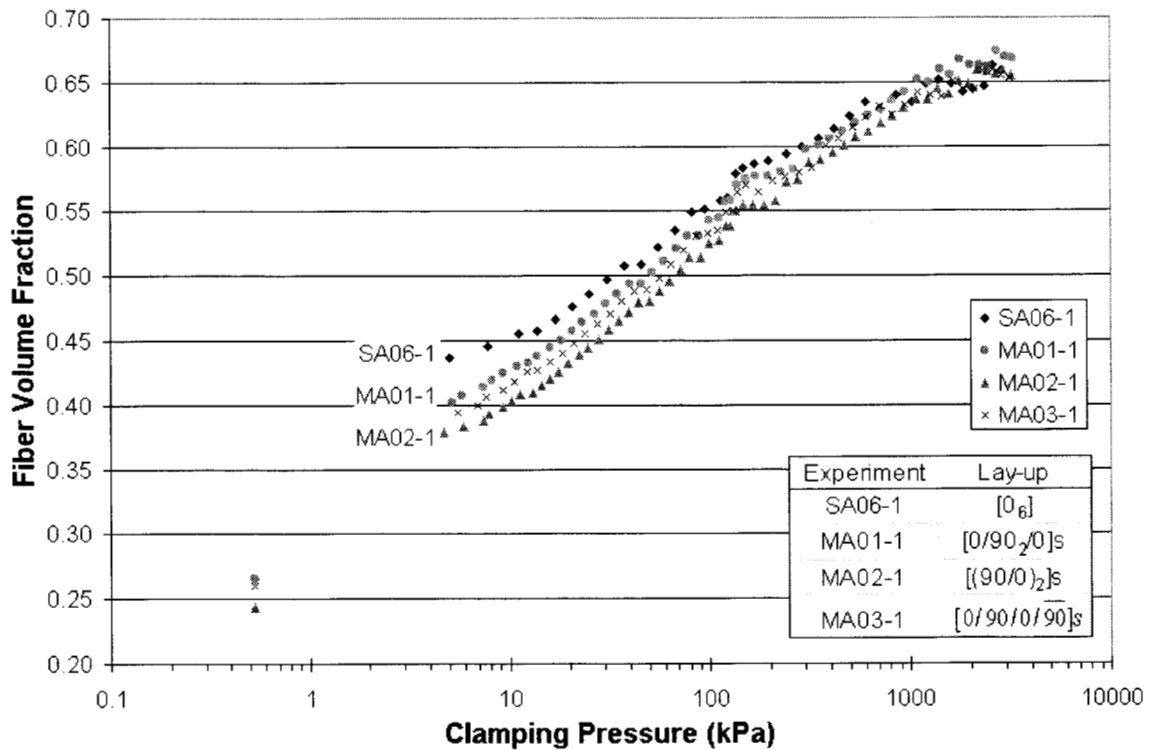
Figure 36. Effects of lay-up on A130 fabric stacking.

Ply stacking order was significant when dealing with the D155 fabrics. As one

can see, the unidirectional lay-up maintained a significantly higher fiber volume fraction

per clamping pressure than any other of the lay-ups, Figure 37. Also, as predicted, the

MD01 lay-up had the second highest fiber volume fraction per clamping pressure.

However, it had a significant drop-off from the unidirectional lay-up since it contained

four 0° to 90°interface regions over the eight ply lay-up. As expected, the MD02 and

MD03 lay-ups had the lowest fiber volume fraction for a given pressure. The D155

fabrics showed a greater sensitivity to fabric orientation than the A130 fabrics. This is

due to the fact that the geometry of the D155's allow fiber bundles that are aligned in

parallel to easily nest together, but this nesting is impossible when layers are stacked

perpendicular to each other.
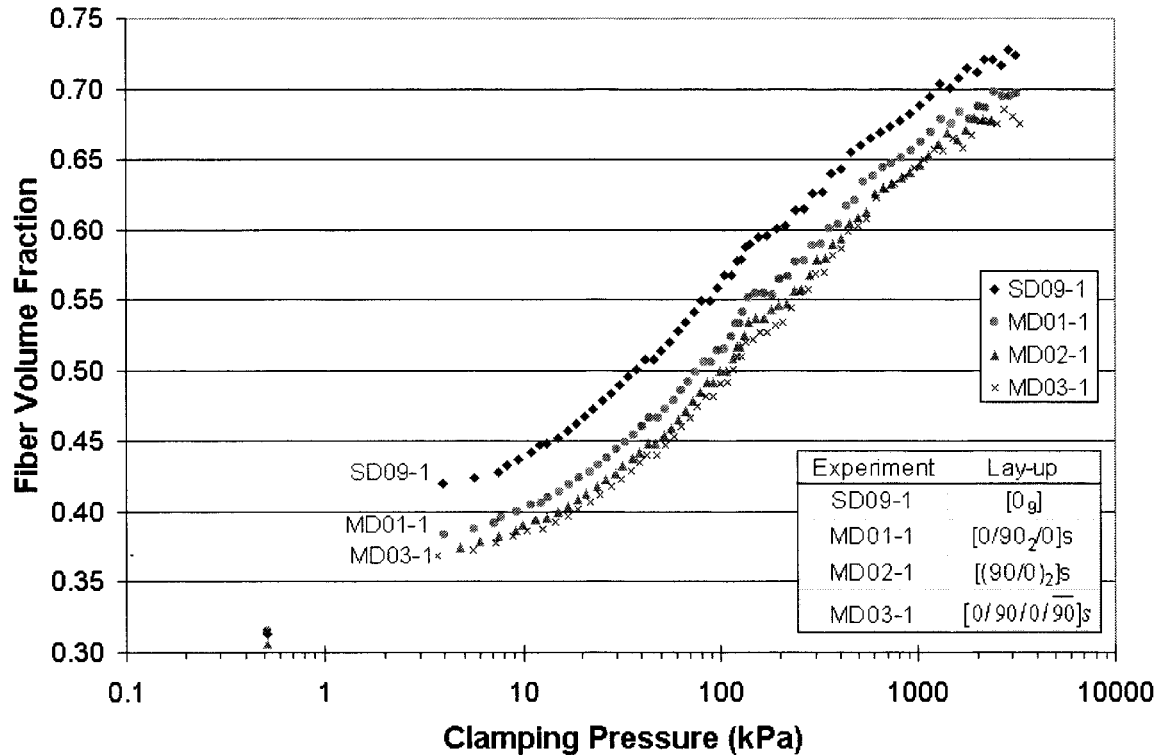
Figure 37. Effects of lay-up on D155 fabric stacking.

Finally, the effect of mixing different fabrics on the fiber volume fraction of a

lay-up was investigated. Both unidirectional fabrics were combined with the DB120

fabric. Fabric compression tests were performed on both the Mx04 and Mx05 series

lay-ups. Both lay-ups gave identical results, so only the Mx04 series results are shown in

Figure 38. Adding the DB120 fabric to a lay-up significantly reduced the fiber volume

fraction of the overall laminate, but as one can observe from the graph, the local fiber

volume fraction in the unidirectional layers was much higher than the fiber volume

fraction in the ±45° layers. This is of importance if one wants to estimate permeabilities

of a mixed fabric lay-up since permeability varies greatly with fiber volume fraction. In addition, it is desirable to know how much relative thickness each layer is taking up in the laminate.

Experiment	Lay-up	Fabric
SA06-1	$[0_6]$	A130
MA04-1	$[0/\pm45_2/0]s$	A130/DB120
SD09-1	$[0_9]$	D155
MD01-1	$[0/\pm45_2/0]s$	D155/DB120
SB12-1	$[0_{12}]$	DB120
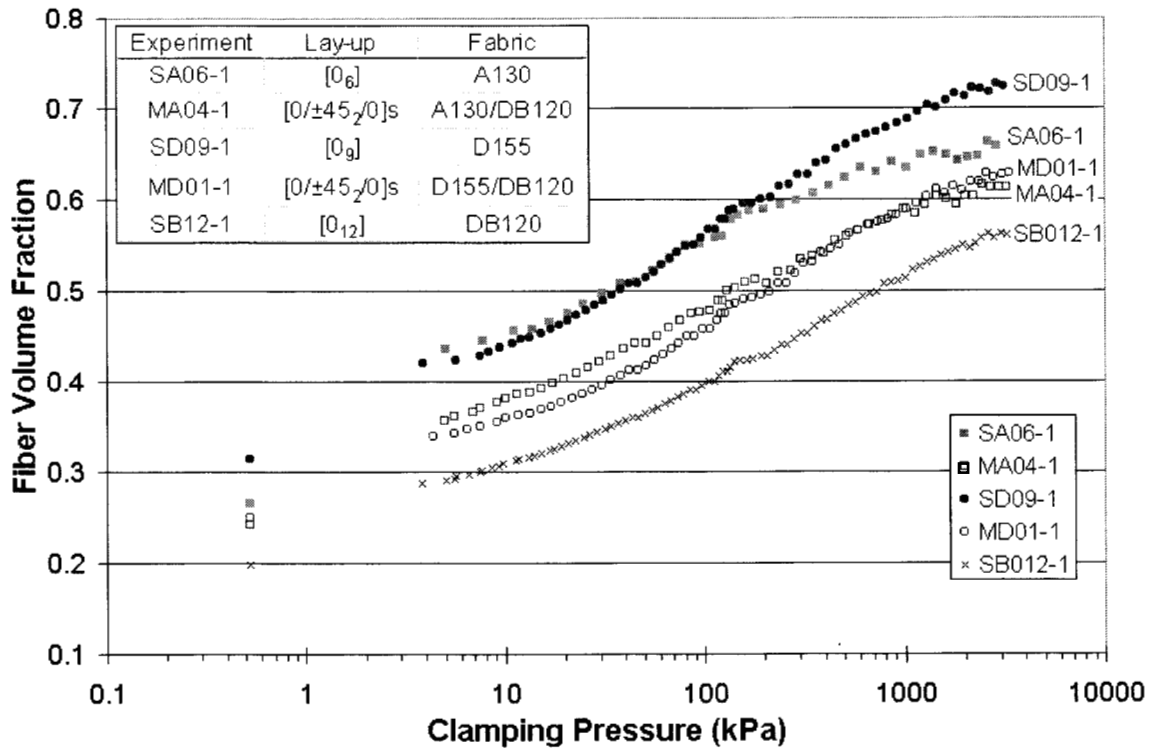
Figure 38. Effect of mixed fabrics on fiber volume fraction.

Permeability

Permeability values were determined for A130, DB120 and D155 fabrics at several fiber volume fractions. Permeability data are the primary input for any flow model, so the accuracy of the measurements and calculations is of utmost importance. Flow results are presented as flow front position versus time in the flat plate mold, see Figure 20.

A130 Fabric

As stated earlier, A130 fabric is a woven, unidirectional glass fabric. The fiber tows are woven over a thermoplastic coated glass bead. The thermoplastic bead inhibits flow through the thickness of a laminate and can create preferential flow between plies. The glass beads are spaced about every 3 to 4 cm. The perpendicular glass beads create a channel area that helps in wetting the fabric in the transverse direction.

A contour plot of the resin flow front position over time is shown in Figure 39. Contours were traced from digitized images of the experiments. The digitized images were then transformed to a normal unit of measure by knowing distance between pixels. The mold stiffeners caused the blank areas in the contour plots.

As one can see, the flow fronts were not exactly symmetrical. At the beginning of the experiment there was some preferential flow on the left-hand side of the mold (negative x-direction). As the experiment progressed, the flow front shape on the right hand side of the mold (positive x-direction) passed the flow on the left side. After 30 minutes the right-hand side finished approximately 4 cm further along than the left side. The transverse direction, however, remained relatively symmetrical. This effect was commonly observed in unidirectional experiments with the A130 fabrics.

In order to determine the experimental permeabilities, the distance from the inlet port to the maximum flow front locations in both the transverse and longitudinal directions were measured and plotted versus time. Since the flow fronts were not symmetrical, average values were taken in both directions. Figure 40 is a plot of permeability versus fiber volume fraction.
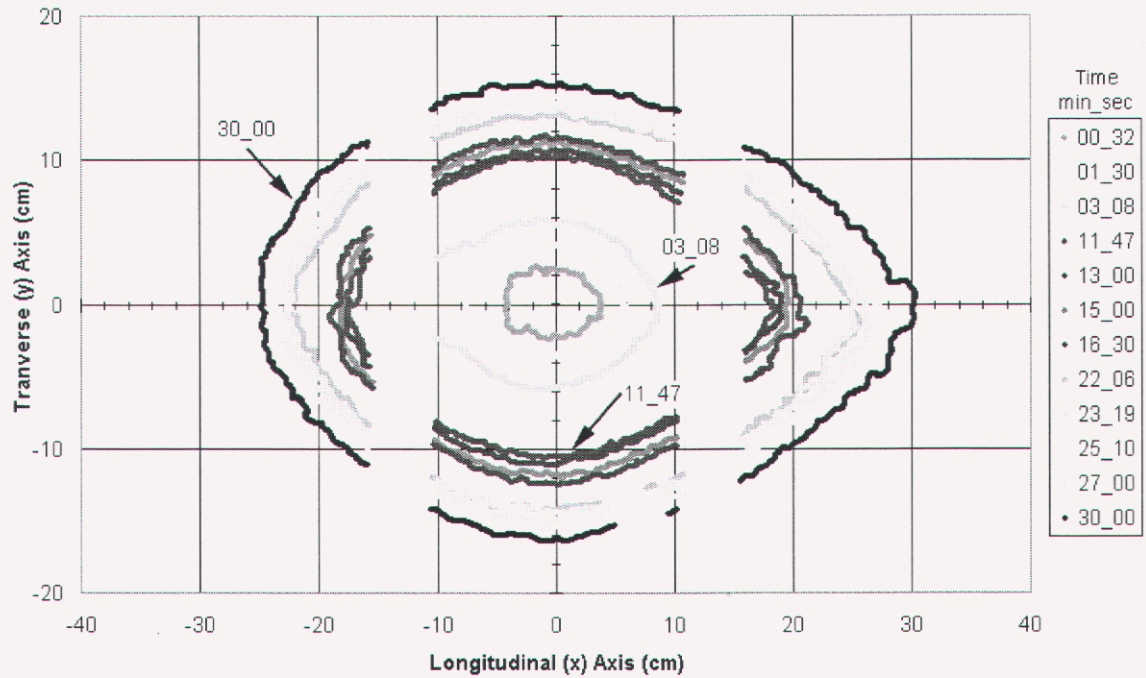
Figure 39. Contour plot for experiment SA08-1. Times are listed in minute_second format on the legend. The lay-up consisted of 8 layers of A130 fabric with a fiber volume fraction of 0.40. Fibers aligned in the x-direction.

The equations shown in the figure:

$$K_x = 5.85 \cdot 10^{-8} e^{-15.9 v_f}$$
$$R^2 = 0.943$$
$$K_y = 1.13 \cdot 10^{-9} e^{-8.63 v_f}$$
$$R^2 = 0.968$$
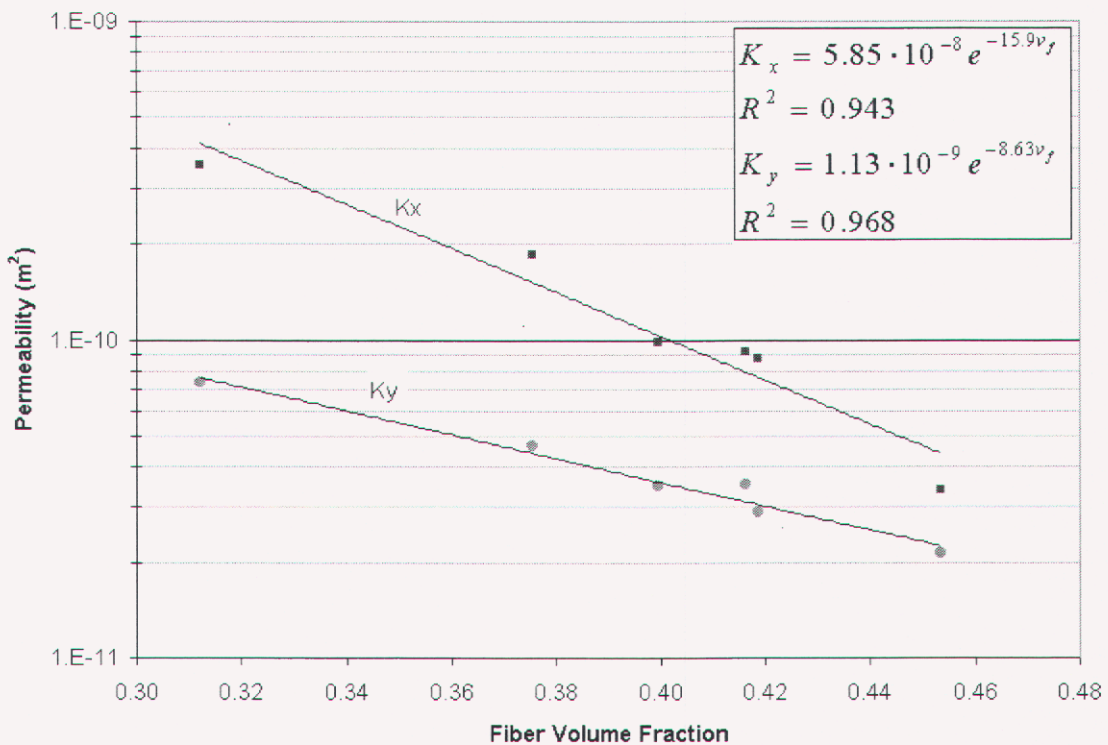
Figure 40. A130 unidirectional permeability versus fiber volume fraction.

As expected, permeability decreased with increasing fiber volume fraction. The permeability in the longitudinal direction (K_x) was affected to a greater degree than in the transverse direction by changing fiber volume fraction.

DB120 Fabric Results

Of the three fabrics tested, the DB120 fabric wet out the most evenly. In addition, it had a very high through-thickness permeability, due to the fact that it is a stitched fabric and its fiber bundles are spaced the farthest apart of the three fabrics, Figure 10. Furthermore, flow experiments with the DB120 fabrics had the smallest region of unsaturated flow. In most experiments an unsaturated flow region was not noticeable.

One might expect that, since the DB120 contained ±45° plies stitched together, both the longitudinal and transverse flow directions would be identical, but that is not the case as can be seen in Figure 41. The exact fiber orientation was checked to see if it was influencing the flow of resin, however, fibers were orientated 3° towards the transverse direction. This implies that the increased resin flow in the DB120's is due to the presence of the stitching material, which ran parallel to the longitudinal direction.

Comparing Figure 39 and Figure 41, the DB120 fabric shows a much more symmetrical flow front shape than the A130 fabric. During the course of the experiment, there was never more than a one cm difference in the two longitudinal flow front positions. After approximately 2.5 minutes, there was not a significant difference in the two transverse flow fronts. Similar results were observed with other DB120 fabric tests.
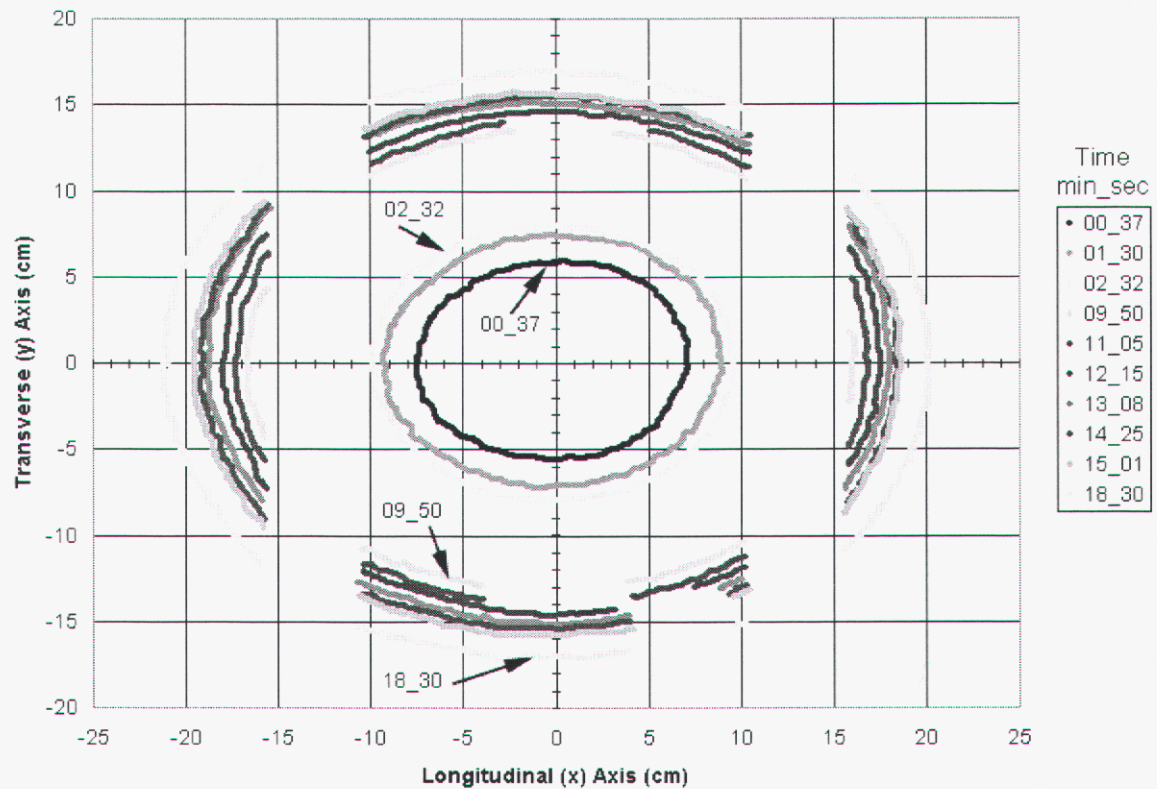
Figure 41. Contour plot for experiment SB08-1. Times are listed in minute_second format on the legend. The lay-up consisted of 8 layers of DB120 fabric with a fiber volume fraction of 0.31.

Permeabilities of the DB120 fabrics show linear behavior in Figure 42 when plotted versus fiber volume fraction on a semi-log graph. In addition, both the longitudinal (K_x) and the transverse (K_y) permeabilities had similar slopes. This is expected since fabric architecture is similar in both directions.

$$K_x = 6.39 \cdot 10^{-9} e^{-13.2 v_f}$$

$$R^2 = 0.953$$

$$K_y = 6.44 \cdot 10^{-9} e^{-14.7 v_f}$$

$$R^2 = 0.923$$
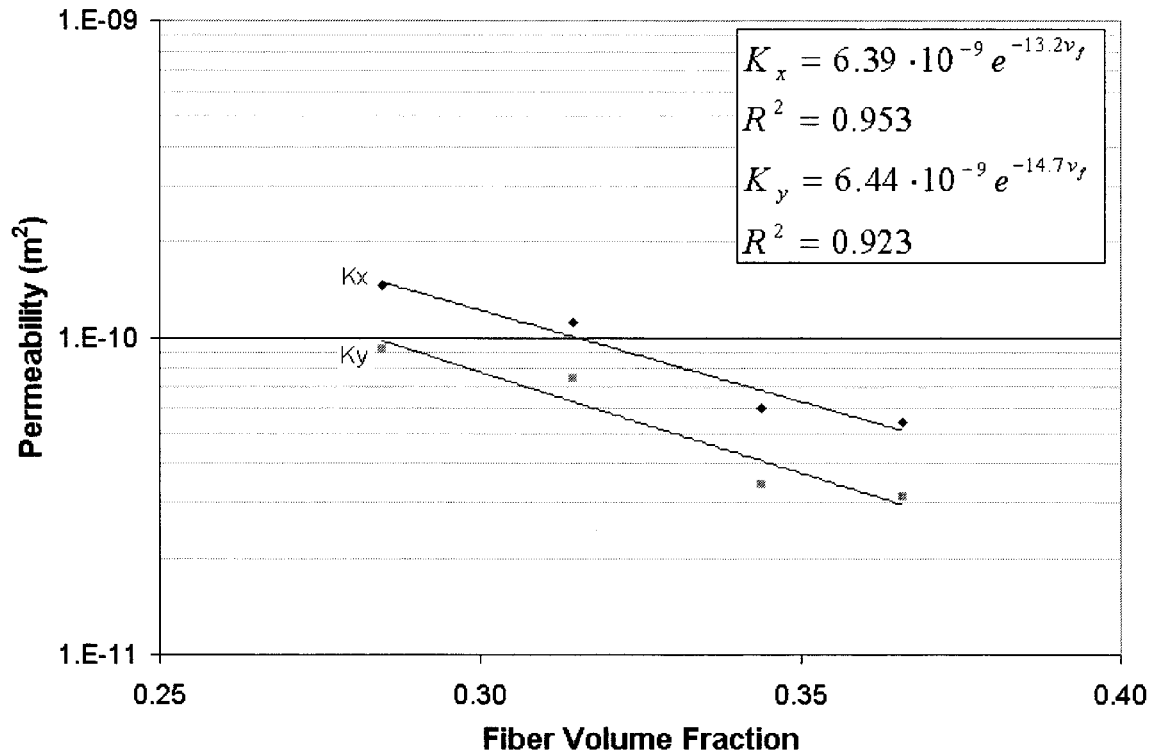
Figure 42. Permeability versus fiber volume fraction for DB120 fabric.

D155 Fabric

Like the DB120 fabric, the unidirectional D155 fabric consists of stitched fiber

bundles. There were gaps parallel to the direction of the fibers. These gaps create

regions of high permeability. As a result the D155 fabric exhibited highly anisotropic

flow patterns shown in Figure 43. The gaps also raise the through thickness permeability

of the D155 fabric, so preferential flow between fabric layers was not a problem. In

addition, distances between unsaturated flow region were barely noticeable.
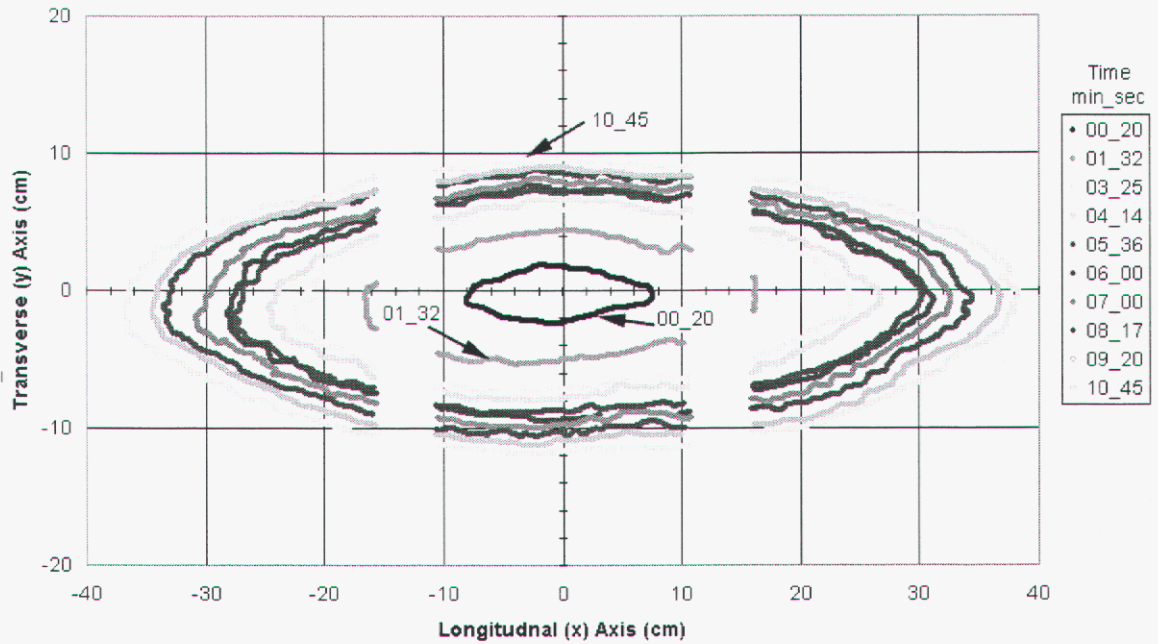
Figure 43. Contour plot for experiment SD06-1. Times are listed in minute_second format on the legend. The lay-up consisted of 6 layers of D155 fabric with a fiber volume fraction of 0.40. Fibers aligned with x-axis.

Both the longitudinal and the transverse flow fronts remained relatively symmetric. While the shape at the longitudinal ends of the flow front changed slightly on either side, the maximum flow points from the injection port remained within one cm of each other throughout the course of the experiment. The maximum flow positions of transverse flow fronts also remained within one cm of each other throughout the course of the experiment.

Transverse permeabilities were approximately ten times lower than the longitudinal permeabilities as shown in Figure 44. Also, as the fiber volume fraction was increased, the permeability in the transverse direction decreased at a faster rated than the permeability in the longitudinal direction.
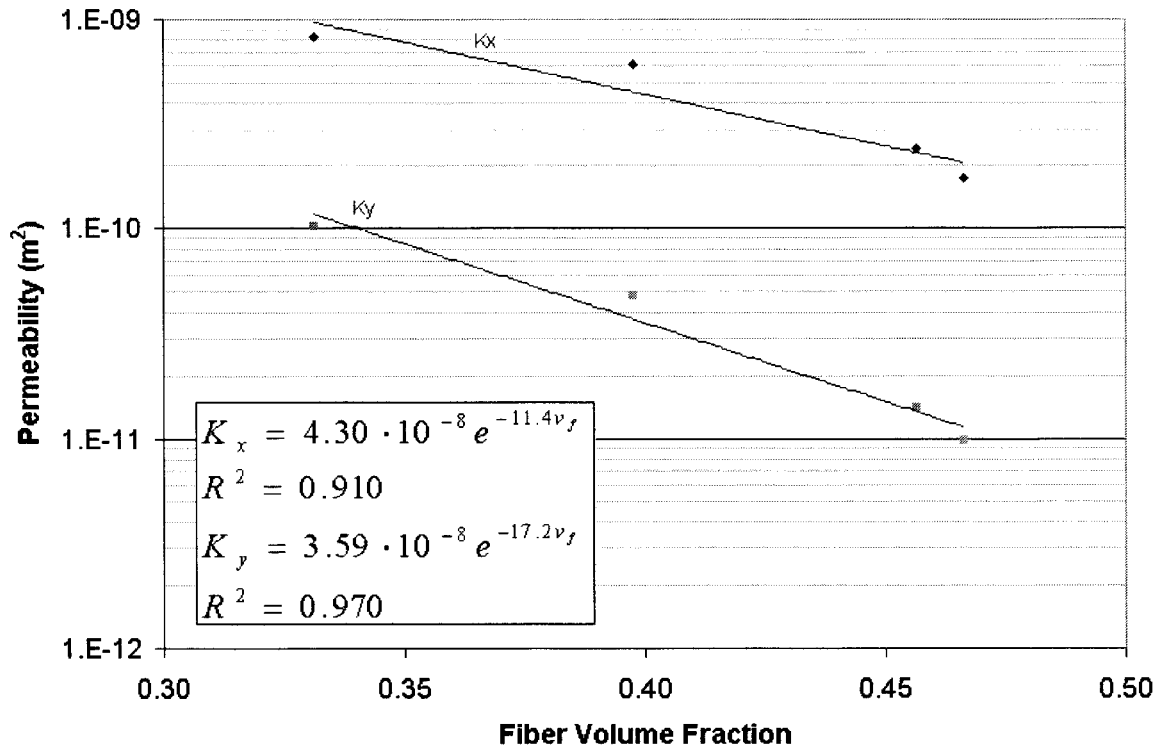
Figure 44. D155 permeability versus fiber volume fraction for a unidirectional lay-up.

The equations shown in the figure are:

$$K_x = 4.30 \cdot 10^{-8} e^{-11.4v_f}$$

$$R^2 = 0.910$$

$$K_y = 3.59 \cdot 10^{-8} e^{-17.2v_f}$$

$$R^2 = 0.970$$

Permeability Discussion

Defining the position of the saturated flow boundary can be a source of error when calculating permeabilities. An example of this type of flow front is shown in Figure 45.

Unsaturated flow was a problem primarily in the A130 fabric. In order to estimate how repeatable these permeability experiments were, a set of three experiments were performed on an eight-layer lay-up of A130 fabric. Results are summarized below in Figure 46.
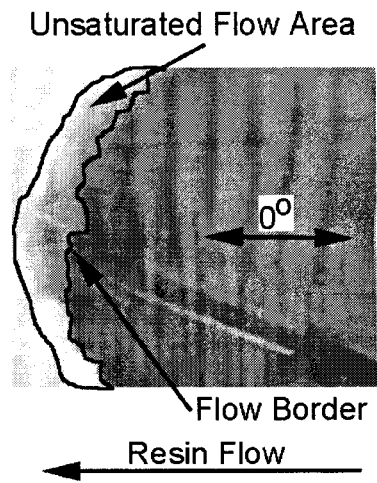
Figure 45. Unsaturated flow occurring in a unidirectional A130 lay-up.
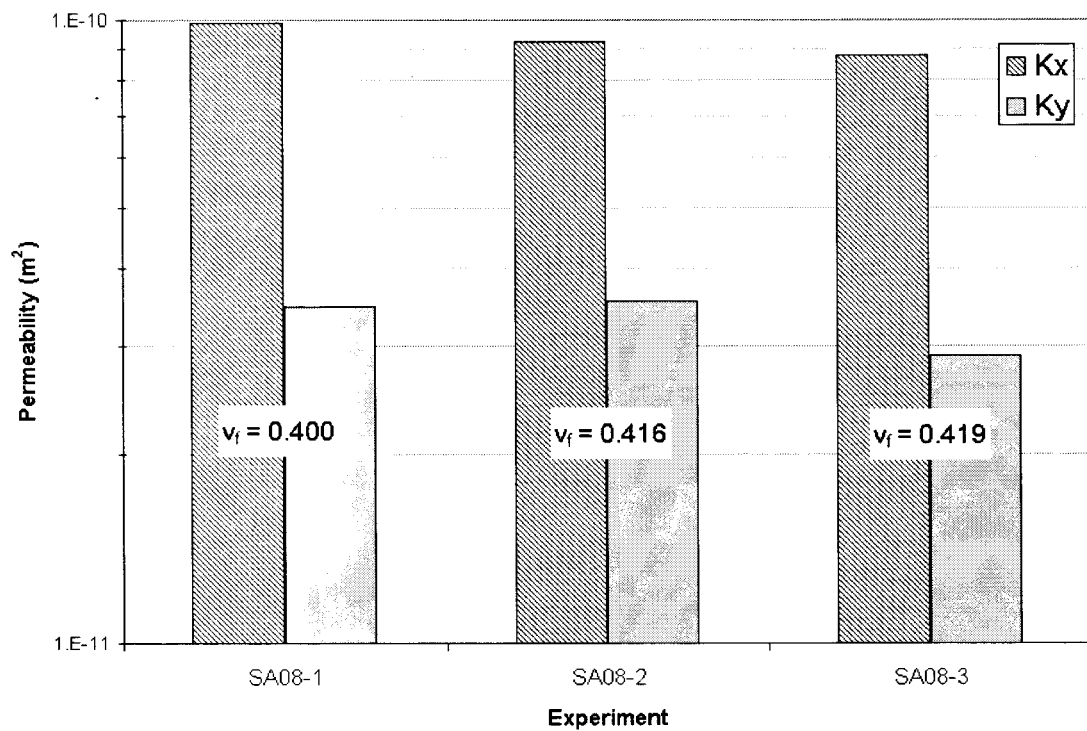
Figure 46. Permeability variation for three experiments with A130 fabrics.

Experiments SA08-1 to SA08-3 used slightly increased fiber volume fraction so a slight decrease in the longitudinal permeability is expected. However, flow in the transverse direction did not follow this pattern. The K_y value for the SA08-2 experiment was slightly higher that the SA08-1 experiment even though it had a one percent higher fiber volume fraction. In addition, flow in the transverse direction is governed by the density of cross beads. This tends to vary significantly throughout a roll of fabric. If one compares the K_x to K_y ratios of the three experiments they differ by about 10% due to the variability in the K_y measurements.

Permeabilities are summarized for all three fabrics and compared with values from the NIST Permeability Database[18] in Figure 47. Only the NIST permeabilities
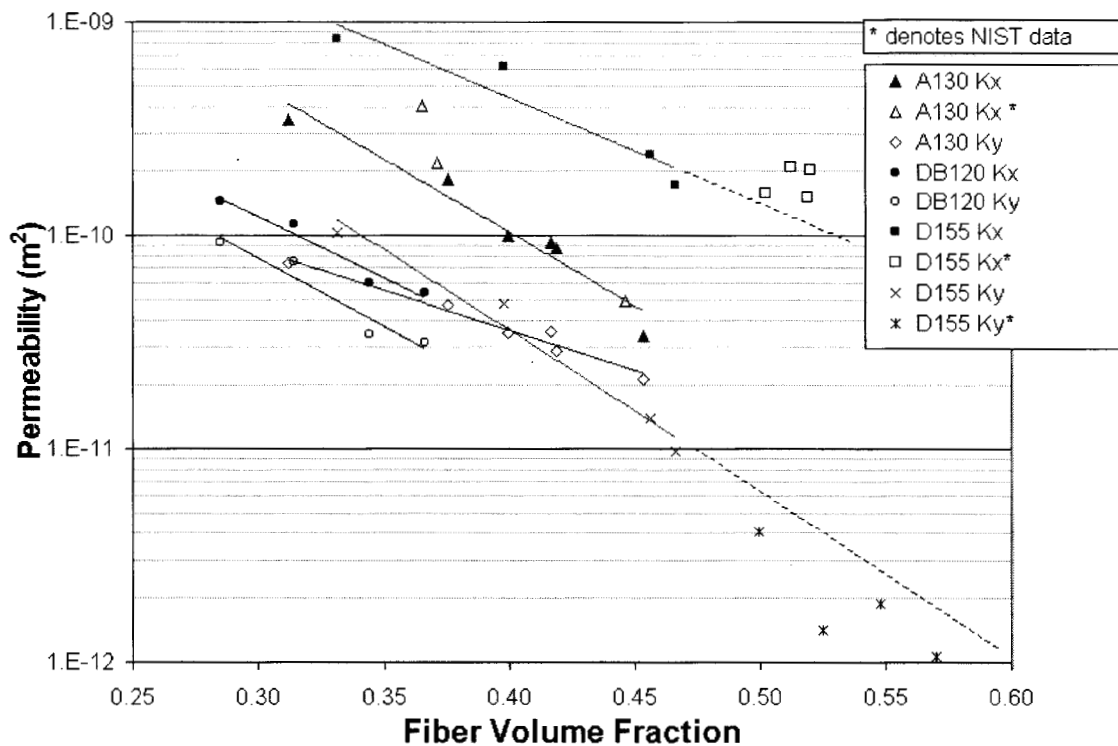
Figure 47. Summary of single fabric permeability data.

determined through saturated flow experiments were plotted. The unsaturated flow experiments gave higher permeabilities and may have been influenced by mold deflections. Trend lines do not include NIST database values.

The longitudinal permeability for the A130 fabric is approximately five times lower at a given fiber volume fraction than that of the D155 fabric. The decrease in permeability is due to the smaller channels between fiber bundles in the A130 fabric. Another factor that restricts flow through the A130 fabric is the glass bead as well as the thermoplastic used to hold the fiber tows together.

Since fibers are orientated at ±45° relative to the direction of flow, it is not surprising that the DB120 fabric had the lowest permeability in the longitudinal direction. However, one can see that below a fiber volume fraction of 0.37 the DB120 fabric has lower permeabilities than the transverse permeability of the D155 fabric. This may be due to the lack of compressibility observed in the DB120 fabrics. While both the D155 fabric and the DB120 fabric have the same volume of fibers, the D155's have their fibers concentrated into denser bundles. This can leave inter-laminar flow channels at low fiber volume fractions and increase the transverse permeability of the D155's.

Another point of interest is how the transverse permeabilities of the A130 and D155 fabrics varied over the range of fiber volume fractions. At low fiber volume fractions, the D155 fabric is more permeable than the A130 fabric, but as the fiber volume fraction increases, the permeability of the D155 fabric decreases at a faster rate than for the A130 fabric, eventually surpassing it at a fiber volume fraction of 0.40. Because of the D155 fabric architecture, fiber bundles nest tightly together blocking

transverse flow. The A130 fiber bundles, however, are woven over glass beads orientated in the transverse direction. These weave points create channels in the transverse direction, even at high fiber volume fractions.

The two unidirectional fabrics, D155 and A130, have large differences between their longitudinal and transverse permeabilities. D155's have the largest difference of approximately an order of magnitude. This is because the D155 fabric has a larger channel between fiber tows than the other fabrics. The A130 fabric is also different in that its longitudinal and transverse permeabilities seem to be converging as the fiber content increases. The A130's are a woven fabric, so the transverse glass bead creates a channel, raising the transverse permeability. As expected, the DB120 fabric has a relatively similar permeability in the two directions since they consist of plies in both the ±45° directions. The DB120's display slightly anisotropic permeabilities, which is most likely due to the stitching orientated in the longitudinal direction.

The NIST database contains permeabilities for a large variety of fabrics. NIST permeability values for the A130 and D155 fabrics are compared with experimental results from this study to verify that the data are consistent. The NIST database contains no values for the DB120 fabric, and had no transverse flow properties for the A130 fabric.

Three longitudinal permeability values are given for the A130 fabric in the NIST Database. They range in fiber volume fraction from 0.365 to 0.446. As one can see in Figure 47, two of the three NIST Database values agree well with the data from the present study, 0.446 and 0.371. The other point at 0.365 is approximately twice as high

as the results from the present study.

Four longitudinal permeability values are given for the D155 fabric in the NIST Database. They fell in the fiber volume fraction range of 0.501 to 0.520. If one extrapolates the curve fit from the present study to this range, the NIST data fall slightly above the extrapolated trend line, but in the general range predicted.

Finally, the NIST Database gave four transverse permeabilities for the D155 fabric. They fall in the fiber volume fraction range of 0.499 to 0.570. Extrapolation of the trend predicted from the data from the present study falls slightly above the NIST data.

Thus, the experimentally determined permeabilities seem to be consistent with saturated flow experiments measured independently by NIST. The individual fabric permeability values are now used to predict permeability values for lay-ups containing various fiber orientations as well as different combinations of fabrics.

Mixed Fabric

The objective of the mixed fabric experiments was to observe the results of lay-ups containing various fabric orientations as well as lay-ups containing multiple fabric types. The results were also used to develop a predictive capability for mixed fabrics.

Experimental Results

A total of ten lay-ups are compared in this section. Their permeabilities are summarized graphically in Figure 48. The naming convention of these lay-ups was consistent with the rest of the experiments. Lay-ups covered include Mx01 to Mx05.

Experiment	Fabric	Lay-up
MA01-1	A130	[0/90₂/0]s
MA01-2	A130	[0/90₂/0]s
MD01-1	D155	[0/90₂/0]s
MA02-1	A130	[(90/0)₂]s
MD02-1	D155	[(90/0)₂]s
MA03-1	A130	[0/90/0/90]s
MA03-2	A130	[0/90/0/90]s

Experiment	Fabric	Lay-up
MD03-1	D155	[0/90/0/90]s
MA04-1	A130-DB120	[0/±45₂/0]s
MD04-1	A130-DB120	[0/±45₂/90]s

Experiment	Fabric	Lay-up
MA05-1	D155-DB120	[0/±45₂/0]s
MD05-1	D155-DB120	[0/±45₂/90]s
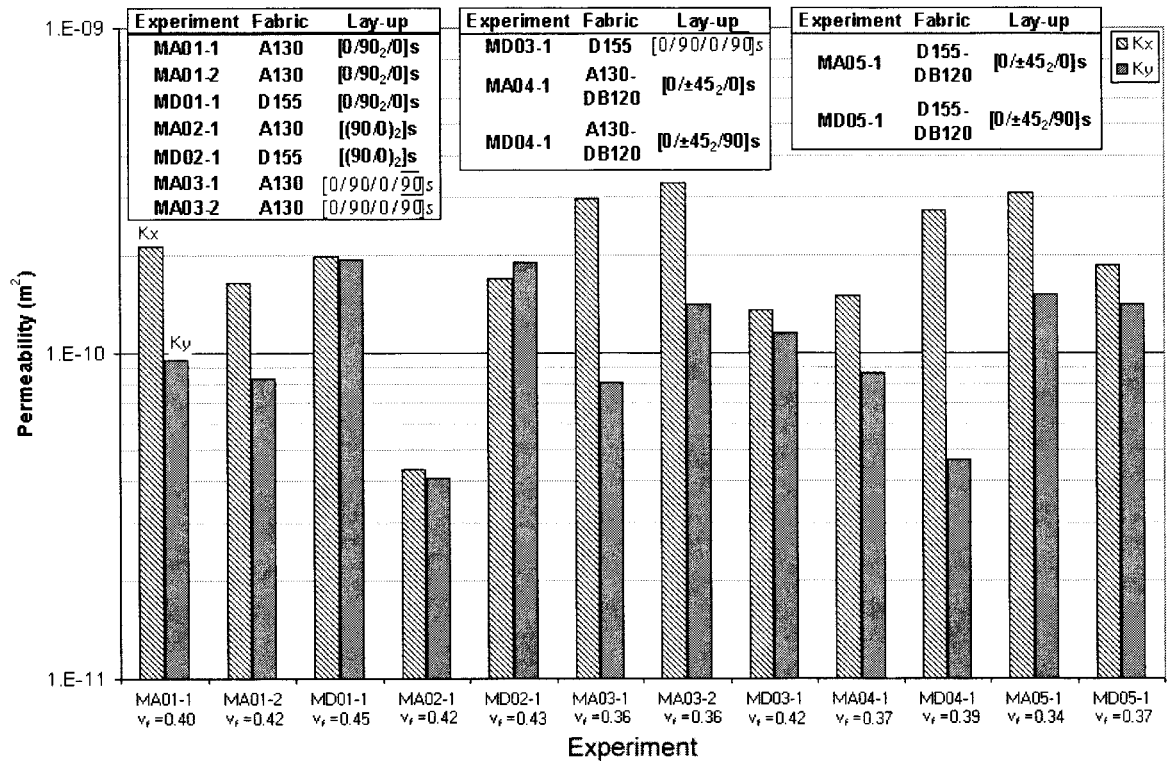
Figure 48. Transverse and longitudinal permeabilities for mixed fabric experiments.

The x designates that either A for A130's or D for D155's were the unidirectional material of the lay-up.

The first lay-up investigated was the Mx01 series lay up, [0/90₂/0]s. Since the lay-up contains four layers of fabric in both the 0° and 90° directions, one would expect the K_x and K_y values to have no significant difference; this is the case with the D155 fabric. The K_x value is 1.98×10^{-10} m^2 while the K_y value is 1.93×10^{-10} m^2. The A130 fabric, however, has a significant difference between its K_x and K_y values. A K_x to K_y ratio of 2.1:1 is observed. This experiment was repeated with the same result to ensure that the result was not due to experimental error.

The next lay-up investigated was the Mx02 series, [(90/0)₂]s. Once again, this lay-up contains an equal number of plies in the 0° and 90° directions. Both lay-ups with

the A130s and the D155s show almost no significant difference between their K_x and K_y permeabilities. One interesting point to note: there is a significant drop in the overall permeability from the MA01 lay-up to the MA02 lay-up. While fiber volume fraction can play a part in the loss of permeability, experiments MA01-2 and MA02-1 had nearly identical fiber volume fractions, 0.421 and 0.423, but their permeabilities differ by a factor of 3.8 for the K_x and 2.0 for the K_y. This effect, however, did not appear between the MD01 and MD02 lay-ups.

The Mx03 lay-up, $[0/90/0/\overline{90}]$s, is nearly identical to the Mx02 lay-up if it were rotated 90°. The only difference being that it does not repeat the 90° layer at the center of the lay-up. Since it has one less layer than the two previous lay-ups, it has a lower fiber volume fraction for the same thickness. Thus, it would be expected that the Mx03 lay-up would have a higher permeability. The data do show this for the A130 lay-up, but not for the D155 lay-up. Another observation of interest is that the A130 fabric has a rather large K_x to K_y ratio, while the D155 fabric K_x to K_y ratio is small in comparison. This would be expected to be the other way around, since the D155 fabric has much higher K_x to K_y ratios in the unidirectional permeability experiments. One last point to note: experiment MA03-1 was repeated because it did not contain enough measurements to give an accurate estimate of the permeabilities; results for the two experiments are similar.

The next lay-up examined was the Mx04 series, $[0/\pm45_2/0]$s. Either A130 or D155 fabrics were used for the 0° layers and the DB120 fabric was used for the ±45° layers. The addition of the DB120 fabric drops the fiber volume fraction of the lay-up

significantly, but at the same time has little influence on flow. This can be explained because the DB120 fabric has relatively low permeabilities even at low fiber volume fractions. A slight drop in permeability is observed between the MA03 and MA04 lay-ups even though both have the same relative fiber volume fraction.

Flow front shapes were quite different between the A130 fabric and the D155 fabric under this lay-up. The A130 lay-up has a much lower K_x to K_y ratio than the D155 lay-up. This is expected since the D155 fabric has a much higher permeability in the longitudinal direction than the A130s

The final mixed fabric lay-up studied was the Mx05 series, [0/±45/90]s. This lay-up is identical to the Mx04 series except that the 0° plies in the center of the lay-up are replaced with 90° plies. The addition of the 90° plies would be expected to lower the longitudinal permeability and raise the transverse permeability relative to the Mx04 lay-up. This is the case in the D155 lay-up, but the A130 lay-up shows a significantly different result. The MA05 lay-up shows an increase in both longitudinal and transverse permeabilities when compared with the MA04 lay-up. While the MA05-1 lay-up had a lower fiber volume fraction than MA04-1, it was not low enough to cause this large of a change.

Predictive Data used

Permeability data as a function of fiber volume fraction was necessary in order to predict permeabilities for mixed fabric lay-ups. These data were determined from an exponential fit to experimentally determined single fabric permeability data, Table 14.

Table 14. Correlations for permeability as a function of fiber volume.

Fabric	Relation	R^2
A130	$K_x = 5.85 \cdot 10^{-8} e^{-15.9 v_f}$	0.943
	$K_y = 1.13 \cdot 10^{-9} e^{-8.63 v_f}$	0.968
DB120	$K_x = 6.39 \cdot 10^{-9} e^{-13.2 v_f}$	0.953
	$K_y = 6.44 \cdot 10^{-9} e^{-14.7 v_f}$	0.923
D155	$K_x = 4.30 \cdot 10^{-8} e^{-11.4 v_f}$	0.910
	$K_y = 3.59 \cdot 10^{-8} e^{-17.3 v_f}$	0.970

The other set of information necessary for predicting permeability in mixed fabric lay-ups was layer thickness as a function of clamping pressure. These data were taken from a logarithmic curve fit to experimental fabric compression data, Table 15. Since clamping pressures were low, only fabric compression data in the range of 3 to 70 kPa was used to form the correlation. Initial stacking thickness was left out of the curve fit since it was for fabric under relatively little pressure.

Table 15. Ply thickness versus clamping pressure relationships.

Fabric	Relationships	R^2
A130	$ply\_thick = -3.23 \cdot 10^{-3} \ln(p) + 4.64 \cdot 10^{-2}$	0.983
DB120	$ply\_thick = -4.21 \cdot 10^{-3} \ln(p) + 5.52 \cdot 10^{-2}$	0.993
D155	$ply\_thick = -4.06 \cdot 10^{-3} \ln(p) + 5.66 \cdot 10^{-2}$	0.984

Predictive Results

Graphs comparing the predictions for the Mx01, Mx02 and Mx03 lay-ups to actual experimental permeability results are shown in Figure 49 and Figure 50. Only the volume fraction prediction method, Equation 23, is used in these experiments since results from the fabric stacking experiments were not accurate enough to be able to

determine thickness effects between plies orientated in a unidirectional manner and those with 0° /90° intersections.

Since all A130 or D155 fabrics were assumed to have the same ply thickness, a lay-up containing an equal number of plies in the 0° and 90° directions was predicted to have equal K_x and K_y values as long as it contained only one type of fabric.

This, however, was not the case with the MA01 lay-up. As one can see from Figure 49 it had a significantly anisotropic flow front. In order to insure that this result was not caused by an experimental error, the experiment was repeated with the same result. Permeabilities in both the longitudinal and transverse directions actually are higher than for a unidirectional lay-up orientated in either direction, Figure 49. This result is puzzling because a unidirectional lay-up composed of the same material and
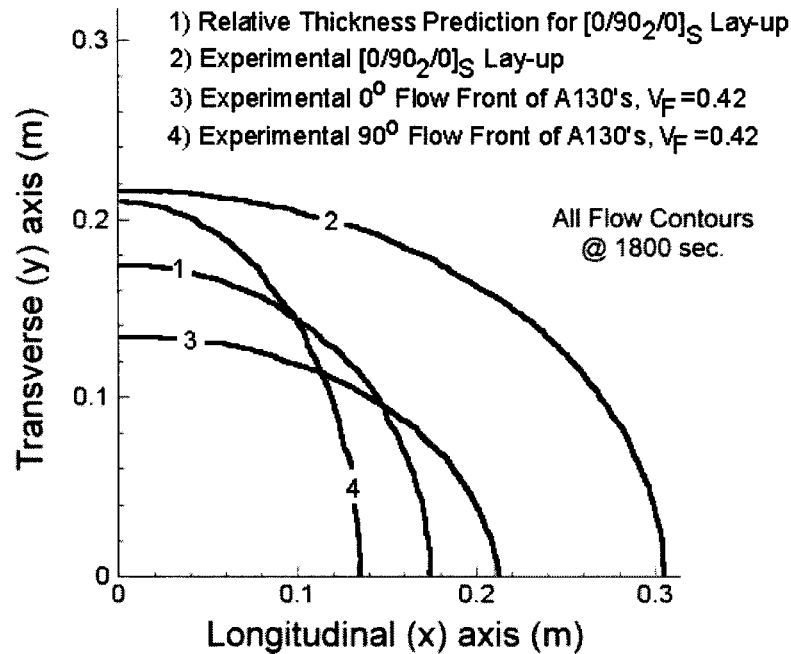
Figure 49. Plot of experimental and predicted flow fronts for test MA01-2 at 1800 sec. with an injection pressure of 86.2 kPa.

fiber volume fraction should have a higher permeability. The predictions of the

permeability for this lay-up not only fail to capture the general shape of the flow front,

they also under predict flow in the longitudinal direction by 43% and under predict flow

in the transverse direction by 17% after 1800 s.

Flow fronts were next plotted for the MD01 lay-up in Figure 50. Once again

relative thickness estimates used the information in Table 14 and Equation 23 to estimate

permeability for the relative thickness method.

The MD01 lay-up had an isotropic flow front as predicted. Once again flow was

under predicted. However flow in the D155 fabric stayed within the range predicted by
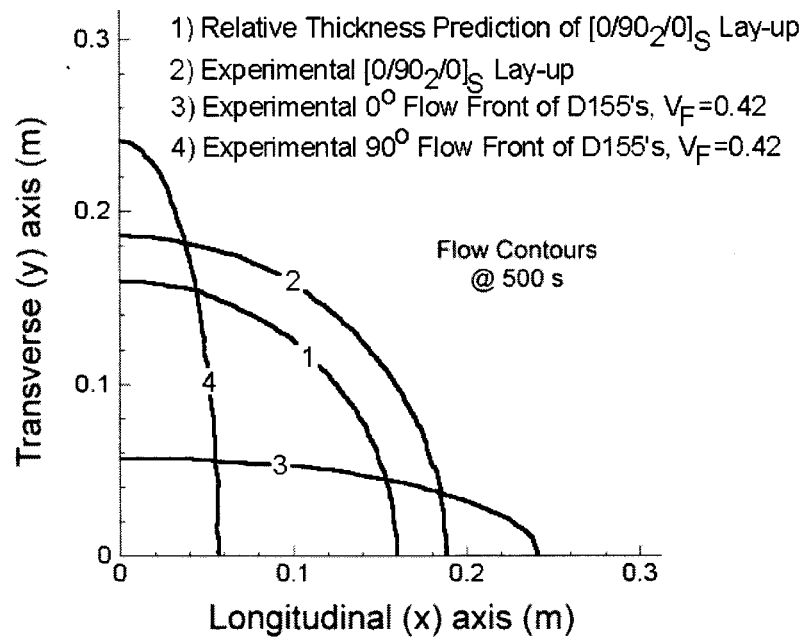
Figure 50. Plot of experimental and predicted flow front positions for test MD01-1 at 500 sec. with an injection pressure of 89.7 kPa.

105

the longitudinal and transverse permeabilities for a unidirectional lay-up at the same fiber volume fraction. While permeabilities were off by nearly 30%, flow front position in the transverse and longitudinal was under predicted by only 15%. A probable cause of the under prediction in flow is that flow permeates the fabric faster in the 0° layers, thus wetting out the 90° plies through the thickness of the fabric.

Both the MA02 and the MD02 lay-ups had isotropic flow fronts. The permeability of the MA02 lay-up dropped by a factor of 3.8 in the longitudinal direction compared to the MA01 lay-up. This lay-up was much closer to the predicted permeability, with permeability over predicted by 15%.

The experimental permeabilities of the MD02 lay-up dropped compared to MD01 even though they were predicted to increase, due to a decreased fiber volume fraction, Figure 51 and Figure 52. This decrease in permeability is most likely due to experimental variation, as the permeabilities of the MD02 experiment are only under predicted by 11%.

Since the Mx03 series of lay-ups had four layers in the 0° direction and only three in the 90° direction it was predicted that the permeability of these lay-ups would be higher in the longitudinal direction. Although this was the case, the magnitude of the difference between the longitudinal and the transverse permeabilities was not accurately predicted for all cases. The MA03 lay-up was under predicted by a factor of 2.5 in the longitudinal direction but only under predicted by 22% in the transverse direction. It is worth noting that the trend of significantly under predicting longitudinal permeabilities was also observed in the MA01 lay-ups. This, however, is not as readily dismissed in the

MA03 lay-up since this lay-up does not contain any adjacent layers with the same orientation.
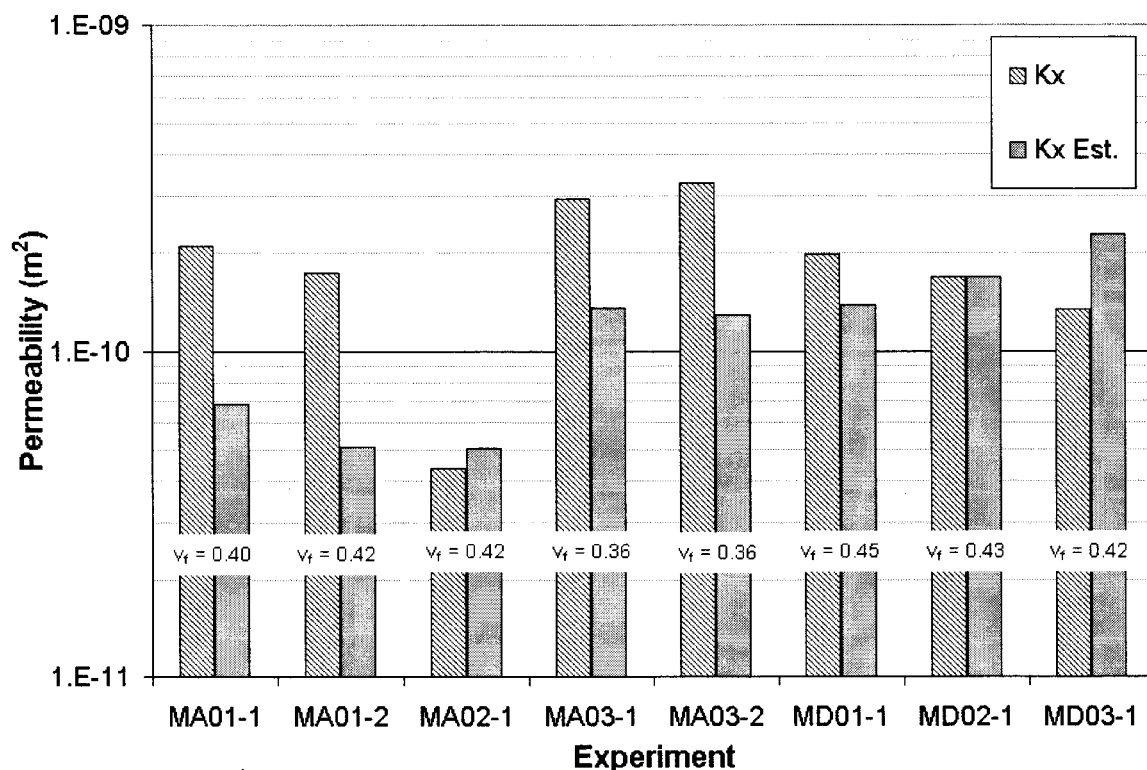
Figure 51. Summary of longitudinal permeability estimates versus experimentally determined permeabilities for the Mx01, Mx02 and Mx03 series lay-ups.

The predicted shape of the MD03 lay-up flow front was much closer to experimental observations than was the case with the MA03 lay-up. A K_x to K_y ratio of 1.28 was predicted, while a K_x to K_y ratio of 1.17 was observed. Longitudinal permeability values were over predicted by 55% while the transverse permeabilities were over predicted by 69%.
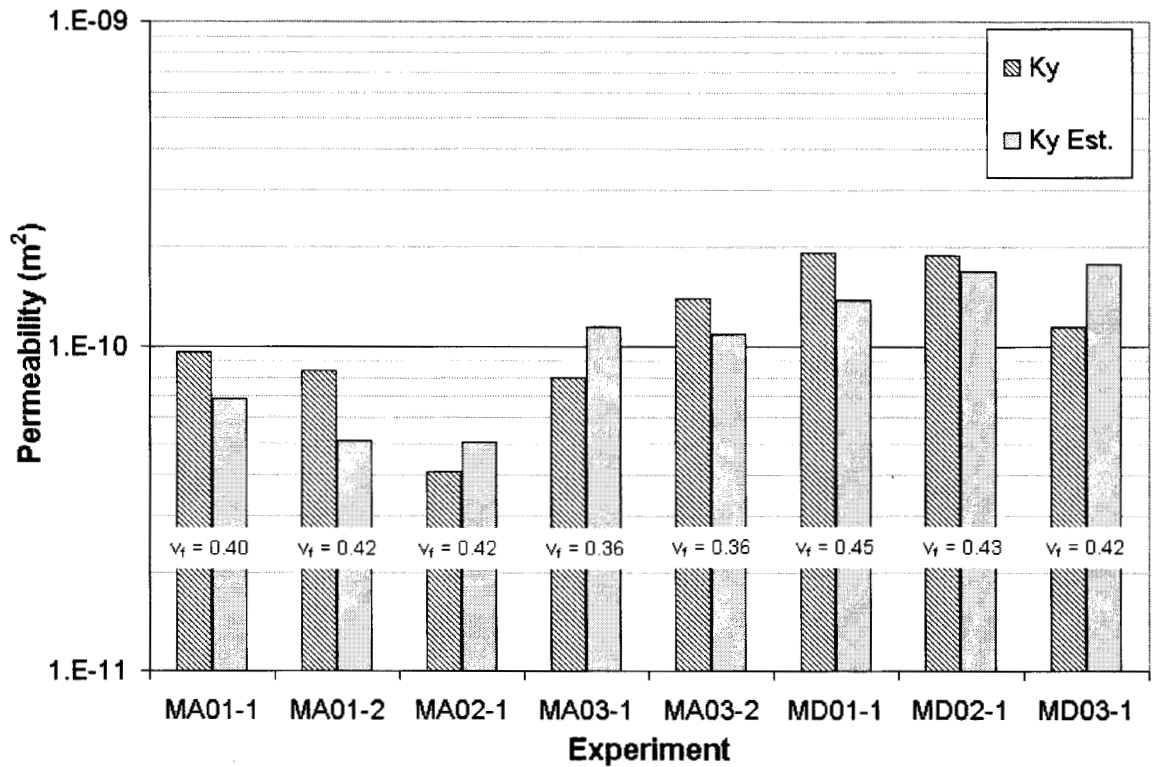
Figure 52. Summary of transverse permeability predictions versus experimentally determined permeabilities for the Mx01, Mx02 and Mx03 series lay-ups.

Graphs comparing both the relative thickness and the clamping pressure predictive methods of the Mx04 and Mx05 lay-ups to experimental results are shown in Figure 53 and Figure 54.

As mentioned earlier, the relative thickness method used the fiber volume fraction of the entire lay-up to predict permeabilities for each fabric layer. Then, the number of plies of a given fabric and its relative thickness are used to estimate its overall fraction of the lay-up.

The clamping pressure method, on the other hand, used a clamping pressure to determine the thickness and fiber volume fraction of each individual fabric present in the

lay-up. Table 16 compares input data for the Mx04 and Mx05 lay-ups.

The relative thickness method predicts the same fiber volume fraction for both the unidirectional layer and the DB120 layer, while the clamping pressure method predicts the DB120 fabric will have a lower local fiber volume fraction than the unidirectional fabric. Also, the clamping pressure method predicts that the DB120 fabric will take up a larger fraction of the composite than does the relative thickness method.

Table 16. Predicted lay-up composition and permeabilities for Mx04 and Mx05 lay-ups.

Lay-Up	Method	% DB120 by volume	v_f for 0° layer	v_f for DB120's	K_x (m²)	K_y (m²)
MA04	Rel. Thk.	44.6	0.340	0.340	1.11×10^{-10}	3.80×10^{-11}
	clamp	53.9	0.445	0.306	8.22×10^{-11}	4.91×10^{-11}
MD04	Rel. Thk.	44.6	0.394	0.394	3.00×10^{-10}	3.11×10^{-10}
	clamp	49.0	0.462	0.324	1.56×10^{-10}	3.28×10^{-11}
MA05	Rel. Thk.	40.2	0.366	0.366	1.14×10^{-10}	1.03×10^{-10}
	clamp	54.1	0.415	0.284	1.06×10^{-10}	7.88×10^{-11}
MD05	Rel. Thk.	40.2	0.367	0.367	2.33×10^{-10}	2.25×10^{-10}
	clamp	49.1	0.432	0.301	1.43×10^{-10}	1.22×10^{-10}

The clamping pressure method consistently predicts lower permeabilities in the longitudinal direction than the relative thickness method, see Figure 53. This is a direct result of the thicker DB120 layers predicted by this method and the higher local fiber volume fractions in the unidirectional material. As was demonstrated earlier, the DB120 fabric has a much lower permeability than the unidirectional material in the longitudinal direction even at much lower fiber volume fractions, see Figure 47. This effect is magnified in the MD04 and MD05 series since the permeability of the D155s is much higher in the longitudinal direction than for the A130s.

In general, predictions from the relative thickness method were closer to the experimentally observed K_x results than the predictions from the more complex clamping

pressure method. The clamping pressure method was able to predict a large relative

increase between the MA04 and MA05 lay-up while the relative thickness method was

not. In addition, the clamping pressure method consistently under predicts permeabilities

in the longitudinal direction while the relative thickness method underpredicts for the

A130 lay-ups and overpredictes the D155 lay-ups.
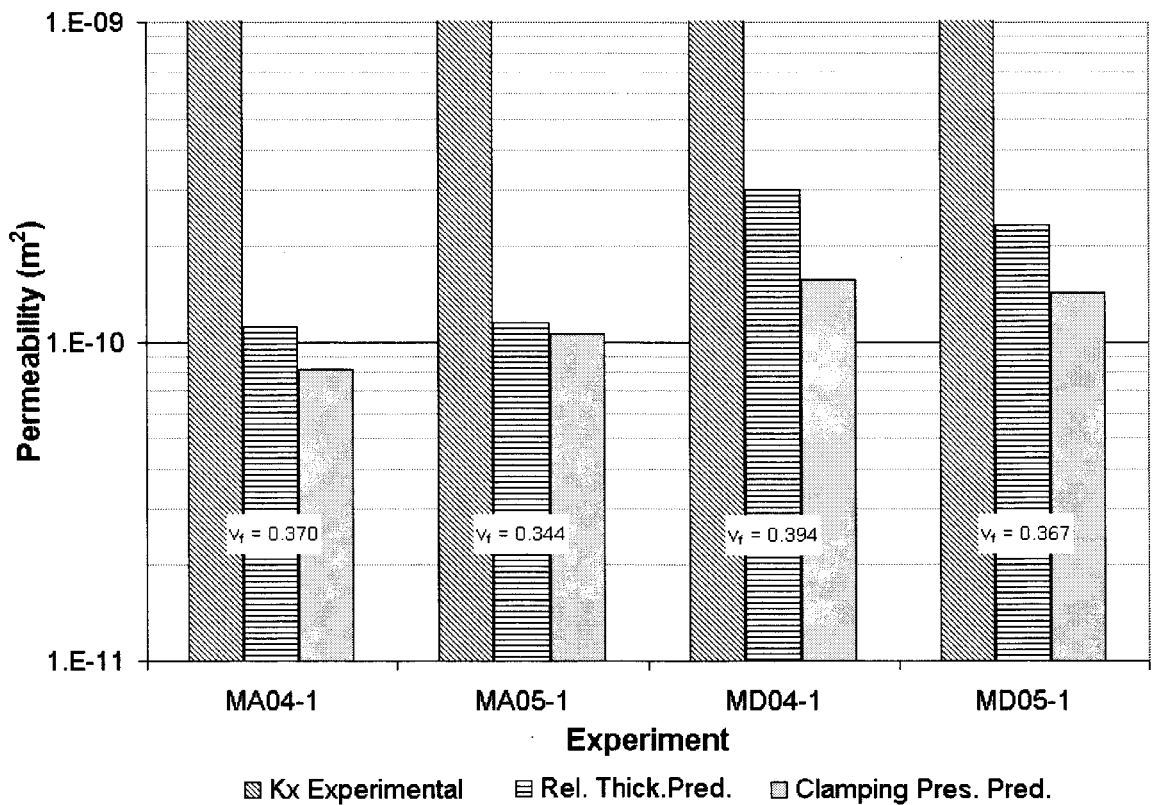
Figure 53. Predicted versus experimental K_x values for the Mx04 and Mx05 lay-ups.

It is shown in Figure 54 that the clamping pressure method estimates the effect of

the addition of 90° plies to the lay-up more accurately than does the relative thickness

method. The relative thickness method greatly exaggerates this effect in both the A130

and D155 lay-ups, while the clamping pressure method follows the experimental data

more closely. Once again, the clamping pressure method consistently under estimates the

permeabilities in the y direction while the relative thickness method under predicts for all but the MD05 experiment. Also, the clamping pressure method predicts permeabilities closer to the experimentally observed K_y values for all the experiments except MA04.
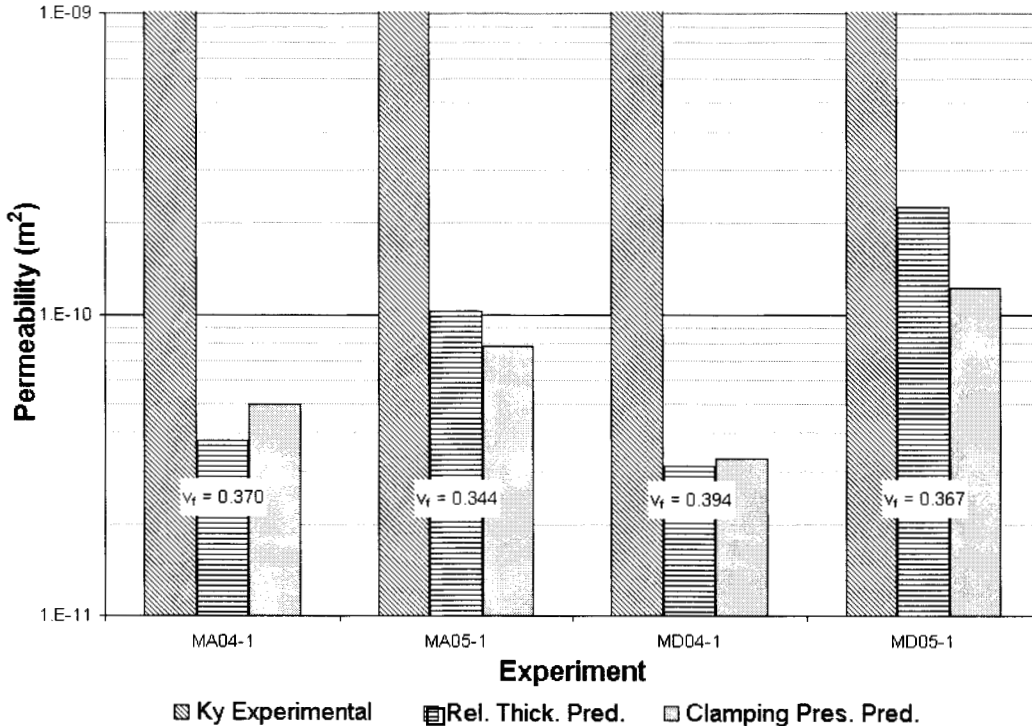
Figure 54. Predicted versus experimental K_y values for the Mx04 and Mx05 lay-ups.

Table 17 indicates that the clamping pressure method flow front predictions were closer to experimental than those predicted by the relative thickness method for all experiments. Both methods failed to capture the flow front change between the MA04 and MA05 experiments. Because the clamping pressure method under predicts flow fronts in the longitudinal direction, its flow front ratios, while close, were consistently lower than the experimental ratios. The relative thickness method over predicts the flow contribution in the longitudinal direction for the Mx04 experiments, and under predicts

its contribution in the Mx05 experiments. This trend was most obvious with the D155 lay-ups. Overall, the clamping pressure method did a better job of capturing flow effects in mixed fabric lay-ups.

Table 17. Comparison of predicted to experimental flow front shapes.

Experiment	Experimental K_x/K_y	Clamping Pressure K_x/K_y	Relative Thickness K_x/K_y
MA04-1	1.72	1.67	2.93
MA05-1	2.03	1.34	1.11
MD04-1	5.85	4.74	9.67
MD05-1	1.32	1.17	1.04

Summary

Although both the A130s and D155s are unidirectional fabrics, they did not always follow the same trends. One would expect the Mx01 series lay-up to have equal permeabilities in both principal directions. However, the flow front for the MA01 lay-up with A130 fabric was highly orientated in the longitudinal direction. It was not uncommon for lay-ups containing two consecutive layers of 90° plies to have much higher permeabilities in the longitudinal direction than expected, examples are MA01 and MA05.

Two predictive methods were used to estimate the permeability of a mixed fabric lay-up. The first method was the relative thickness method. In order to determine the composition of a lay-up containing two separate fabrics, the relative thickness data for each fabric was used to estimate their fraction of the lay-up. Then, the fiber volume fraction of the entire lay-up used for each ply, whether they were different fabrics or not. The clamping pressure method used clamping pressure data to estimate the thickness

contribution of each fabric as well as its fiber volume fraction. That way each fabric may be at a different fiber volume fraction. Once again, the layer permeabilities are combined into a single permeability using Equation 23.

The methods were able to predict the general trends for most lay-ups. Both methods were not able to accurately predict flow in lay-ups containing A130's orientated at 90°. Generally, flow was greatly under predicted in these lay-ups. In addition, permeabilities predicted by the clamping pressure method represented what was observed experimentally, both in shape and magnitude, and were closer than the relative thickness method.

T-Section

The foregoing findings were next applied to the T-section geometry, Figure 21 and 55, which has three-dimensional flow characteristics. This mold contained two intersecting flow planes as well as three regions of differing thickness. Experiments were performed with both central and end injection points: TA01 and TD01 were central injections and TA02 was an end injection. The lay-ups orientation and fiber contents for each section are given in Table 9.

TA01

A plot showing flow contours for the TA01 experiment is given in Figure 56. Contours are separated into the web and skin planes because information would have been lost in a three-dimensional plot. The skin surface of the mold was aligned perpendicular to the ground, and the web plane was parallel to the ground. Injection took

place from two symmetrically spaced injection ports. The ports were located halfway along the length and injected through the flange area of the mold, Figure 56. Also, the lay-up was selected to keep similar fiber volume fractions in all three sections of the mold: skin, flange and web.

At the injection ports in the flange region, the part was approximately 1.30 cm thick, while farther on the skin stepped down to 0.284 cm thick. Resin first penetrates the skin at this step area at the 46-second mark—approximately 4.6 cm from the skin-web intersection. As one can see, it took a considerable amount of time before the resin penetrated through the fabric comprising the flange and skin. In addition it took a considerable amount of time, 6 minutes, before the flange was fully wet-out near the injection ports. Resin did not penetrate the skin surface symmetrically. The resin penetrated the bottom half of the skin nearly 2 minutes before it started penetrating through the top half of the skin. Wet-out in the skin surface of the mold was achieved by the bottom half of the mold filling. At this time, the preferential flow along the edges of the mold was the primary source of flow. This eventually created an air pocket on the top half of the skin section. Injection was halted after fifteen minutes and this region failed to completely wet out.

Flow proceeded at a much more rapid rate in the web section. Even though the photographs at the web did not turn out, resin had penetrated beyond the region blocked by the mold at the time the first images were recorded, 1 min 24 s. Since resin was able to stay in the plane of the fibers in the web section, the majority of the resin went there instead of flowing through the plane of the fabric into the skin/flange section. Once

again, preferential flow occurred along of the boundary of the mold, trapping an air pocket in the web section.

Around the three-minute mark, resin had penetrated the entire length of the web section. A factor that greatly increased the permeability in the x-direction of the mold was a region of low fiber volume fraction caused by the fabric architecture at the skin-web interface as shown in Figure 55. A cross-section of an actual composite part showing this void area can be see in Figure 13.
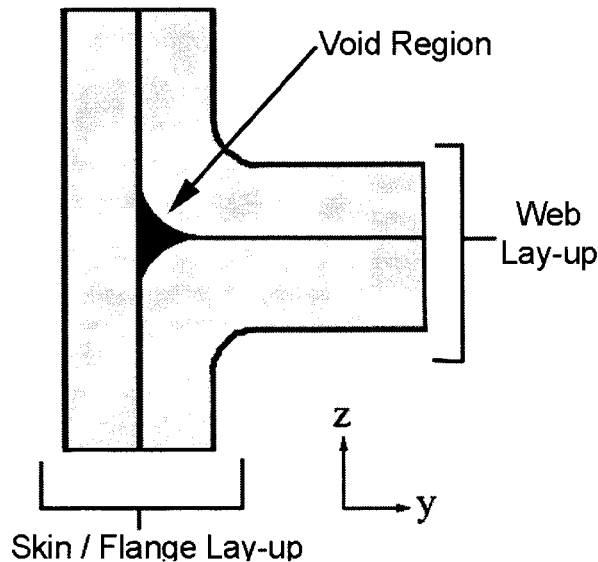
Figure 55. Source of high permeability in T-sections.

Unfortunately, it was difficult to eliminate preferential flow (race tracking) problems in the thick flanged T-mold. Even if one was careful cutting and placing fabric, the shape of the mold along the z borders of the skin plane make it impossible to prevent preferential flow in that direction. Preferential flow also occurred in the region where the flange stepped into the skin, as a result of the void region created by the lay-up geometry. In addition, the low out-of-plane permeability of the A130's created preferential flow

between layers. Flow in the flange region progressed through the bottom layers first before it penetrated the entire thickness. An example of flow patterns caused by preferential flow between layers can be seen in Figure 56.
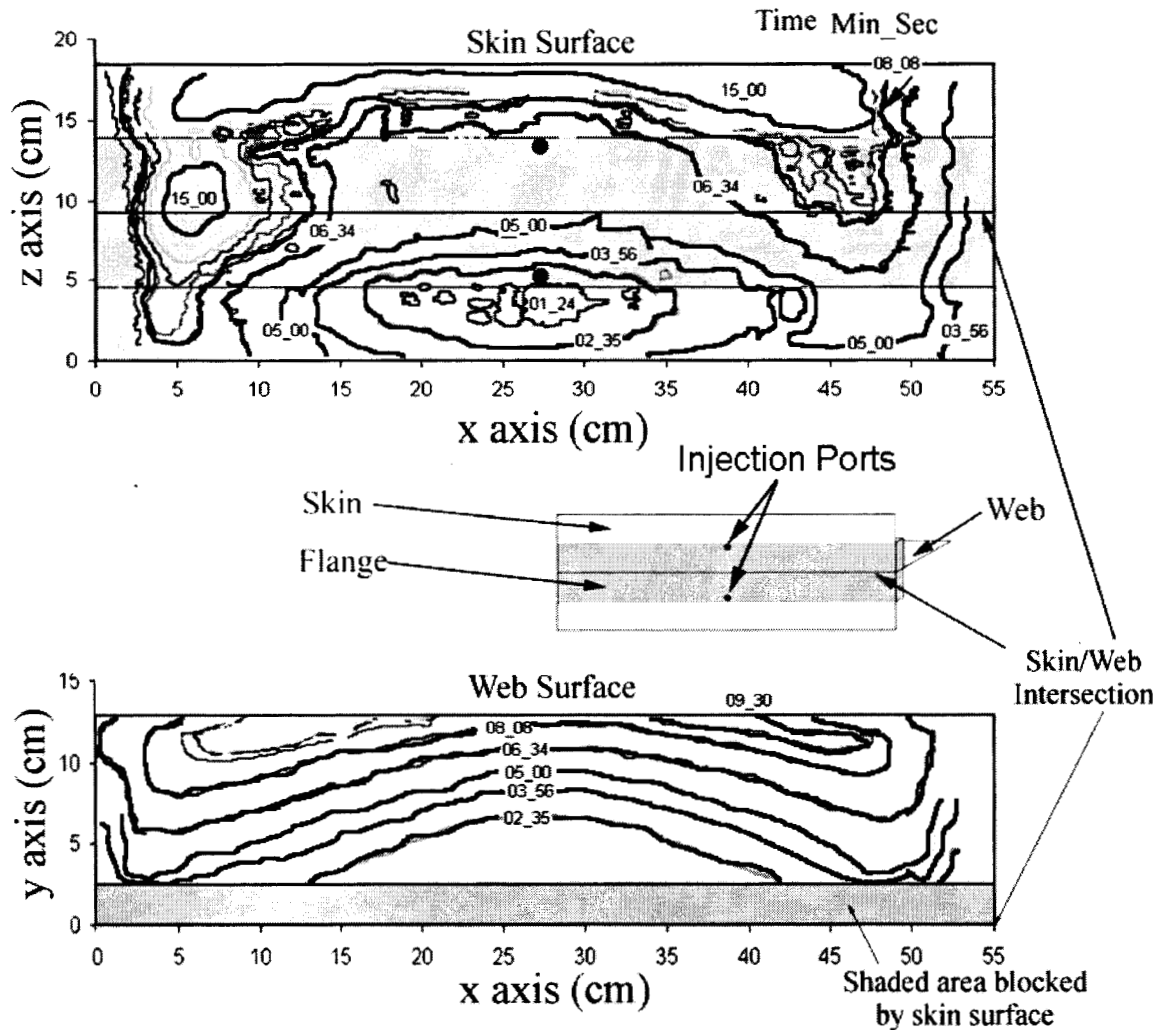
Figure 56. Flow front positions for TA01. Injection was from two central injection ports (shown as black dots) at a pressure of 82.7 kPa.

TD01

A plot containing flow contours for TD01 is shown in Figure 57. The mold and setup procedures were identical to those used for the TA01 experiment. In addition to

using D155s instead of A130s, the lay-up of the TD01 differed from the two A130 T-section lay-ups. The A130 lay-ups were chosen to give similar fiber volume fractions in the skin, flange and web sections of the mold. This experiment, however, had significantly different permeabilities in each section.

Unlike the A130 lay-up, the D155 fabric allowed the resin to penetrate the skin surface easily. In addition, flow patterns from both injection ports were relatively symmetrical, the flow front from the upper port advancing slightly faster. Flow advanced faster on the left side of the mold. It nearly completed filling around the 11 minute mark, while a substantial air pocket still existed along the right side of the mold after 15 minutes. It can be seen from the flow fronts that the permeability of the skin region on the skin surface was lower than the permeability in the flange region. This was a result of the skin region having a much higher fiber volume fraction than the flange region.

Flow was not visible in the T-section until three minutes and 45 seconds into injection. Resin penetrated the y direction slowly since it was flowing normal to the D155 fibers . Flow progressed across the right side of the web faster than it moved through the left side, opposite of the skin surface. Flow had completely filled the right hand side of the web at the 12 minute 14 second mark.

Race tracking occurred in the both the skin and the web sections of the mold, but race tracking was not nearly as pronounced as with the A130 fabric. In addition, the high permeability through the plane of the D155's allowed the resin to evenly penetrate the flange section of the mold, unlike with the A130's. This gave flow fronts with smooth surfaces and no resin pockets ahead of the main flow front. Flow into the web section

117

was hindered by the low permeability normal to the D155 fibers. This is evident by the

flat flow fronts in that section, and is contrasted by the A130 lay-up.
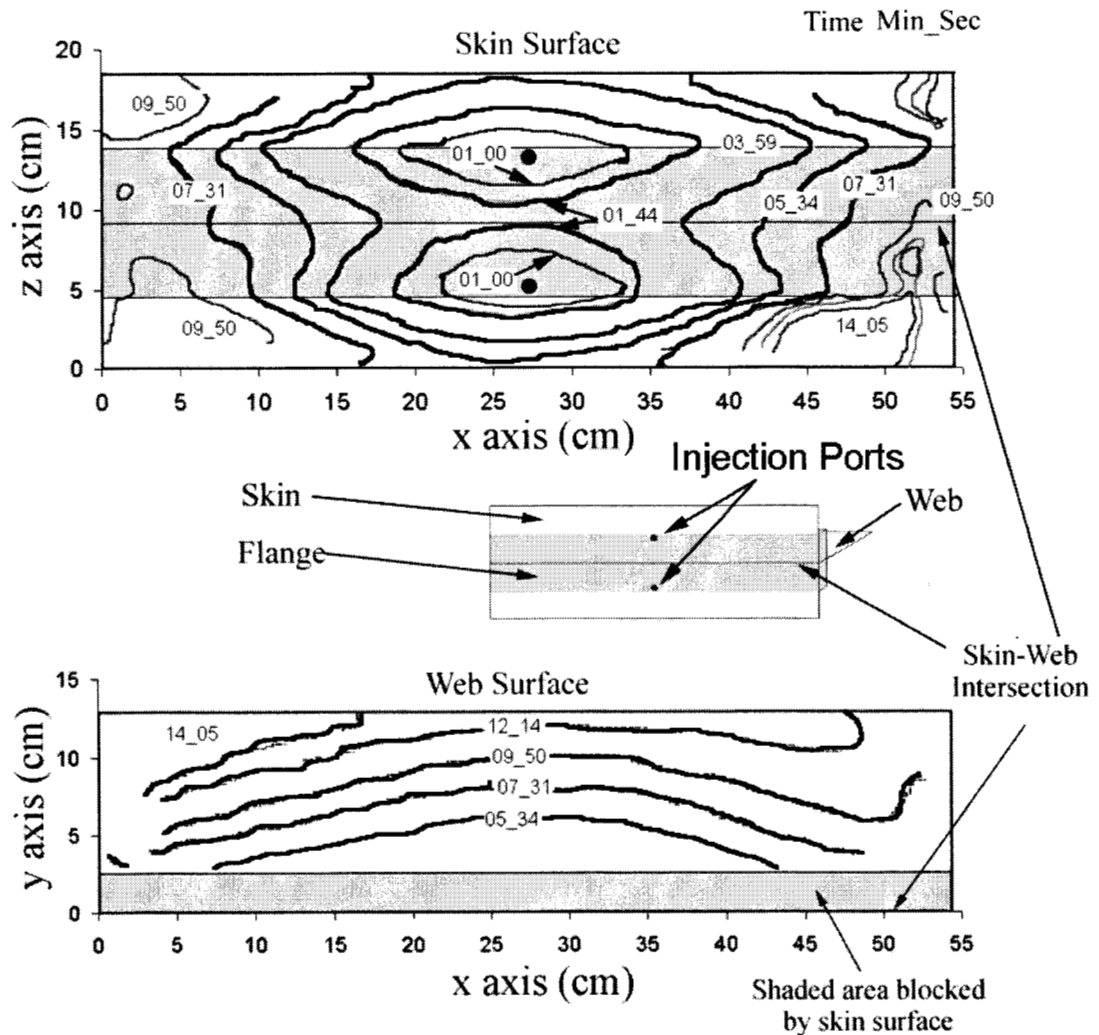
Figure 57. Flow front positions TD01. Injection was from two central injection ports
(shown as black dots) at a pressure of 82.7 kPa.

TA02

A plot containing flow contours for TA02 is shown in Figure 58. The mold and

setup procedures were identical to those used for the TA01 experiments. The only

difference being that injection took place at the end of the mold instead of at the center.

Although the injection ports were located at the flange, resin quickly spread across the skin surface in the z direction as well as through the thickness of the flange due to race tracking. As one can see, flow along the skin surface started out symmetrical. Then, after three minutes, edge effects as well as the seemingly lower permeability of the flange region gradually influenced flow. Resin reached the far end of the skin section around 11 minutes, but as in the previous experiment, this was simply a result of preferential flow along the edges of the mold. Flow then trapped an air pocket in the skin section around the 16-minute mark. The skin surface finally finished wetting out 25 minutes 17 seconds into the experiment.

The main mechanism of flow in the web section was flow along the web/skin intersection. This problem was exacerbated by the fact that skin and web mold faces were not exactly aligned, so the actual thickness of the part was 0.5 mm greater in this region. At the time the resin reached the end of the mold in the web section, it had traveled nearly 55 cm, while at the same time resin had only advanced 25 cm in the skin section. After the resin reached the end the mold, it traveled to the skin layer as well as down into the web section. Judging by the flow fronts, preferential flow was once again a factor along both x boundaries as well as the y boundary of the web. Air was also trapped in the web section, and the web finished wetting out after 29 minutes.

In addition to race tracking complications, inter-laminar preferential flow was present in the skin section. Although it was not as pronounced as in the TA01 experiment, pockets of resin were observed ahead of the flow front between times of 7 to 10 minutes.
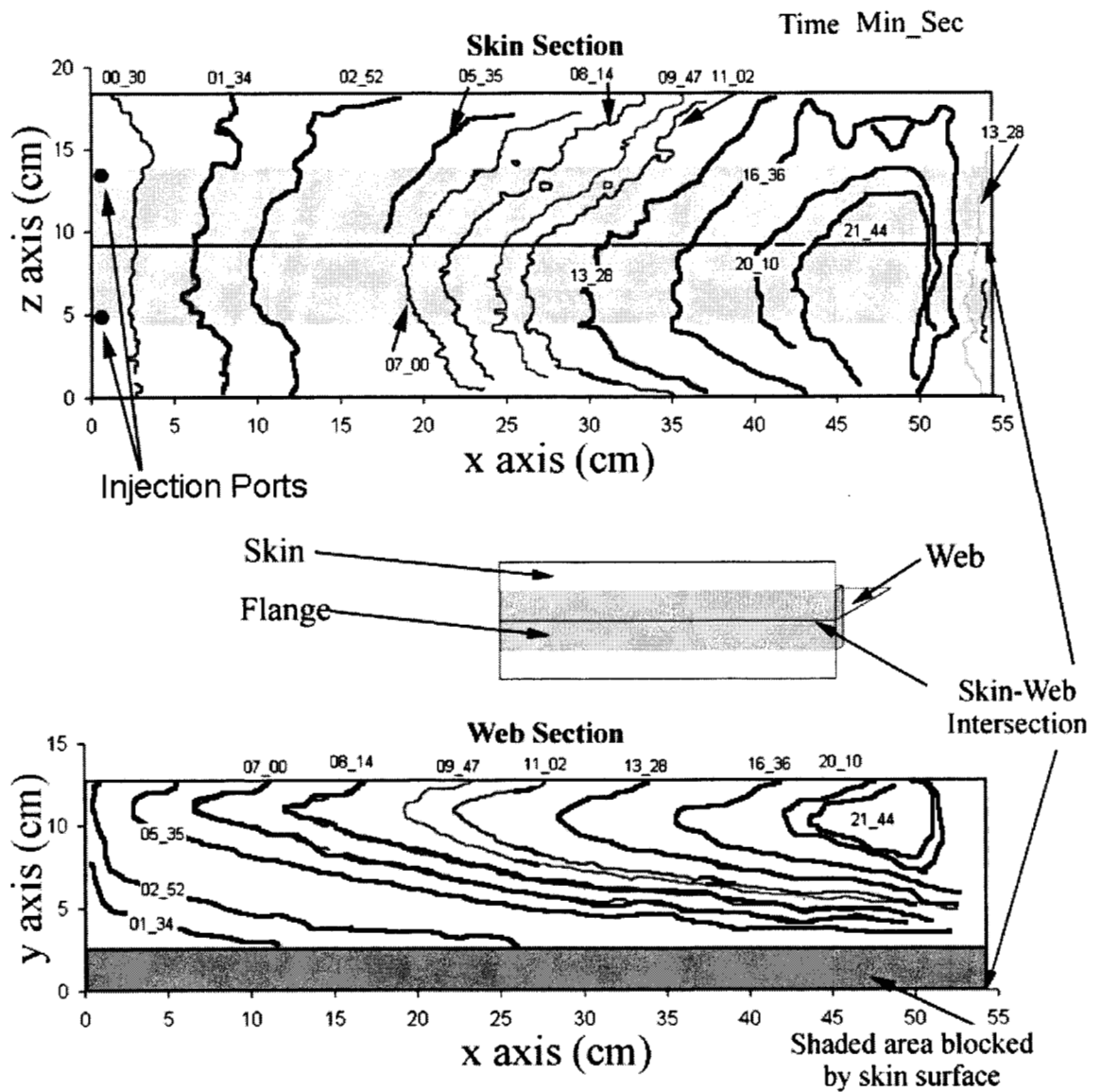
Figure 58. Flow front positions for TA02. Injection was from two injection ports located at the end of the mold. Injection pressure was at 82.7 kPa.

Steel Root Insert Mold

Since the steel insert mold was opaque, a partial injection was required to get an idea of the filling patterns inside the mold. The mold was filled for 160 seconds and then

the resin was allowed to cure. After the part cured it was removed and the flow fronts were analyzed. As one can see from Figure 59, filling patterns differed on the skin and inner surface sides of the mold. This was a result of the injection port being located under the steel insert on the skin side of the mold.

Flow first progressed across the skin side of the mold. The flow seemed slightly biased along the length of the mold. As one can see there was a bit of race tracking on the top half of the skin. Additional fabric was placed in this region to build up the fiber volume fraction, but it may have been displaced when the mold was put together.

Flow may have reached the inner-surface face of the mold by either of two mechanisms. Either flow progressed through the lay-up and around the steel insert, or it reached the boundary of the mold on the skin surface and penetrated to the surface. Judging by the lengths of the two flow fronts on the inner-surface mold, it is expected that the flow reached the boundary before flow had completely penetrated into the inner surface side of the mold. This, however, was due to race tracking, and judging by the results it appears that normally flow would penetrate the inner-surface face of the laminate before flow reached the boundary on the skin face.

During the complete filling of the mold, flow reached the vent port on the insert side of the mold approximately 238 seconds after injection. The mold was completely filled at 741 seconds.
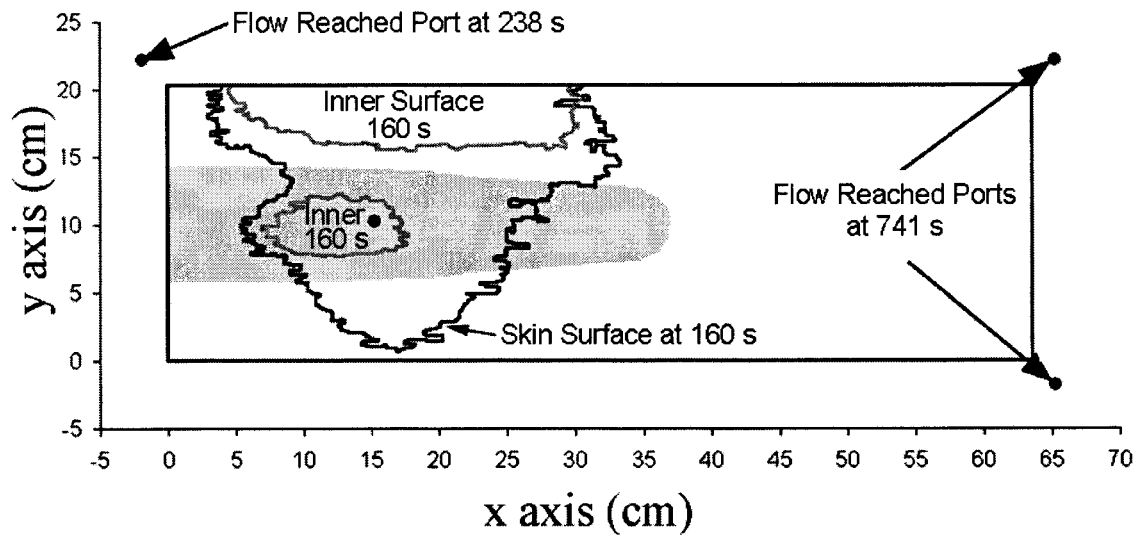
Figure 59. Filling pattern of insert mold with an injection pressure of 96.5 kPa.

CHAPTER 5

NUMERICAL RESULTS AND CORRELATION WITH EXPERIMENTS

LIMS basics

Liquid Injection Modeling Simulation 4.0 (LIMS) is a finite element based program that is specialized for modeling fluid flow in RTM molds. LIMS only accepts a mesh composed of 4 node quadrilateral elements. LIMS uses Darcy's law combined with a boundary element method to advance flow, and conservation of mass issues are addressed by assigning a fill factor to the nodes.

In order to analyze flow for a given mold one must follow these steps: create and mesh the model; define permeabilities throughout the mold on an element by element basis; set the port type, initial value and nodal location; and record or display the desired information.

Model Creation

One feature that sets LIMS apart from other RTM modeling software packages is its ability to read models created from third party software. LIMS will read finite element models created in PATRAN and exported as neutral files. A limitation of LIMS is that it requires linear quadrilateral elements. These shell elements allow one to model three-dimensional shapes, but do not account for flow through the thickness of a laminate. LIMS requires that all duplicate nodes at intersections must be removed, and

the model must be renumbered so the list of nodes and elements is continuous. In addition, one must keep track of element normals to insure proper translation of the model.

One parameter of interest is the sensitivity of the results to the density of the mesh. To determine this, test runs were done at several mesh densities. A common way to do this is to vary the mesh size and solve the model. As the mesh size is decreased, the solutions should converge. The only parameters varied in this set of tests were the element size and the injection pressure (flow rate). A matrix of numerical sensitivity tests performed is shown in Table 18. Tests were done simulating a center injection on the flat plate mold. Flow distances were then recorded along the x and y axes with the injection port being located at the origin. In addition, two pressures were used to see if the accuracy of the model depends on the velocity of the flow front.

Although boundary conditions may not be specified into LIMS, it is possible to exploit symmetry since flow along a plane of symmetry and flow along a solid boundary are treated the same. This was verified by comparing two models with the same element

Table 18. Matrix of mesh sensitivity runs on a 510 mm by 810 mm plate model with quarter symmetry and the injection port located at the origin.

Trial	element length (mm)	Injection Press. (kPa)	x direction times (s)	y direction times (s)
1	50.8	89.7	150, 450, 900	150, 450
2	25.4	89.7	150, 450, 900	150, 450
3	12.7	89.7	150, 450, 900	150, 450
4	6.35	89.7	150, 450, 900	150, 450
5	50.8	160	150, 450	150, 450
6	25.4	160	150, 450	150, 450
7	12.7	160	150, 450	150, 450
8	6.35	160	150, 450	150, 450

edge length, one with quarter symmetry and one without. Therefore, in the mesh sensitivity runs, the model employed quarter symmetry on the flat plate mold in order to minimize the number of elements required and solution time.

As one can see from the results, Table 19, at lower mesh densities flow seems to be faster. If one had a poorly meshed model errors could become quite large. In addition, as time progressed the difference between the dense and fine mesh increased slightly. As one can see from trials 1 to 4, flow values in the y direction were much closer at the different mesh densities than in the x direction. It was of interest to see if the rate of flow made a difference in the accuracy of the results, so the pressure of the experiment was increased. As one can see from trials 5 to 8 there was less of a difference between the fine and coarse meshes as the flow rate increased.

Table 19. Mesh sensitivity flow results.

trial	x flow distance (cm)			y flow distance (cm)	
	@ 150 s	@450 s	@900 s	@150 s	@450 s
1	16.33	25.98	35.06	10.85	17.39
2	14.66	23.75	32.38	9.97	16.28
3	13.5	22.11	30.24	9.28	15.32
4	12.59	20.71	28.41	8.73	14.42
5	20.89	33.27	na	13.84	24.2
6	18.87	30.78	na	12.91	21.19
7	17.51	28.71	na	12.07	19.92
8	16.37	26.97	na	11.37	18.78

Judging from the convergence runs, the error of a model tended to be on the order of the element size. Early in the experiment, 150 seconds, the error was approximately half the size of an element, and towards the end, at 900 seconds, it was slightly larger than the size of an element.

Once meshed, a LIMS model must be formatted. In addition to creating a list of node locations and element connectivities, LIMS gathers the model parameters given in Table 20 from user input.

Table 20. LIMS input parameters

K_{11}	v_f
K_{22}	resin viscosity
K_{12}	element thickness
I_{AX}	port information

K_{11} is the permeability of the fabric in the longitudinal direction, K_{22} the permeability in the transverse direction and K_{12} the flow coupling term in the permeability tensor. In addition, the fiber volume fraction (v_f) as well as resin viscosity were needed. The I_{AX} term defines the longitudinal direction of an element in the global x-y-z coordinates of the mold. The designation 1 would mean the longitudinal direction is the x direction, a 2 would mean it was in the y direction and a 3 would make the longitudinal direction the z direction. If one selects a value for I_{AX} that is perpendicular to the element, an error results. Next, LIMS requires an element thickness; element thickness does not seem to have an effect on the flow, as shown by trials done with models having two different element thicknesses. Finally, injection and vent port information may be added at this time. LIMS supports three types of injection ports: constant pressure, constant flow rate and mixed gates. Mixed gates generally are a constant flow rate gate that can not exceed a maximum pressure, so once that maximum pressure is reached it becomes a constant pressure gate.

Recording information

Another feature of LIMS is its flexibility in recording data. It contains a set of commands called lBasic that allow the user to manipulate the injection and record results. LBasic allows the user to control ports during the course of an injection as well as record information at any node in the model. Parameters that may be monitored include: time, fill factor, pressure, number of empty or filled nodes during last time step and fill time for a particular node. If one wishes to learn more about the features available they should refer to the LIMS users manual, Reference 36. Once the model has been solved LIMS may also format the results for plotting. Available FEA post processing formats include Tecplot and PATRAN.

Flat Plate models

The first step in modeling parts was to verify the accuracy of the model on a simple flat plate structure. The model was used to determine the experimental errors associated with calculating permeabilities. Then A130 and D155 lay-ups were investigated to see if LIMS could accurately predict flow front shapes of the more extreme experimental results. Next, permeability predictions for lay-ups combining unidirectional fabric with the DB120 fabric were examined. Finally, lay-ups that were not well predicted by the permeability estimation schemes were analyzed.

Two different models were used to represent the flat plate. The first had an element edge length of 12.7 mm and modeled the entire plate. The other model used quarter symmetry and an element edge length of 6.35 mm. All models represented the mold with an injection port at the center. In addition, the injection was placed at the

127

origin for all flat plate runs.

Experimental Error

There were several sources of error when determining and locating the flow front positions. There was a ±3.45 kPa pressure difference, generally ±3.8%, during the experiment. Errors measuring fiber volume fraction and part thickness contributed to incorrect input into the model. Also, the process of digitizing the flow fronts added some error to flow front measurements.

Of the above mentioned sources of error, pressure fluctuation during the course of an experiment was the most significant. It could result in a maximum flow front position error of one cm after 1200 seconds of injection time. A similar magnitude of error could be realized if the fiber volume fraction was off by more than 0.03; typical experimental errors are in the ±0.01 range. The inaccuracy associated with measuring part thickness and errors from digitizing flow fronts only contributed errors on the order of 1mm or less.

A130 0_8 Lay-up (SA08-1)

All the single fabric experiments should have been modeled exactly since the permeability is reduced from the experiment it is modeling. This particular lay-up, however, had an asymmetrical flow front. Most lay-ups had higher permeability in the longitudinal direction than in the transverse direction, but this lay-up had slightly different permeabilities in all four directions. This phenomenon happened in a few of the experiments, but was the most severe with this lay-up.

As one can see from the diagram in Figure 60, experimental flow in the

longitudinal direction initially started out faster on the left-hand side of the mold. At 150

seconds flow on the right side of the mold exceeded flow on the left and that trend

continued for the remainder of the experiment. By 1620 seconds there was

approximately a 4 cm difference in flow between the two longitudinal flow fronts. LIMS

seemed to slightly under predict flow in the longitudinal direction throughout the course

of the experiment and the difference was at a maximum of 8% at 1620 seconds.
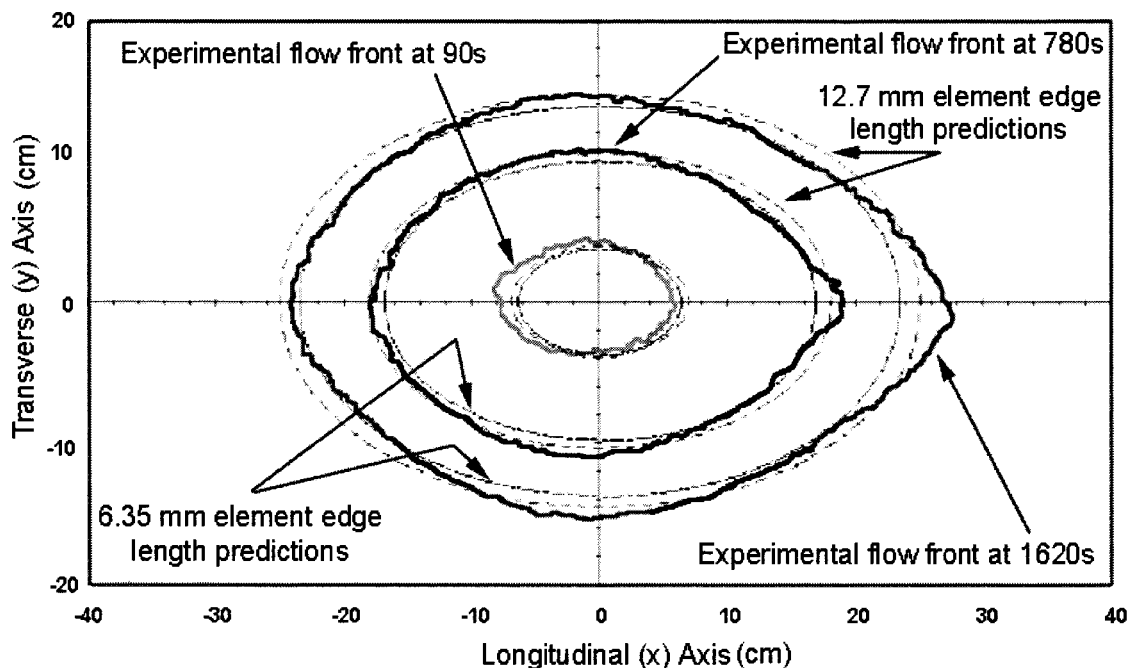
Figure 60. Experimental versus predicted flow front positions for SA08-1, single fabric
A130. K_x=9.90x10^{-11} K_y=3.47x10^{-11}, v_f=0.400, μ=0.195 kg/m·s and P=89.7 kPa.

Flow in the transverse direction was much more symmetric than in the

longitudinal direction, and the model predicted flow results much closer than those in the

longitudinal direction. Once again, however, the model under predicted flow, with flow

being under predicted by a maximum of 11% at 1620 seconds.

The model predicted a smooth, rounded flow front. As one can see, the flow front

129

shapes predicted by the model were quite close to those observed experimentally. The left-hand side of the plate was modeled within experimental error. However, flow on the right-hand side of the mold came to a point and was approximately 4 cm ahead of the model prediction at the end of the experiment (1620 s). The shape of the model along the transverse flow front closely matched the experimental shapes on both sides. Since the model assumed symmetry, differences from symmetrical flow fronts could not be predicted, nor could they have been if the whole plate were modeled.

D155 0_6 Lay-up (SD06-1)

The SD06-1 experiment was also a single fabric lay-up used to determine permeability. Because of the large difference between the permeabilities of the longitudinal and transverse directions, it was of interest to see if the model would accurately predict the shapes of the flow fronts as well as the curvature along the longitudinal axis.

As shown in Figure 61, flow distances along the longitudinal axis were predicted relatively well using the higher mesh density model. The maximum error in predicting the flow distance was roughly 1 cm after 560 seconds of injection time. The lower mesh density model, element edge length of 12.7 mm, was not as accurate. In the worst case it over predicted flow by nearly 4 cm along the longitudinal axis. Thus the error is greater using lower mesh densities when the flow fronts have a tighter radius.

Experimental flow in the transverse direction was shifted towards the bottom half of the mold; however, flow was well predicted by both models. Flow distances were predicted to within 1 cm.

Flow front shapes predicted by the model were close to those observed experimentally. Experimental flow fronts tended to have a smaller radius for the longitudinal direction. This caused the model to slightly over predict flow in the transverse direction near the tip of the longitudinal flow front.
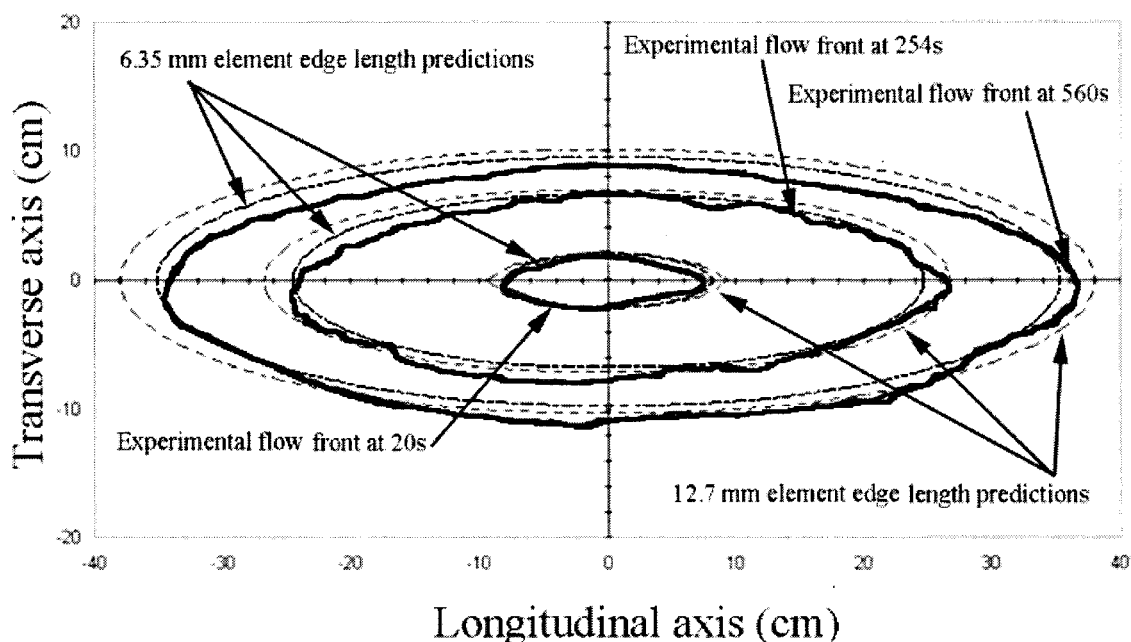
Figure 61. Experimental versus predicted results for SD06-1, single fabric D155. $K_x=6.16 \times 10^{-10}$ $K_y=4.80 \times 10^{-11}$, $v_f=0.398$, $\mu=0.195$ kg/m·s and P=89.7 kPa.

A130-DB120 [0/±45₂/0]s Lay-up

The objective of modeling the MA04-1 lay-up was to show how the two permeability estimation schemes, relative thickness and clamping pressure, compared with experimental results. Since it has already been demonstrated that experimentally determined permeabilities accurately represent flow even in the extreme cases, experimentally determined permeabilities were used to give the flow front locations of the experiment instead of actual experimental data in Figure 62. While experiments with

the D155 and DB120 fabrics were better predicted than those with the A130 and DB120 fabrics, the latter results are given in Figure 62 because they better represented the MSU composite version of the AOC 15/50 blade.

Neither of the models predicted flow accurately. The relative thickness method was the least accurate of the two, under predicting flow by 3 cm after 1800 seconds in the longitudinal direction and under predicting flow by nearly 7 cm in the transverse direction after 1800 seconds. In addition, it failed to calculate the proper shape of the flow front. While the clamping pressure method under predicted flow in the longitudinal and transverse directions by approximately 5 cm, it captured the proper shape of the flow front. The greater accuracy of the clamping pressure method appears to validate one of its main features: fiber volume fraction varies in plies with different fabrics.
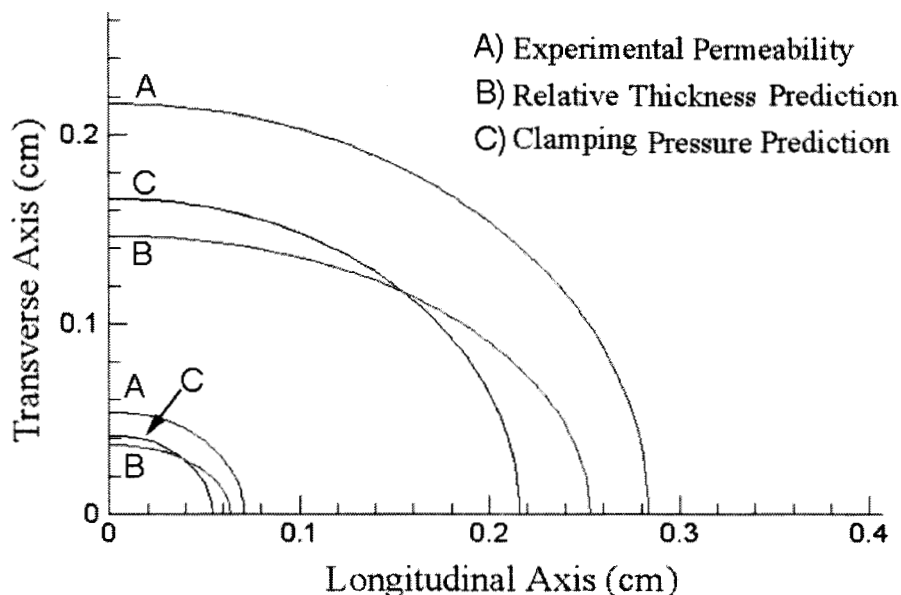
Figure 62. Flow contours comparing the experimentally determined permeability with two predictive methods. Flow front times are at 85 and 1800s from an injection port located at the origin. Quarter symmetry was assumed.

A130 [0/90/0/$\overline{90}$]s Lay-up

The MA03-2 lay-up was selected because it was a worst case scenario. Of all the mixed fabric permeability cases, the MA03 lay-up resulted in one of the least accurate predictions using unidirectional ply permeability data.

As one can see from Figure 63, flow is relatively well predicted in the transverse direction. However, the flow front location in the longitudinal direction is nearly 580 s behind after 900 s of injection. Because of this, the predicted permeability fails to capture the correct shape of the flow front. While these results are not encouraging, they are only a factor of 2 off at a worst case scenario. However, if one wants to accurately model flow front shapes and injection times, it would be best to determine the exact permeability from an experiment instead of trying to produce permeabilities from unidirectional fabric permeabilities.
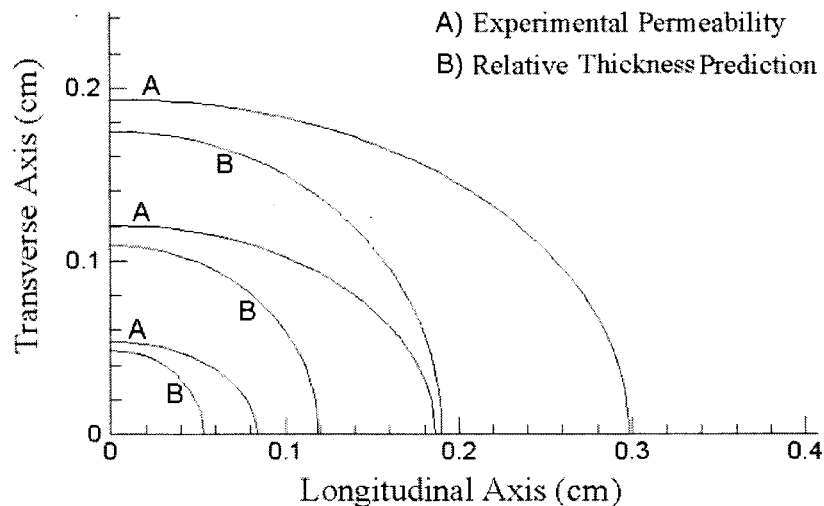
Figure 63. Flow contours comparing the experimentally determined permeability with the relative thickness predictive method for the MA03-2 lay-up (0/90/0/$\overline{90}$)s. Flow front times were at 54 s, 320s and 900 s from an injection port located at the origin. Quarter symmetry was assumed.

T-section Results

T-intersections are a major feature of a turbine blade geometry, and also represent a basic three-dimensional geometry case. T-sections were modeled with injection ports located at both the center of the mold and at the ends using mixed lay-ups of either A130 or D155 fabric with the DB120 fabric.

Thick flanged T model

The thick flanged T was modeled with half symmetry along the web plane. Quarter symmetry was not chosen because injections were also performed from the ends of the mold and it was desired that the same model be used for both the end and central injections.

In order to take into account the different geometries and lay-ups present in the thick flange T-mold, it was divided into three regions with different permeability properties: skin, flange and web. The meshed version of this model is shown in Figure 64. The model contained 2376 elements, with a maximum edge length of 5 mm. Elements 1-1296 made up the web section, elements 2397 to 1836 made up the flange region, and elements 1837 to 2376 made up the skin region. Since the permeabilities of the three regions varied from experiment to experiment they will be detailed in the relevant sections.
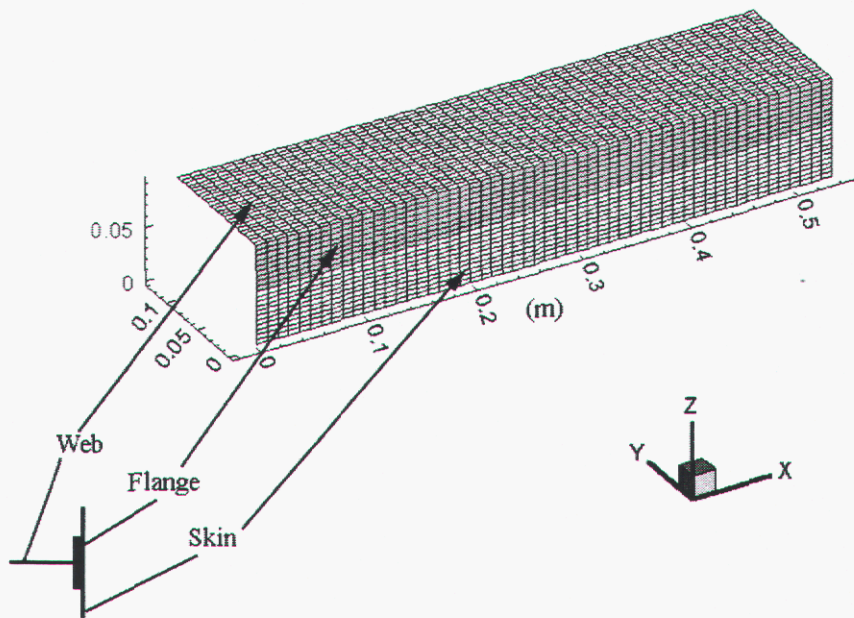
Figure 64. Meshed T-mold showing the three different lay-up regions.

A130 Center Injected T-mold (TA01)

The LIMS input parameters used for modeling the TA01 experiment are shown in Table 21. All permeabilities were calculated by using the clamping pressure method. The lay-up was chosen to give a consistent fiber volume fraction throughout the part.

Table 21. Fabric related LIMS input properties for thick flanged T model TA01. Injection took place at 82.7 kPa from a central injection port and with a resin viscosity of 0.195 kg/m·s.

	Skin	Flange	Web
K_x (m^2)	$1.41 \cdot 10^{-10}$	$1.63 \cdot 10^{-10}$	$9.91 \cdot 10^{-11}$
K_y (m^2)	$7.10 \cdot 10^{-11}$	$9.29 \cdot 10^{-11}$	$6.10 \cdot 10^{-11}$
v_f	0.346	0.316	0.342
Thickness (cm)	0.283	1.283	0.532
elements	1837 - 2376	1297 - 1836	1 - 1296

As one can see from Figure 65 it is difficult to determine how accurate the model was in predicting flow patterns. There was a considerable amount of interlaminar flow

that the LIMS model cannot predict because it uses 2-D shell elements which do not account for flow through the thickness of the element nor does allow for an element to be composed of several layers of material. In addition to the interlaminar flow, there was a considerable amount of racetracking present along the borders of the mold in the experiment. This is most visible in the web section where flow quickly progressed along the mold border in the y direction. The model gives an accurate prediction of flow front shape in the web section of the part. This indicates that the K_x and K_y permeabilities in that region were in the same relative magnitude to each other as were the experimental values. However, the model did not predict flow to be at the first experimental contour level, 155 seconds, until 300 seconds had passed. Although the filling patterns in the rest of the mold were inconclusive, the filling time predicted by the model, 1032 seconds, is close to the experimental filling time of 1200 seconds.

D155 Center Injected T-mold (TD01)

The LIMS input parameters used for modeling the TD01 experiment are shown in Table 22. Once again injection took place at centrally placed injection ports. This lay-up was selected to contrast the filling patterns of the A130 fabric since the through-thickness permeability of the D155's is considerably higher than that of the A130's. Permeabilities in the three sections differed a bit more than for the A130 lay-ups. All permeabilities were calculated by using the clamping pressure method.

Table 22. Fabric related LIMS input properties for thick flanged T model TD01. Injection took place at 82.7 kPa from a central injection port and with a resin viscosity of 0.195 kg/m·s.

	Skin	Flange	Web
K_x (m^2)	$2.17 \cdot 10^{-10}$	$7.13 \cdot 10^{-10}$	$7.25 \cdot 10^{-10}$
K_y (m^2)	$8.64 \cdot 10^{-11}$	$1.90 \cdot 10^{-10}$	$1.94 \cdot 10^{-10}$
v_f	0.333	0.273	0.271
Thickness (cm)	0.294	1.281	0.515
elements	1837-2376	1297-1836	1-1296
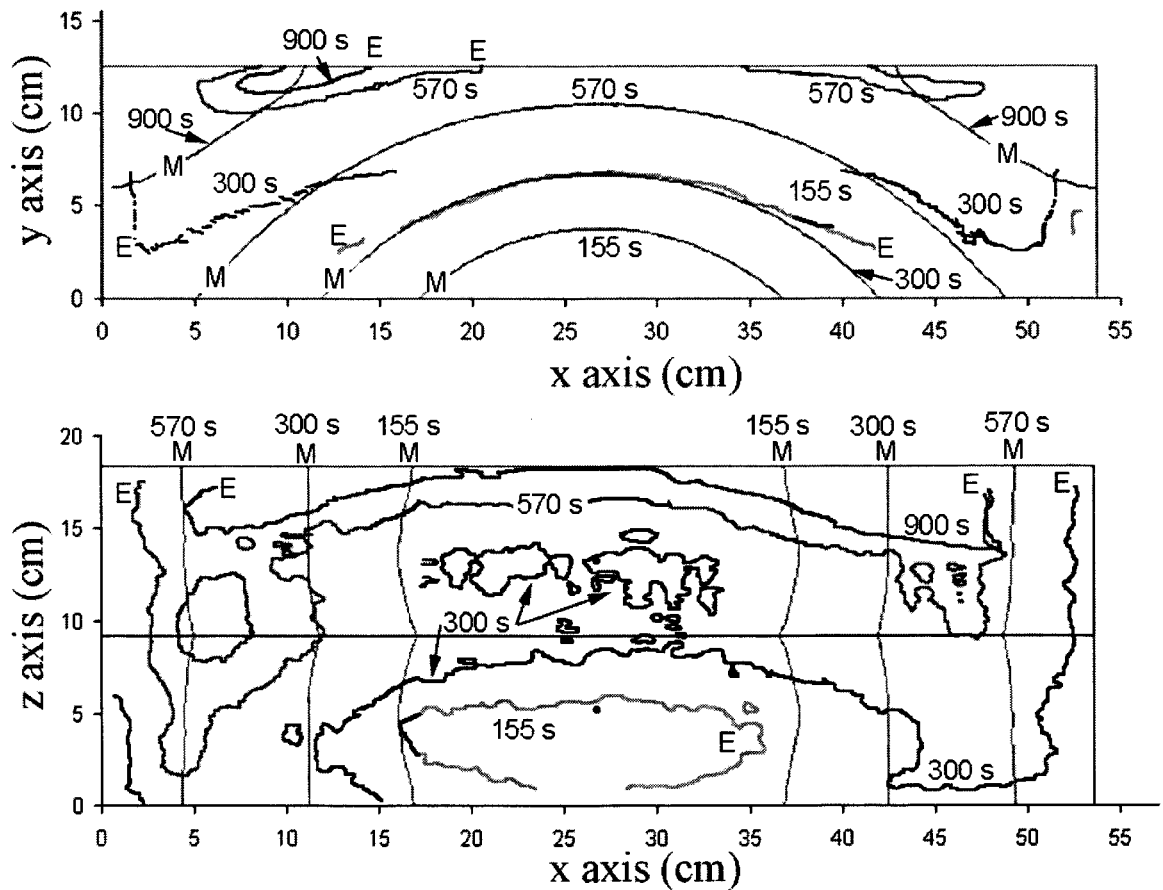
Figure 65. Predicted versus experimental results for case TA01.

The predicted filling times shown in Figure 66 do not match well to the experimental flow fronts. The model predicts filling times to be significantly shorter than experimental values. The flat plate cases gave predicted results which showed that permeabilities were consistently under predicted, giving longer than actual filling times. The cause of this was that the experiment had problems with the mold sealing. This was most likely the cause of the discrepancy between the predicted filling time of 337 seconds and the actual filling time in excess of 900 seconds for the T-section case TD01.

Although the filling times did not match, the flow front shapes seem to be reasonably close to those predicted by the model. Both the model and the experiment show a higher transverse permeability in the flange region. In addition, the relative differences between the transverse permeabilities in the flange and skin sections seems to be predicted relatively well. Also, flow fronts predicted in the web region have nearly the same shape as those observed experimentally. This leads one to believe that the transverse and longitudinal permeabilities in the web have the correct relative magnitudes. There was race tracking observed in the mold, but it was significantly less than the amount present when using the A130 fabric in the same mold.
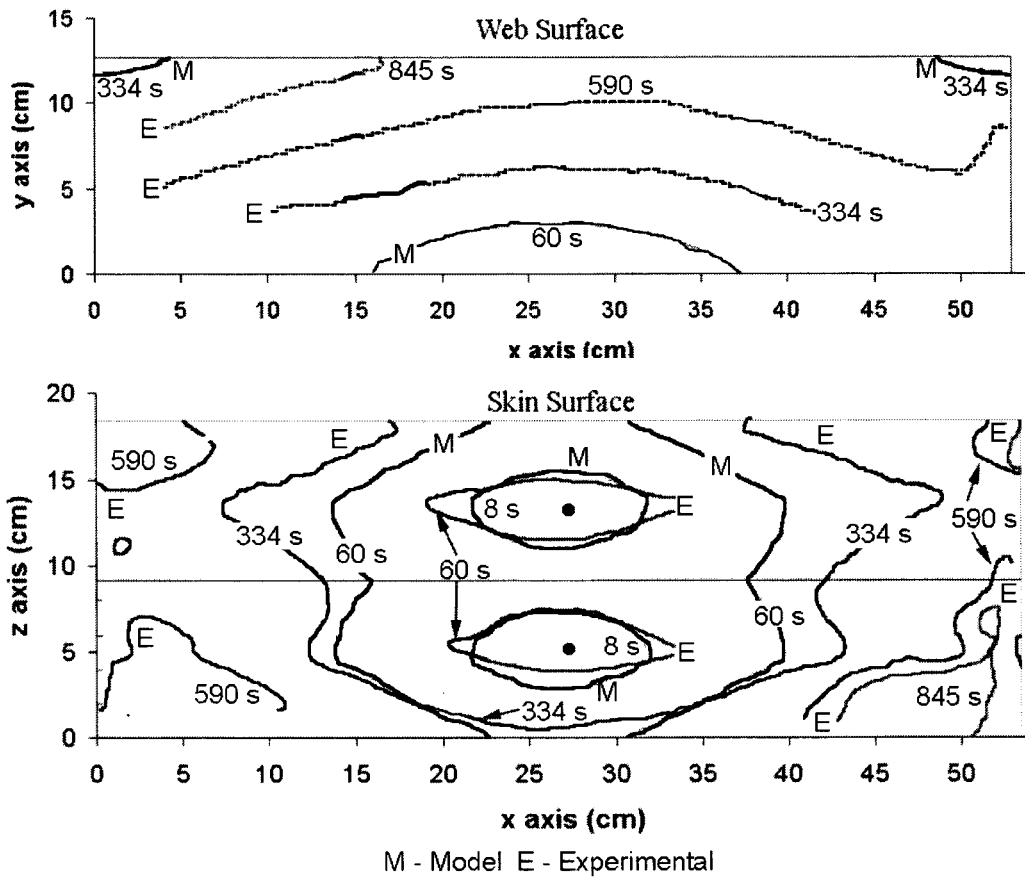
Figure 66. Predicted versus experimental results for case TD01.

A130 End Injected T-mold (TA02)

The LIMS input parameters used for modeling the TA02 case are shown in Table 23. All permeabilities were calculated by using the clamping pressure method. Injection was from the end of the mold instead of in the center as in the previous two cases. Due to the shape of the mold, a large resin rich region filled at the start of the injection along the skin surface. To model this effect more accurately, injection ports were located along the length of the skin in the z direction instead of at a single node.

Table 23. Fabric related LIMS input properties for thick flanged T model TA02. Injection took place at 82.7 kPa from an end of the skin. A resin viscosity of 0.195 kg/m·s was used.

	Skin	Flange	Web
K_x (m^2)	$1.72 \cdot 10^{-10}$	$1.78 \cdot 10^{-10}$	$9.75 \cdot 10^{-11}$
K_y (m^2)	$8.31 \cdot 10^{-11}$	$1.01 \cdot 10^{-10}$	$6.00 \cdot 10^{-11}$
v_f	0.331	0.310	0.343
Thickness (cm)	0.295	1.31	0.530
elements	1837-2376	1297-1836	1-1296

Once again flow front shapes were not well predicted. The model predicted the flange region to be slightly less permeable than the rest of the skin section. Judging from the experimental results, the model seemed to under predict the magnitude of the difference. However, race tracking along the skin boundaries in the x direction also contributed to the higher permeabilities, so it is difficult to determine whether the model predicted the correct ratio of permeabilities between the flange and skin regions. Experimentally, flow in the web was governed by transverse flow into the web from the skin/flange intersection, while the model predicted flow to originate from a single point at the skin/flange intersection. As one can see, the experimental flow front reached the end of the mold, along the skin/flange intersection, after 420 seconds, but the model predicted flow to be slightly less then halfway across the mold at this time. The two flow fronts are considerably different. Despite the inability to predict the preferential flow in the experiment, the filling times predicted by the model are close to experimental values. The model predicted filling to be completed at the 1886 s mark, compared to the experimental value of 1740 seconds.

Figure 67. Experimental versus predicted results for TA02.

Steel Insert Results

The steel insert mold provides several interesting features. First, it has a very complex lay-up containing ply-drops, several fabrics and even fabric rolled into dart shapes. All these effects will be taken into account with a smeared permeability. In addition, the mold is relatively thick, and experimentally it was shown that flow through the thickness was significant around the steel insert. The objective of attempting to model this part was to see how much error results from permeability estimates, as well as the inability of the modeling program to deal with fully three dimensional flow patterns.

Insert Model

Due to the location of the injection port half symmetry was used along the x axis of the part, Figure 68. The insert mold was modeled with two surfaces. The first was the flat, skin surface of the mold. The skin surface covered the entire mold. The other was the curved, inner-surface side that was only present in the insert region. The geometry of the model did not allow for flow through the thickness of the insert region of the part. LIMS does not take into account flow through the thickness of a lay-up and it was not possible to provide a flow channel through the thickness of the part due to meshing constraints.
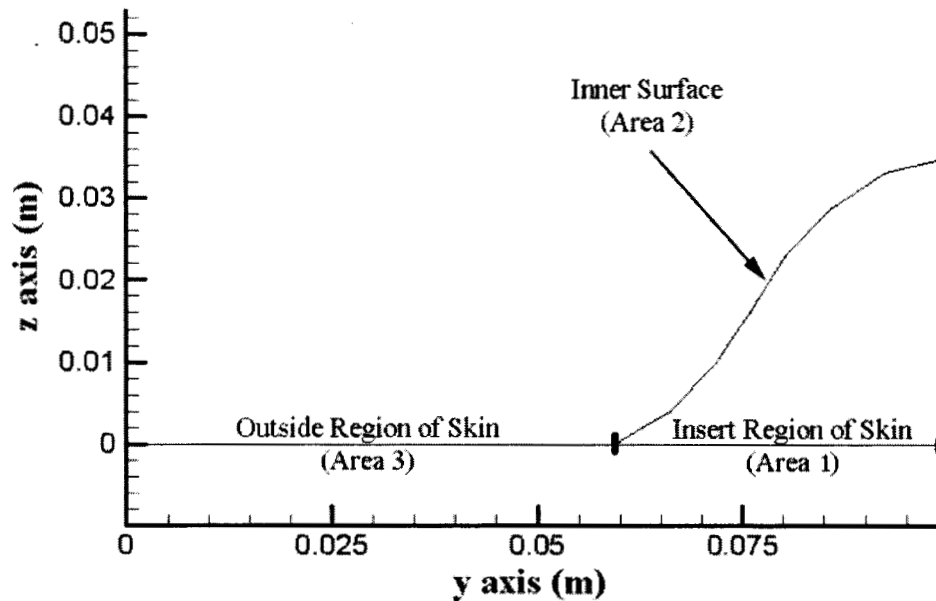
Figure 68. Sections of insert model.

The skin surface was divided into two regions. The first was insert area, the area under the insert, and the other was the remainder of the skin surface. The regions were divided because the lay-ups in the two regions were different, and because the skin surface outside the insert region also included fabric from the inner surface layer. Fiber

volume fractions in each of the three regions were based on the average thickness of the region and its lay-up. Permeability, layer thickness and layer fiber volume fraction data were calculated using the clamping pressure method. A list of material properties for the two skin regions as well as the inner surface region is shown in Table 24.

Table 24. Fabric related LIMS input properties for steel insert model. Injection took place at 96.5 kPa with a resin viscosity of 0.195 kg/m·s.

	Area 1	Area 2	Area 3
Lay-up	[±45/0$_2$/±45]s	[±45/0/±45/0$_2$/±45]s	[±45/0$_2$/±45]s & [±45/0/±45/0$_2$/±45]s
K_x (m^2)	$3.46 \cdot 10^{-10}$	$8.60 \cdot 10^{-10}$	$1.01 \cdot 10^{-9}$
K_y (m^2)	$8.47 \cdot 10^{-11}$	$2.38 \cdot 10^{-10}$	$2.88 \cdot 10^{-10}$
v_f	0.330	0.258	0.245
Thickness (cm)	0.423	0.813	1.424
elements	1-213	214-426	427-837

The meshed model is shown in Figure 69. As mentioned earlier, the model was limited to 4 node elements, which posed a problem when meshing the model at the insert
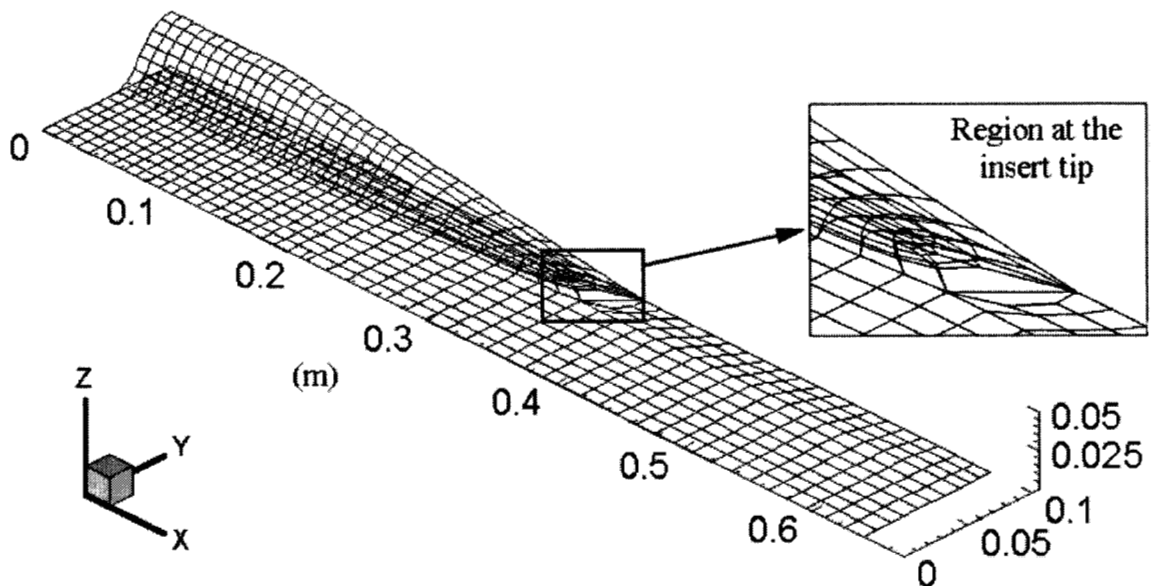
Figure 69. Meshed insert model with a close up at the insert tip region.

tip. A large element was required in that area in order for the meshing algorithm to make an acceptable mesh for LIMS. Other than at the insert tip, the maximum element edge length was around 1.1 cm.

Results

As shown in Figure 70, the model did not do a very good job of matching the experimental results. The longitudinal flow front prediction seems close at 160 seconds, but the transverse permeability is severely underestimated. Although the flow front at 160 seconds is close to the experimental flow front, the model does not do well in predicting complete filling of the mold. The model predicted flow to reach ports 2 and 3 at 2489 seconds, while the experiment reached that location in 741 seconds. Preferential flow should not have been a factor because injection stopped when resin reached the vent ports, and there were no dry spots in the final part.

The large errors in filling time are a result of two factors: LIMS is not able to account for through thickness effects of a lay-up and it is not possible to get an accurate estimate of the permeability around the insert region.

It can be observed from experimental results that flow through the thickness of the part is significant. Not only does the model assume flow rates are equal through the thickness of an element, but the geometry of the model prevents flow between the two flow planes in the insert region since they are only joined at the skin/inner surface intersection.

In addition to the limitations of the actual model, permeabilities around the steel insert were impossible to estimate accurately. There are multiple ply-drops in this region,

a third fabric with an unknown permeability, and D155 fabric rolled into darts, see Figure 31.
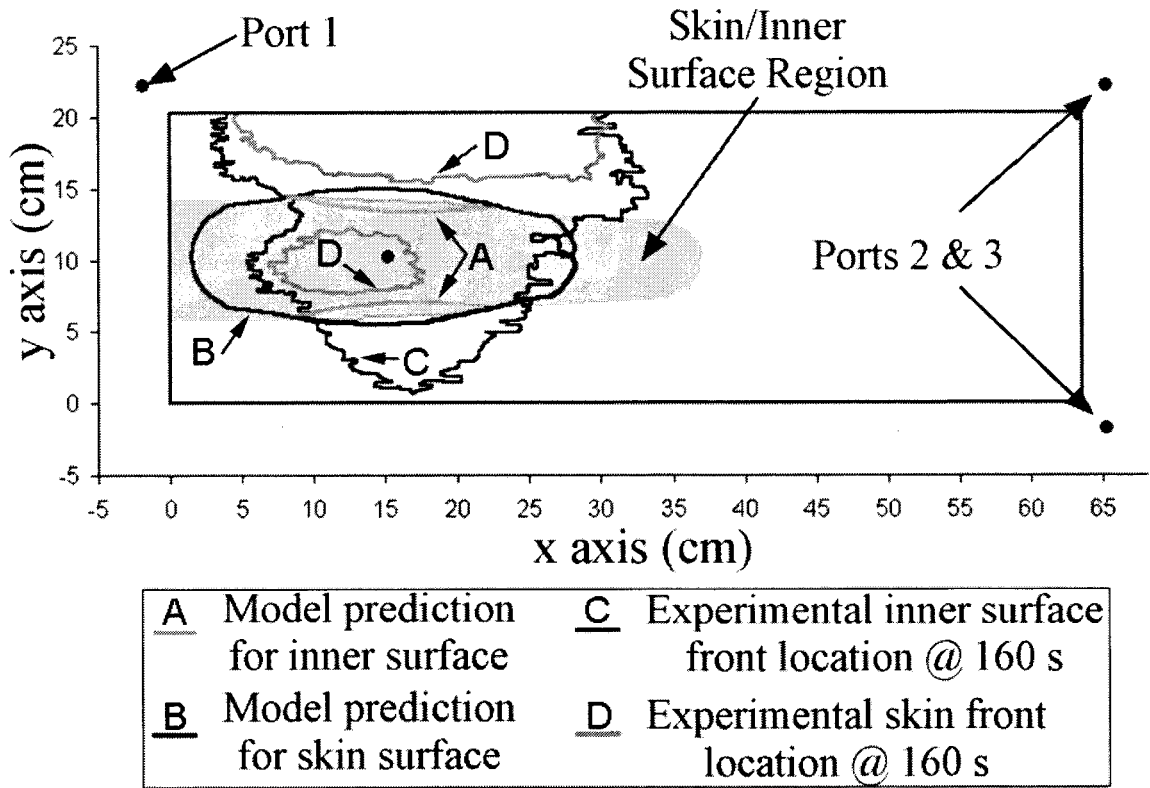
Figure 70. Insert Model versus experimental results. Injection at 96.5 kPa.

Blade Models

The final step of the research was to apply the LIMS modeling package to a full-scale blade injection. The objectives were to get an estimate on the filling time of a blade and observe general filling patterns. An end injection was performed as well as one involving multiple injection ports.

Model

The composite version of the AOC 15/50 blade[3,43] was selected as a model. Blade geometries were taken from reference 43 and the lay-up schedule and part thickness were taken from reference 3. The blade was created from 10 cross sections, separating it into 9 regions. The regions were numbered starting from the root end of the blade. Each region was composed of the following sections: web, spar cap, flange, leading edge and trailing edge, see Figure 71. Lay-ups and permeabilities of these sections are detailed in the appendix.
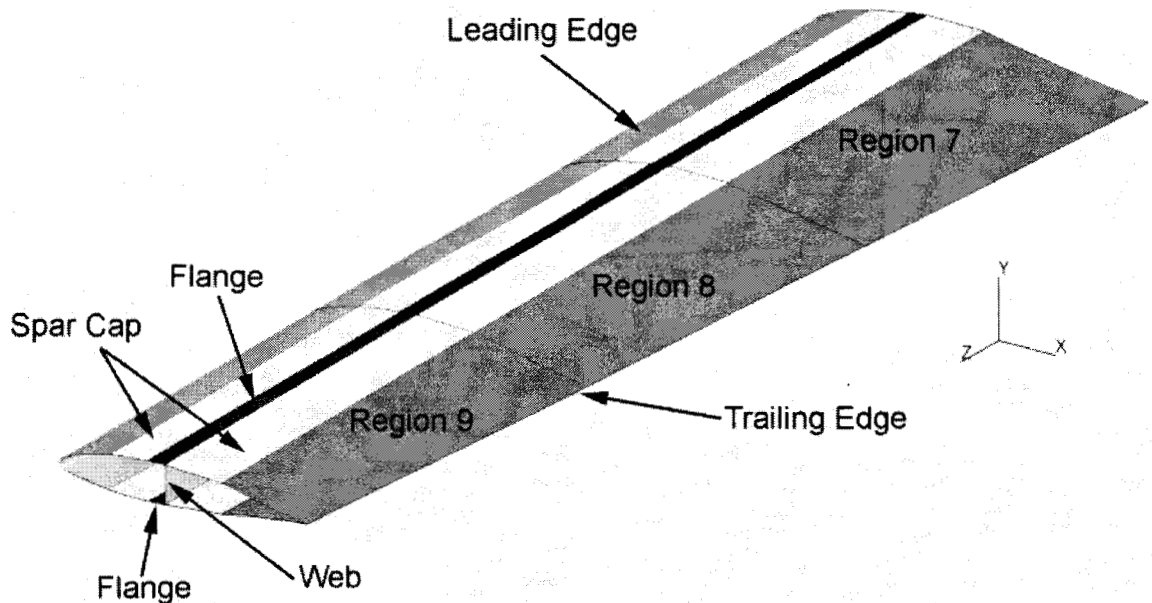
Figure 71. Tip end of AOC 15/50 blade.

End Injection

Two injection ports were located at the root end of the blade in region 1. An injection pressure of 266 kPa was used. The blade filled in a regular manner as shown in Figure 72. Filling patterns were similar on both sides of the mold as well as in the web section, although they are not visible in the figure. A filling time of approximately 10.5

146

hours was predicted. Given that the injection ports were located at an end, and they were

at a constant pressure, this long fill time is not surprising.
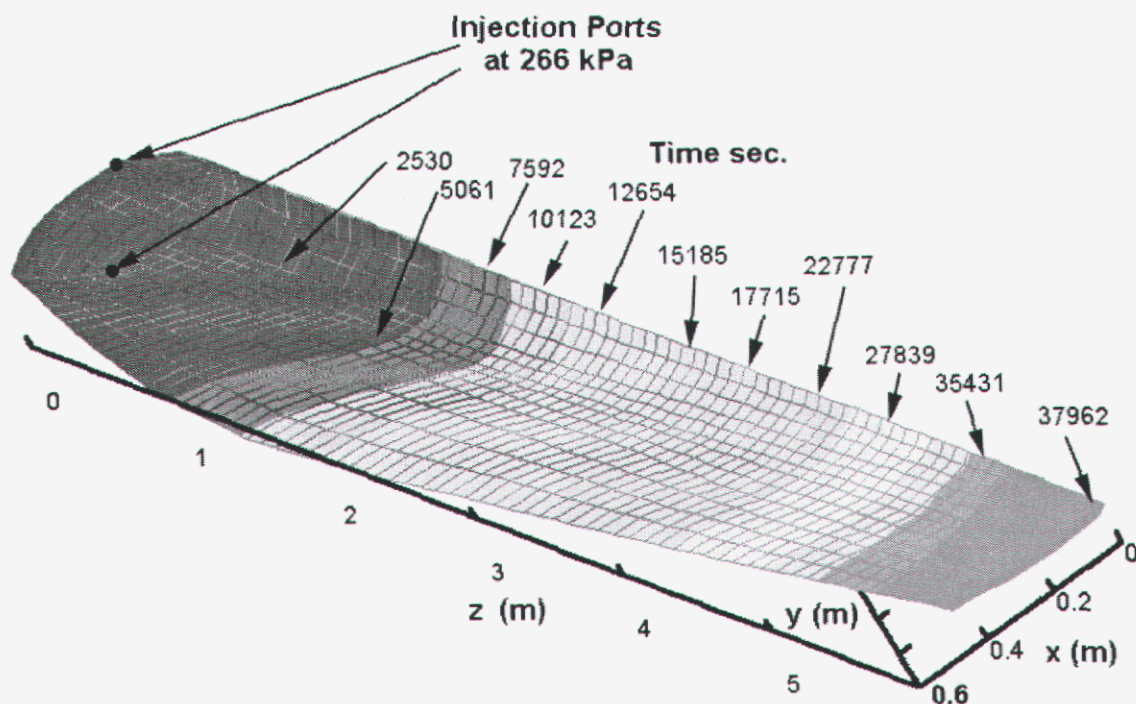
Figure 72. End injection of AOC 15/50 blade. View is from the low pressure side of the
blade.

Multiple Port injection

Injection ports for this simulation were located in three different regions at the

skin-web intersection on both faces of the blade as shown in Figure 73. This gave a total

of six injection ports. Once again filling occurred in a similar manner on both sides of

the blade. Also, flow in the web section kept up with flow along the skins of the blade.

Although the number of ports increased by a factor of 2 from the previous model, the

filling time has decreased by a factor of 10. This is due to better positioned ports and the

fact that as one progress away from a constant pressure injection port the flow rates do

not drop in a linear manner. Obviously, if one were interested in producing blades, the

time saving would be well worth the added cost of multiple injection ports.
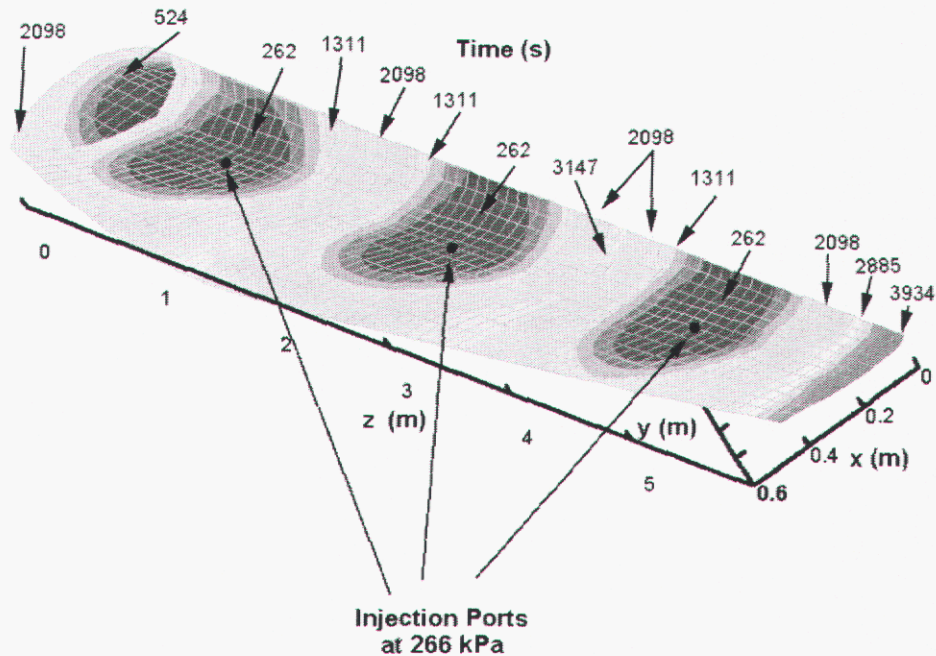
Figure 73. Multi-port injection of AOC 15/50 blade. Six injection ports were located at three locations along the blade length on both the low and high-pressure sides of the blade at the web skin intersection. View is from the low-pressure side of the blade.

Discussion

Based on results from permeability and substructure experiments, there is reason

to believe that flow front shapes should be accurate, however filling times may be over

predicted.

Flow front shapes were accurately predicted in the A130/DB120 lay-ups when the

clamping pressure method was used. In addition, there are no A130 plies oriented in

the 90° direction, which was the major source of error when predicting flow front shapes

148

with the A130 fabric. Also, there are no unconventional fabric geometries or large concentrations of ply-drops present in the lay-up, and the geometric scale of the blade should make through thickness flow insignificant. These were a major source of error in steel root insert model. Another source of error in predicting flow front shapes that can be avoided is preferential flow that was present in the skin/web intersection in the T-geometry. The blade uses a C-channel instead of a T-intersection, and the resin rich area at the skin/web intersection can be avoided with a properly shaped mold.

Based on the results from the permeability experiments, filling times should be over predicted. While the clamping pressure was able to accurately predict flow front shapes, filling times tended to be under estimated. In addition, the farther the flow is from a constant pressure injection port, the greater the error in flow front predictions. For this reason errors in filling time related to the end injection are much greater than those associated with the multi-port injection. The filling times of the multi-port injection were on the same order as experimental results, so errors in filling times should be comparable to those observed in the substructure experiments (approximately 30%).

CHAPTER 6

RESULTS SUMMARY, RECOMMENDATIONS AND FUTURE WORK

A summary of the experimental and modeling work is included in this section as well as recommendations for further study in this area.

Fabric Characterization

- The volume of glass fibers per unit area for the A130, DB120 and D155 fabrics are 0.0174 cm^3/cm^2, 0.0140 cm^3/cm^2 and 0.0209 cm^3/cm^2 respectively.

- Binder or stitching content of the fabrics was also calculated. The A130 fabric was composed of 2.44% thermoplastic binder by weight. The DB120 fabric was composed of 4.83% stitching by weight; and the D155 fabric was composed of 1.94% stitching by weight.

- Maximum fiber volume fractions were computed for the three fabrics using clamping pressure data. The A130 fabric was able to reach a maximum fiber volume fraction of 0.67; the DB120 fabric was able to reach a maximum fiber volume fraction of 0.55; and the D155 fabric was able to reach a maximum fiber volume fraction of 0.72.

- Stacking order affected the unidirectional fabrics. A unidirectional lay-up would have a lower thickness at a given fiber volume fraction than one with alternating 0° 90° plies. This effect was more pronounced in the D155 fabric than in the A130 fabric.

Permeability

Single Fabric Permeability

- A130 fabric permeabilities were calculated in the fiber volume fraction range of 0.31 to 0.45 and the following relationships were determined for permeabilities:
  $K_x = 5.85 \cdot 10^{-8} e^{-15.9 v_f}$ and $K_y = 1.13 \cdot 10^{-9} e^{-8.63 v_f}$ (permeability is given in m^2).

- DB120 fabric permeabilities were calculated in the fiber volume fraction range of 0.28 to 0.37 and the following relationships were determined for permeabilities:

$K_x = 6.27 \cdot 10^{-9} e^{-13.2 v_f}$ and $K_y = 6.35 \cdot 10^{-9} e^{-14.7 v_f}$ (permeability is given in m^2).

- D155 fabric permeabilities were calculated in the fiber volume fraction range of 0.33 to 0.47 and the following relationships were determined for the permeabilities: $K_x = 4.30 \cdot 10^{-8} e^{-11.4 v_f}$ and $K_y = 3.59 \cdot 10^{-8} e^{-17.3 v_f}$ (permeability is given in m^2).

- The DB120 fabric had the lowest permeability per fiber volume fraction of the three fabrics in both the longitudinal and transverse directions.

- The D155 fabric had the highest permeability of the three fabrics in the longitudinal direction and in the transverse direction at higher volume fractions.

- The transverse permeability of the A130 fabric increased relative to the other fabrics as fiber volume fraction increased. This was likely the result of its woven structure as opposed to the other two stitched fabrics.

Mixed Fabric Permeability

- The relative thickness method—based on the rule of mixtures—was used to estimate the permeabilities of lay-ups from unidirectional permeability data. This method was not able to accurately estimate individual permeability values as well as the relative differences between the longitudinal and transverse permeabilities.

- A method based on clamping pressure was used to estimate the permeability of lay-ups containing a unidirectional fabric mixed with the DB120 fabric. It under estimated flow levels, but was able to accurately capture the shape of flow fronts. The method implies different fiber volume fractions in different fabric layers and, perhaps, other flow channels between the layers.

Modeling

Thick Flange T Mold

- Injection through the flange resulted in three-dimensional flow fronts with the A130 fabric. The same injection method with D155 material resulted in two-dimensional flow patterns.

- Race tracking along the skin/web intersection was observed, and resulted in flow nearly two times faster than predictions.

- LIMS was able to predict approximate filling times for the T-mold. Flow front shapes were close, but race tracking along the borders of the mold and the skin flange region had the potential to significantly alter filling patterns.

Steel Insert Mold

- Experimental results show that filling patterns in the insert mold were highly three-dimensional. Flow patterns along the skin surface of the mold differed significantly from those along the inner surface in the region of the steel insert.

- It was not possible to predict the permeability of the insert mold by the clamping pressure method. Filling times were under predicted by a factor of 3.5 and flow front patterns were also poorly predicted. This was likely due to the inhomogeneous lay-up of the mold as well as the varying thickness of the part.

Blade

- An injection with a single set of injection ports at the root end of the blade as well as one with three sets of injection ports along the length blade were modeled. The run with multiple injection ports reduced the filling time of the blade by a factor of 10.

- Based on results from the substructures, it is anticipated that the flow front shapes should be accurate.

Recommendations

- For consistent results, locate injection ports so they wet the entire thickness of part, or use fabrics that have high through thickness permeabilities (D155 and DB120).

- Using the A130 fabric as a 90° ply precludes predictions of the flow fronts.

- A double biased fabric with smaller gaps between fiber bundles would provide higher fiber volume fractions than are attainable with the DB120 fabric. Also, a fabric with less stitching would increase transverse permeabilities over the DB120 fabric.

- For best results, use experimentally determined permeabilities for a given lay-up.

- To get a lower limit on injection times when the lay-up does not contain 90° plies, the following method may be used. Use the highest permeability of the individual fabric layers as the permeability in the principal direction. Then find the other permeability value using the shape, Kx to Ky ratio, predicted by the clamping pressure method.

- Attempt to account for race tracking at the mold edges as well as any T intersections of a part by raising the permeability in these regions.

- Small parts with thick, complicated lay-ups, such as the steel root insert geometry, are not suited for modeling with LIMS. Through thickness flow can significantly alter flow front shapes, and in-plane permeabilities are difficult to predict.

Future Work

- More accurate clamping pressure experiments could determine the effect of 0°-90° intersections on the stacking thickness of a unidirectional fabric.

- A modeling package that took into account three-dimensional filling patterns would be useful for predicting flow in parts such as the root, as well as predicting flow in detail regions such as the skin-web intersection of the thick flange T mold.

- An alternative to the DB120 fabric that had higher fiber volume fractions and higher permeabilities would be useful.

REFERENCES CITED

[1] Swanson, R.W., Introduction to Design and Analysis with Advance Composite Materials, Prentice Hall, NJ, 1997.

[2] Mallick, P.K., Fiber-Reinforced Composites, Marcel Dekker, Inc., New York, 1988.

[3] Carins, D.S., et al., "Design/Manufacturing Synthesis of a Composite Blade for the AOC 15/50 Wind Turbine," *Proceedings of 37th AIAA Aerospace Sciences Meeting and Exhibit, 1999 ASME Wind Energy Symposium*, Reno, NV, 11-14 January, 1990, AIAA/ASME, NY, 58-65.

[4] Skramstad, J.D. "Evaluation of Hand Lay-Up and Resin Transfer Molding in Composite Wind Turbine Blade Manufacturing," Master's Thesis in Mechanical Engineering, Montana State University-Bozeman, August 1999.

[5] Mandell, J.F., Sutherland, H.J. and Samborsky, D.D., "Effects of Materials Parameters and Design Details on the Fatigue of Composite Materials for Wind Turbine Blades," *Proceedings of 1999 European Wind Energy Conference and Exhibition*, Nice, France, 1-5 March, 1999, WIP-Munich, Germany, 1999.

[6] Orozco, R., "Effects of Toughened Matrix Resins on Composite Materials for Wind Turbine Blades," Master's Thesis in Chemical Engineering, Montana State University-Bozeman, July 1999.

[7] Li, M., "Temperature and Moisture Effects on Composite Materials for Wind Turbine Blades," Master's Thesis in Chemical Engineering, Montana State University-Bozeman, March 2000.

[8] Mandell J.F., Samborsky, D.D., "DOE/MSU Composite Material Fatigue Database: Test Methods, Materials and analysis," *Sandia National Laboratories Contractor Report*, SAND97-3002. December, 1997.

[9] Rosen, S. L., Fundamental Principles of Polymeric Materials, John Wiley & Sons, New York, 1993.

[10] Hedley, C.W., Mold Filling Parameters in Resin Transfer Molding of Composites," Master's Thesis in Chemical Engineering, Montana State University-Bozeman, April 1994.

[11] Kruckenberg T., Paton, R. etal., "Resin Transfer Moulding for Aerospace Structures," Kluwer Academic Publishers, MA, 1998.

[12] Samborsky, D.D., "Fatigue of E-Glass Fiber Reinforced Composite Materials and Substructures," Master's Thesis in Civil Engineering, Montana State University-Bozeman, December 1999.

[13] Bird R.B., Stewart W.E. and Lightfoot, E.N., "Transport Phenomea," John Wiley & Sons, New York, 1960.

[14] Scheidegger, A.E., "The Physics of Flow Through Porous Media," The MacMillan Company, NY, 1957.

[15] Calhoun, J.C., Yuster, S.T., "A Study of the Flow of Homogenous Fluids Through Porous Media," *Drilling and Production Practice*, 1946

[16] Schwartz, C.E., Smith, J.M., *Industrial and Engineering Chemistry*, Vol. 45, p. 1209, 1953.

[17] Parnas, R.S., Flynn, K.M. and Dal-Favero, M.E., "A Permeability Database for Composites Manufacturing," *Polymer Composites*, Vol. 18, No.5, 1997.

[18] Parnas, R.S., Flynn, K.M. and Dal-Favero, M.E., "NIST Database on Reinforcement Permeability Values Data on Composite Reinforcement Materials Used in Liquid Composite Molding," U.S. Department of Commerce, Gaithersburg, MD.

[19] Parnas, R.S., Howard, J.G., Luce, T.L. and Advani, S.G., "Permeability Characterization. Part 1: A Proposed Standard Reference Fabric for Permeability," *Polymer Composites*, Vol. 16, No. 6, Dec. 1995.

[20] Simacek, P. and Advani, S.G., "Permeability Model for a Woven Fabric," *Polymer Composites*, Vol. 17, No. 6, Dec. 1996.

[21] Cai, Z. and Berdichevsky, A.L., "Numerical Simulation on the Permeability Variations of a Fiber Assembly," *Polymer Composites*, Vol. 14, No. 6, Dec. 1993.

[22] Skartsis, L., Kardos, J.L. and Khomami, B. "Resin Flow Through fiber Beds During Composite Manufacturing Processes, Part 1: Review of Newtonian Flow Through Fiber Beds," *Polymer Engineering and Science*, Vol. 32, No. 4, 1992. p.221

[23] Skartsis L., Khomami, B. and Kardos, J.L., "Resin Flow Through fiber Beds During Composite Manufacturing Processes, Part 2: Numerical and Experimental Studies of Newtonian flow Through Ideal and Actual Fiber Beds," *Polymer Engineering and Science*, Vol. 32, No. 4, 1992. p 231

[24] Larson, R.E. and Higdon, J.L.L., *Journal of Fluid Mechanics*, Vol. 178, p. 119, 1987.

25 Cairns, D.S., Humbert, D.R. and Mandell, J.F., "Modeling of Resin Transfer Molding of Composite Materials with Oriented Unidirectional Plies," *Composites: Part A* Vol. 30, 1999.

26 McCabe, W.L., Smith, J.C. and Harriott, P., "Unit Operations of Chemical Engineering," McGraw-Hill, NY, 1993.

27 Gebart, B.R., "Permeability of Unidirectional Reinforcements for RTM," *Journal of Composite Materials*, Vol. 26, No. 8, 1992.

28 Chan, A.W., Hwang, S.T., "Anisotropic In-Plane Permeability of Fabric Media," *Polymer Engineering and Science*, Vol. 31, No. 16, Aug. 1991.

29 Lai, Y.H., "Measuring Permeability of Preforms," Masters Thesis in Chemical Engineering, Washington University, May 1996.

30 Bear, J., "Dynamics of Fluids in Porous Media," Am. Elsevier, NY, 1972.

31 Adams, K.L., Russel, W.B. and Rebenfeld, L., *Int. J. Multiphase Flow*, 14, 203, 1988.

32 Skartsis, L., Khomami, B. and Kardos, J.L., "The effect of Capillary Pressure on the Impregnation of Fibrous Media," *SAMPE Journal*, Vol. 28, No. 5, 1992.

33 Ahn, K.J., Seferis, J.C. and Berg, J.C., "Simultaneous measurements of Permeability and Capillary Pressure of Thermosetting Matrices in Woven Fabric Reinforcements," *Polymer Composites*, Vol. 12, No. 3, June 1991.

34 Humbert, D.R., "Modeling of Resin Transfer Molding of Composite Materials with Oriented Unidirectional Plies," Master's Thesis in Chemical Engineering, Montana State University-Bozeman, Apr. 1996.

35 Teukolsky, S.A., Vetterling, W.T. and Flannery, B.P., "Numerical Recipes in C," Cambridge University Press, NY, 1992.

36 Simacek, P., Sozer, E.M. and Advani, S.G., "User Manual for DRAPE 1.1 and LIMS 4.0 (Liquid Injection Molding Software)," University of Delaware Center for Composite Materials Technical Report, CCM Report 98-01, 1998.

37 Janssen, L.P.B.M., Warmoeskerken, M.M.C.G., "Transport Phenomenon Data Companion," Delftse Uitgevers Maatschappij, Delftse, The Netherlands, 1987.

38 Snell, F.D., Hilton, C.L., "Encyclopedia of Industrial Chemical Analysis," Vol. 3, Interscience Publishers, NY, 1966.

[39] Mogavero, J. and Advani, S.G., "Experimental Investigation of Flow Through Multi-Layered Preforms," *Polymer Composites*, Vol. 18, No. 5, Oct, 1997.

[40] Adams, K.L. and Rebenfeld, L., "Permeability Characteristics of Multilayer Fiber Reinforcements. Part I: Experimental Observations," *Polymer Composites*, Vol. 12, No. 3, June 1991.

[41] Lai, Y.-H, Khomami, B. and Kardos, J. L., "Accurate Permeability Characterization of Preforms Used in Polymer Matrix Composites," *Polymer Composites*, Vol. 18, No.3, June 1997.

[42] Perry R.H., Green, D.W. and Maloney, J.O., "Perry's Chemical Engineering Handbook," McGraw Hill, NY, 1997.

[43] Cairns D.S., McKittrick L., Combs D., Mandell J.F., Rabern D., and VanLuchene R., "Design/Manufacturing Synthesis of a Composite Blade for the AOC 15/50 Wind Turbine Blade" 1999 ASME Wind Energy Symposium, pp. 58-65.

APPENDICES

APPENDIX A

PERMEABILITY EXPERIMENTS

Description of Calculations

The permeability spreadsheets contain all the dimensional information about the given plate as well as maximum flow positions at given times. Permeabilities were determined by a 2-D unsaturated flow method. The spreadsheet for used for the permeability calculations is divided into 9 regions.

- Region 1 contains lay-up, thickness and fiber volume fraction information.

- Region 2 contains the number of plies of each fabric in the lay-up as well as relative thickness information.

- Region 3 contains the times that flow fronts were measured.

- Region 4 contains the pixel to meter calculations for both the x and y directions.

- Region 5 and 6 contain the maximum flow distance from the injection port in both the x and y directions.

- Region 7 contains the fabric hole radius (R_{xo}) the pressure of the experiment, the resin viscosity, permeability calculations and the ratio K_x:K_y.

- Region 8 contains calculations to determine the K_x permeability. R_x/R_{xo} is plotted in one column, the left side of Equation 15 (see chapter 2) is plotted in another and the entire right side of Equation 15 except for K_x is plotted in the third. That way when the equation is plotted the slope gives K_x.

- Region 9 contains calculations for the K_y permeability. The left side of Equation 16 is plotted in one column, and the right side except for K_y is plotted on the other. Once again the slope of this equation will give K_y.

Table 25. Example of a permeability spread sheet.

Region 1		Region 2				
Region 3	Region 4	Region 5		Region 6		
Region 7	Region 8	Region 9				

Single fabric experiments

Table 26. Experiment SA06-1, A130 0_6.

Lay-up	[0_6]							# of plys	rel. thick (cm)
Thickness	0.335								
Fiber Vol.	0.312179						A130	6	1.74E-02
							D155	0	2.09E-02
							DB120	0	1.40E-02

time		total time	x-meas	x-conv	y-meas	y-conv	x-meas dist			left half	right half	average x-radius	y-meas dist	pix		top half	bottom half	average y-radius
min	sec	(sec)	(pix)	m/pix	(pix)	m/pix	left (pix)	elis. (pix)	right (pix)	m	m	m	top	elispe	bottom	m	m	m
0	14	14	1410	0.000558	926	0.000555	77	149	65	0.043	0.0363	0.039649	20	45	22	0.0111	0.0122	0.0117
0	43	43	1413	0.000557	928	0.000554	151	297	142	0.08415	0.07913	0.081638	55	104	49	0.0305	0.0272	0.0288
4	3	243	1411	0.000558	929	0.000554	313	629	319	0.17467	0.17802	0.176342	148	283	135	0.0819	0.0747	0.0783
6	25	385	1415	0.000556	930	0.000553	382	790	407	0.21257	0.22648	0.219526	190	359	173	0.1051	0.0957	0.1004
8	38	518	1416	0.000556	931	0.000552	435	905	463	0.24189	0.25746	0.249677	221	411	196	0.1221	0.1083	0.1152
9	50	590	1419	0.000555	927	0.000555	461	960	496	0.25581	0.27523	0.265519	231	438	209	0.1282	0.116	0.1221
11	0	660	1414	0.000557	930	0.000553	477	1003	519	0.26562	0.28901	0.277316	247	463	218	0.1366	0.1206	0.1286
12	10	730	1413	0.000557	929	0.000554	507	1048	546	0.28253	0.30426	0.293394	255	482	228	0.1412	0.1262	0.1337
13	48	828	1412	0.000558	928	0.000554	538	1118	578	0.30002	0.32232	0.311168	271	510	239	0.1502	0.1325	0.1413
15	0	900	1406	0.00056	930	0.000553	543	1146	606	0.3041	0.33938	0.321736	284	527	243	0.1571	0.1344	0.1457

			R_x/R_{xo}	left side	right side	$R_y{}^2$	$R_x{}^2/K_x$
R_{xo}	0.003175		12.48794	632.52	3.71E+12	0.0001	4459738
del P	89667.5		25.71267	3633.3	1.14E+13	0.0008	18906964
visc	0.195		55.54075	21700	6.45E+13	0.0061	88216740
1-vf	0.687821		69.14205	35723	1.02E+14	0.0101	1.37E+08
K_x	3.53E-10		78.63842	47802	1.37E+14	0.0133	1.77E+08
K_y	7.34E-11		83.62791	54920	1.57E+14	0.0149	2E+08
Kx/Ky	4.799245		87.34371	60572	1.75E+14	0.0165	2.18E+08
			92.40764	68762	1.94E+14	0.0179	2.44E+08
			98.00567	78475	2.2E+14	0.02	2.75E+08
			101.3343	84582	2.39E+14	0.0212	2.94E+08

Table 27. Experiment SA07-1, A130 0_7.

Lay-up	[0_7]									rel. thick							
Thickness	0.325							# of plys		(cm)							
Fiber Vol.	0.375415						A130	7		1.74E-02							
							D155	0		2.09E-02							
							DB120	0		1.40E-02							

time		total time	x-meas	x-conv	y-meas	y-conv	x-meas dist	elis.		left half	right half	average x-radius	y-meas dist	pix		top half	bottom half	average y-radius
min	sec	(sec)	(pix)	m/pix	(pix)	m/pix	left (pix)	elis. (pix)	right (pix)	m	m	m	top	elispe	bottom	m	m	m
1	40	100	806	0.000977	541	0.000951	96	183	91	0.09378	0.0889	0.091342	42	92	49	0.0399	0.0466	0.0433
7	30	450	806	0.000977	541	0.000951	179	375	196	0.17487	0.19148	0.183173	91	193	102	0.0865	0.097	0.0917
9	22	562	805	0.000978	542	0.000949	198	424	222	0.19367	0.21715	0.205409	101	212	112	0.0958	0.1063	0.1011
10	30	630	806	0.000977	542	0.000949	201	438	234	0.19636	0.2286	0.212481	107	225	119	0.1015	0.1129	0.1072
11	25	685	806	0.000977	542	0.000949	212	455	245	0.20711	0.23935	0.223227	112	235	125	0.1063	0.1186	0.1125
12	30	750	804	0.000979	542	0.000949	219	471	251	0.21448	0.24582	0.230148	118	245	129	0.112	0.1224	0.1172
13	40	820	807	0.000976	541	0.000951	234	493	262	0.22832	0.25564	0.241977	122	257	135	0.116	0.1283	0.1222
15	8	908	805	0.000978	542	0.000949	246	521	269	0.24062	0.26312	0.25187	128	269	138	0.1215	0.131	0.1262
17	35	1055	806	0.000977	542	0.000949	262	546	285	0.25595	0.27842	0.267188	142	285	146	0.1348	0.1386	0.1367
20	12	1212	806	0.000977	541	0.000951	288	590	304	0.28135	0.29698	0.289169	152	305	153	0.1445	0.1455	0.145

			R_x/R_{xo}	left side	right side	$R_y{}^2$	$R_x{}^2/K_x$
R_{xo}	0.003175		28.76923	4734.1	2.92E+13	0.0019	45302318
del P	89667.5		57.69231	23667	1.31E+14	0.0084	1.82E+08
visc	0.195		64.69565	30720	1.64E+14	0.0102	2.29E+08
1-vf	0.624585		66.92308	33175	1.84E+14	0.0115	2.45E+08
K_x	1.84E-10		70.30769	37103	2E+14	0.0126	2.71E+08
K_y	4.68E-11		72.48756	39761	2.19E+14	0.0137	2.88E+08
Kx/Ky	3.936506		76.21314	44535	2.4E+14	0.0149	3.18E+08
			79.32919	48755	2.65E+14	0.0159	3.44E+08
			84.15385	55702	3.08E+14	0.0187	3.88E+08
			91.07692	66555	3.54E+14	0.021	4.54E+08

Table 28. Experiment SA08-1, A130 0_8.

Lay-up	[0_8]									rel. thick							
Thickness	0.349							# of plys		(cm)							
Fiber Vol.	0.399542						A130	8		1.74E-02							
							D155	0		2.09E-02							
							DB120	0		1.40E-02							

time		total time	x-meas	x-conv	y-meas	y-conv	x-meas dist			left half	right half	average x-radius	y-meas dist	pix		top half	bottom half	average y-radius
min	sec	(sec)	(pix)	m/pix	(pix)	m/pix	left (pix)	elis. (pix)	right (pix)	m	m	m	top	elispe	bottom	m	m	m
0	32	32	1348	0.000584	894	0.000575	70	135	64	0.04089	0.03738	0.039136	41	82	40	0.0236	0.023	0.0233
1	30	90	1349	0.000584	893	0.000576	104	204	101	0.0607	0.05895	0.059828	66	137	71	0.038	0.0409	0.0395
3	18	198	1351	0.000583	896	0.000574	164	311	146	0.09558	0.08509	0.090338	102	204	102	0.0586	0.0586	0.0586
11	47	707	1353	0.000582	896	0.000574	278	572	297	0.16179	0.17284	0.167315	184	361	178	0.1056	0.1022	0.1039
13	0	780	1352	0.000582	899	0.000572	302	625	323	0.17588	0.18811	0.181999	191	376	184	0.1093	0.1053	0.1073
15	0	900	1355	0.000581	896	0.000574	311	635	325	0.18072	0.18886	0.184792	203	397	194	0.1165	0.1114	0.1139
16	30	990	1355	0.000581	900	0.000572	315	680	358	0.18305	0.20804	0.195543	216	418	201	0.1234	0.1149	0.1192
22	6	1326	1347	0.000585	895	0.000575	374	782	408	0.21862	0.2385	0.228562	246	473	228	0.1414	0.131	0.1362
23	19	1399	1340	0.000588	896	0.000574	384	801	420	0.22564	0.2468	0.23622	249	486	236	0.1429	0.1355	0.1392
25	10	1510	1341	0.000587	893	0.000576	392	829	441	0.23017	0.25894	0.244558	259	501	243	0.1492	0.14	0.1446
27	0	1620	1342	0.000587	898	0.000573	404	862	456	0.23704	0.26755	0.252297	267	524	255	0.1529	0.1461	0.1495
30	0	1800	1342	0.000587	898	0.000573	425	919	502	0.24936	0.29454	0.271952	281	548	267	0.1609	0.1529	0.1569
												10.70678						6.1787

			R_x/R_{xo}	left side	right side	$R_y{}^2$	$R_x{}^2/K_x$
R_{xo}	0.003175		12.32641	612.33	9.72E+12	0.0005	15478741
del P	89667.5		18.84359	1731.1	2.73E+13	0.0016	36173426
visc	0.195		28.453	4612.7	6.02E+13	0.0034	82474275
1-vf	0.600458		52.69771	19244	2.15E+14	0.0108	2.83E+08
K_x	9.9E-11		57.32249	23322	2.37E+14	0.0115	3.35E+08
K_y	3.47E-11		58.20221	24147	2.73E+14	0.013	3.45E+08
Kx/Ky	2.852815		61.58819	27467	3.01E+14	0.0142	3.86E+08
			71.98812	39143	4.03E+14	0.0186	5.28E+08
			74.4	42174	4.25E+14	0.0194	5.64E+08
			77.0261	45616	4.59E+14	0.0209	6.04E+08
			79.46349	48942	4.92E+14	0.0223	6.43E+08
			85.65425	57965	5.47E+14	0.0246	7.47E+08

Table 29. Experiment SA08-2, A130 0_8.

Lay-up	[0_8]								rel. thick			
Thickness	0.335						# of plys		(cm)			
Fiber Vol.	0.416239					A130	8		1.74E-02			
						D155	0		2.09E-02			
						DB120	0		1.40E-02			

time		total time	x-meas	x-conv	y-meas	y-conv	x-meas dist			left half	right half	average x-radius	y-meas dist	pix		top half	bottom half	average y-radius
min	sec	(sec)	(pix)	m/pix	(pix)	m/pix	left (pix)	elis. (pix)	right (pix)	m	m	m	top	elispe	bottom	m	m	m
2	21	141	1352	0.000582	892	0.000577	137	251	114	0.07979	0.06639	0.073091	80	168	88	0.0461	0.0507	0.0484
2	45	165	1351	0.000583	891	0.000577	145	293	145	0.08451	0.08451	0.08451	93	198	104	0.0537	0.06	0.0569
11	30	690	1351	0.000583	892	0.000577	283	574	290	0.16494	0.16902	0.16698	179	368	190	0.1032	0.1096	0.1064
13	43	823	1350	0.000583	891	0.000577	312	621	309	0.18198	0.18023	0.181102	189	399	209	0.1091	0.1207	0.1149
15	0	900	1353	0.000582	891	0.000577	326	646	321	0.18972	0.18681	0.188266	197	410	216	0.1137	0.1247	0.1192
16	0	960	1353	0.000582	892	0.000577	338	667	329	0.1967	0.19147	0.194086	201	423	222	0.1159	0.128	0.122
18	0	1080	1353	0.000582	892	0.000577	370	715	343	0.21533	0.19961	0.207471	210	442	231	0.1211	0.1332	0.1271
19	0	1140	1352	0.000582	892	0.000577	380	732	350	0.22131	0.20384	0.212575	218	452	237	0.1257	0.1367	0.1312
20	0	1200	1354	0.000582	892	0.000577	392	748	356	0.22796	0.20703	0.217495	221	460	241	0.1274	0.139	0.1332
21	40	1300	1354	0.000582	893	0.000576	414	784	366	0.24076	0.21284	0.226799	228	476	250	0.1313	0.144	0.1377
												8.929099						5.4197

			Rx/Rxo	left side	right side	Ry^2	Rx^2/Kx
Rxo	0.003175		23.02071	2795.3	4.41E+13	0.0023	57979028
del P	89667.5		26.61732	3942.4	5.16E+13	0.0032	77510791
visc	0.195		52.59215	19155	2.16E+14	0.0113	3.03E+08
1-vf	0.583761		57.04	23061	2.57E+14	0.0132	3.56E+08
Kx	9.21E-11		59.29638	25194	2.81E+14	0.0142	3.85E+08
Ky	3.53E-11		61.12934	27003	3E+14	0.0149	4.09E+08
Kx/Ky	2.606605		65.34516	31425	3.38E+14	0.0162	4.67E+08
			66.95266	33208	3.56E+14	0.0172	4.9E+08
			68.50222	34978	3.75E+14	0.0177	5.13E+08
			71.43374	38462	4.06E+14	0.019	5.58E+08

Table 30. Experiment SA08-3, A130 0_8.

Lay-up	[0_8]								rel. thick			
Thickness	0.333						# of plys		(cm)			
Fiber Vol.	0.418739					A130	8		1.74E-02			
						D155	0		2.09E-02			
						DB120	0		1.40E-02			

time		total time	x-meas	x-conv	y-meas	y-conv	x-meas dist			left half	right half	average x-radius	y-meas dist	pix		top half	bottom half	average y-radius
min	sec	(sec)	(pix)	m/pix	(pix)	m/pix	left (pix)	elis. (pix)	right (pix)	m	m	m	top	elispe	bottom	m	m	m
9	30	570	1367	0.000576	906	0.000568	337	621	283	0.19411	0.16301	0.178562	173	348	181	0.0982	0.1028	0.1005
10	30	630	1371	0.000574	906	0.000568	347	644	289	0.19929	0.16598	0.182635	180	373	191	0.1022	0.1084	0.1053
11	46	706	1366	0.000576	907	0.000567	365	682	316	0.2104	0.18215	0.196274	187	387	202	0.106	0.1146	0.1103
13	20	800	1369	0.000575	907	0.000567	384	716	332	0.22086	0.19095	0.205909	199	410	212	0.1129	0.1202	0.1165
14	40	880	1368	0.000576	906	0.000568	393	743	351	0.2262	0.20203	0.214118	212	432	221	0.1204	0.1255	0.1229
16	0	960	1368	0.000576	907	0.000567	405	768	363	0.23311	0.20894	0.221025	218	445	229	0.1236	0.1299	0.1267
17	45	1065	1371	0.000574	904	0.000569	417	797	380	0.23949	0.21824	0.228869	228	467	238	0.1297	0.1354	0.1326
19	4	1144	1370	0.000575	907	0.000567	429	813	384	0.24657	0.2207	0.233634	235	475	242	0.1333	0.1372	0.1353
21	5	1265	1370	0.000575	907	0.000567	444	851	410	0.25519	0.23565	0.245416	242	498	255	0.1372	0.1446	0.1409
25	20	1520	1370	0.000575	908	0.000566	489	932	443	0.28105	0.25461	0.267831	266	546	282	0.1507	0.1597	0.1552

			Rx/Rxo	left side	right side	Ry^2	Rx^2/Kx
Rxo	0.003175		56.23994	22329	2.42E+14	0.0101	3.64E+08
del P	89631.49		57.52298	23509	2.68E+14	0.0111	3.81E+08
visc	0.144		61.81845	27701	3E+14	0.0122	4.4E+08
1-vf	0.581261		64.85318	30890	3.4E+14	0.0136	4.84E+08
Kx	8.75E-11		67.4386	33758	3.74E+14	0.0151	5.24E+08
Ky	2.89E-11		69.61404	36279	4.08E+14	0.0161	5.58E+08
Kx/Ky	3.027897		72.08461	39262	4.53E+14	0.0176	5.99E+08
			73.5854	41137	4.86E+14	0.0183	6.24E+08
			77.29635	45978	5.38E+14	0.0199	6.88E+08
			84.3562	56004	6.46E+14	0.0241	8.2E+08

Table 31. Experiment SA09-1, A130 0_9.

Lay-up	$[0_9]$								rel. thick									
Thickness	0.346							# of plys	(cm)									
Fiber Vol.	0.453382						A130	9	1.74E-02									
							D155	0	2.09E-02									
							DB120	0	1.40E-02									
time		total time	x-meas	x-conv	y-meas	y-conv	x-meas dist			left half	right half	average x-radius	y-meas dist	pix		top half	bottom half	average y-radius
min	sec	(sec)	(pix)	m/pix	(pix)	m/pix	left (pix)	elis. (pix)	right (pix)	m	m	m	top	elispe	bottom	m	m	m
0	38	38	1440	0.000547	945	0.000544	73	144	67	0.03992	0.03664	0.038276	39	87	48	0.0212	0.0261	0.0237
1	30	90	1441	0.000546	955	0.000539	102	196	98	0.05574	0.05355	0.054643	58	129	70	0.0312	0.0377	0.0345
2	44	164	1436	0.000548	946	0.000544	125	260	135	0.06854	0.07402	0.071283	80	175	93	0.0435	0.0506	0.047
4	15	255	1441	0.000546	945	0.000544	144	303	158	0.07869	0.08634	0.08251	100	216	115	0.0544	0.0626	0.0585
7	11	431	1442	0.000546	947	0.000543	175	367	189	0.09556	0.1032	0.099381	130	277	145	0.0706	0.0788	0.0747
29	34	1774	1442	0.000546	946	0.000544	314	618	305	0.17146	0.16654	0.169002	243	503	259	0.1321	0.1408	0.1365
30	43	1843	1440	0.000547	944	0.000545	320	628	308	0.17498	0.16842	0.171697	246	507	261	0.134	0.1422	0.1381
32	25	1945	1439	0.000547	945	0.000544	333	648	316	0.18221	0.17291	0.177562	250	517	269	0.1361	0.1464	0.1412
33	8	1988	1441	0.000546	946	0.000544	337	654	319	0.18415	0.17431	0.179228	252	521	271	0.137	0.1473	0.1422
34	15	2055	1443	0.000546	943	0.000545	341	663	321	0.18607	0.17516	0.180616	253	521	270	0.138	0.1473	0.1426

			R_x/R_{xo}	left side	right side	$R_y{}^2$	$R_x{}^2/K_x$
R_{xo}	0.003175		12.05556	579.3	1.27E+13	0.0006	43483229
del P	89667.5		17.21027	1390.4	3E+13	0.0012	88618160
visc	0.195		22.45125	2633.5	5.47E+13	0.0022	1.51E+08
1-vf	0.546618		25.98751	3725.7	8.51E+13	0.0034	2.02E+08
K_x	3.37E-11		31.30097	5769.1	1.44E+14	0.0056	2.93E+08
K_y	2.13E-11		53.22885	19690	5.92E+14	0.0186	8.48E+08
Kx/Ky	1.58311		54.07778	20416	6.15E+14	0.0191	8.75E+08
			55.92495	22044	6.49E+14	0.0199	9.36E+08
			56.44969	22520	6.64E+14	0.0202	9.53E+08
			56.88704	22920	6.86E+14	0.0203	9.68E+08

Table 32. Experiment SB07-1, DB120 0_7.

Lay-up	$[0_7]$								rel. thick									
Thickness	0.345							# of plys	(cm)									
Fiber Vol.	0.284667						A130	0	1.74E-02									
							D155	0	2.09E-02									
							DB120	7	1.40E-02									
time		total time	x-meas	x-conv	y-meas	y-conv	x-meas dist			left half	right half	average x-radius	y-meas dist	pix		top half	bottom half	average y-radius
min	sec	(sec)	(pix)	m/pix	(pix)	m/pix	left (pix)	elis. (pix)	right (pix)	m	m	m	top	elispe	bottom	m	m	m
0	19	19	1361	0.000579	900	0.000579	102	205	103	0.05901	0.05959	0.059301	85	165	80	0.0492	0.0463	0.0477
1	9	69	1362	0.000578	903	0.000577	134	257	125	0.07747	0.07227	0.074867	108	209	101	0.0623	0.0582	0.0603
2	11	131	1361	0.000579	905	0.000575	158	306	149	0.09141	0.0862	0.088807	125	249	124	0.0719	0.0713	0.0716
2	56	176	1365	0.000577	907	0.000574	172	335	163	0.09922	0.09403	0.096622	139	272	133	0.0798	0.0764	0.0781
13	9	789	1374	0.000573	907	0.000574	300	574	276	0.17192	0.15817	0.165045	233	455	223	0.1338	0.128	0.1309
14	9	849	1370	0.000575	905	0.000575	308	591	283	0.17702	0.16265	0.169837	240	469	229	0.1381	0.1318	0.1349
15	9	909	1372	0.000574	906	0.000575	319	609	289	0.18308	0.16586	0.174468	247	483	236	0.142	0.1356	0.1388
17	9	1029	1371	0.000574	908	0.000573	333	637	305	0.19125	0.17517	0.18321	260	507	248	0.1491	0.1422	0.1457
20	39	1239	1340	0.000588	896	0.000581	350	671	321	0.20566	0.18862	0.197144	274	538	265	0.1592	0.154	0.1566
25	9	1509	1341	0.000587	895	0.000582	376	721	346	0.22078	0.20316	0.21197	297	580	285	0.1728	0.1658	0.1693

			R_x/R_{xo}	left side	right side	left side	right side
R_{xo}	0.003175		18.67744	1694.5	2.98E+12	0.0023	24252256.9
del P	55180		23.58003	2959.5	1.08E+13	0.0036	38655028.8
visc	0.195		27.97061	4430.9	2.06E+13	0.0051	54390266.8
1-vf	0.715333		30.43223	5401.2	2.76E+13	0.0061	64385044.4
K_x	1.45E-10		51.98253	18651	1.24E+14	0.0171	187859079
K_y	9.19E-11		53.49197	19914	1.33E+14	0.0182	198927359
Kx/Ky	1.578129		54.95044	21177	1.43E+14	0.0193	209922807
			57.70387	23678	1.62E+14	0.0212	231487282
			62.09254	27981	1.94E+14	0.0245	268037854
			66.76212	32994	2.37E+14	0.0287	309868570

Table 33. Experiment SB08-1, DB120 0$_8$.

Lay-up	[0$_8$]							# of plys	rel. thick (cm)									
Thickness	0.357																	
Fiber Vol.	0.314398						A130	0	1.74E-02									
							D155	0	2.09E-02									
							DB120	8	1.40E-02									

time		total time	x-meas	x-conv	y-meas	y-conv	x-meas dist	elis. (pix)	right (pix)	left half	right half	average x-radius	y-meas dist	pix		top half	bottom half	average y-radius
min	sec	(sec)	(pix)	m/pix	(pix)	m/pix	left (pix)	elis. (pix)	right (pix)	m	m	m	top	elispe	bottom	m	m	m
0	37	37	680	0.000579	933	0.000551	131	251	124	0.07585	0.07179	0.073819	102	205	108	0.0562	0.0595	0.0579
1	30	90	1394	0.000565	928	0.000554	165	320	161	0.0932	0.09094	0.09207	132	261	135	0.0732	0.0748	0.074
2	32	152	1332	0.000591	889	0.000579	168	328	163	0.09931	0.09636	0.097834	138	272	138	0.0798	0.0798	0.0798
9	50	590	1331	0.000592	890	0.000578	282	552	274	0.16683	0.16209	0.164461	222	457	237	0.1283	0.137	0.1326
11	5	665	1331	0.000592	885	0.000581	293	570	286	0.17333	0.16919	0.171264	239	491	247	0.1389	0.1436	0.1412
12	15	735	1330	0.000592	889	0.000579	306	599	297	0.18116	0.17583	0.178497	254	503	253	0.147	0.1464	0.1467
13	8	788	1329	0.000592	886	0.000581	318	621	306	0.18841	0.1813	0.184852	263	519	261	0.1527	0.1515	0.1521
14	25	865	1331	0.000592	890	0.000578	325	636	314	0.19227	0.18576	0.189011	268	532	269	0.1549	0.1555	0.1552
15	1	901	1334	0.00059	889	0.000579	332	645	318	0.19596	0.1877	0.191833	274	541	271	0.1585	0.1568	0.1577
18	30	1110	1331	0.000592	889	0.000579	358	696	342	0.21179	0.20232	0.207055	291	585	294	0.1684	0.1701	0.1692

			R$_x$/R$_{xo}$	left side	right side	left side	right side
R$_{xo}$	0.003175		23.25	2862	9.85E+12	0.0034	48901195
del P	89667.5		28.99857	4823.2	2.4E+13	0.0055	76072306
visc	0.195		30.81381	5561.1	4.05E+13	0.0064	85894325
1-vf	0.685602		51.79865	18500	1.57E+14	0.0176	2.43E+08
K$_x$	1.11E-10		53.9414	20298	1.77E+14	0.0199	2.63E+08
K$_y$	7.48E-11		56.21955	22310	1.96E+14	0.0215	2.86E+08
Kx/Ky	1.489157		58.22122	24165	2.1E+14	0.0231	3.07E+08
			59.53118	25422	2.3E+14	0.0241	3.21E+08
			60.41979	26295	2.4E+14	0.0249	3.3E+08
			65.21412	31282	2.95E+14	0.0286	3.85E+08

Table 34. Experiment SB10-1, DB120 0$_{10}$.

Lay-up	[0$_{10}$]							# of plys	rel. thick (cm)									
Thickness	0.408																	
Fiber Vol.	0.343873						A130	0	1.74E-02									
							D155	0	2.09E-02									
							DB120	10	1.40E-02									

time		total time	x-meas	x-conv	y-meas	y-conv	x-meas dist	elis. (pix)	right (pix)	left half	right half	average x-radius	y-meas dist	pix		top half	bottom half	average y-radius
min	sec	(sec)	(pix)	m/pix	(pix)	m/pix	left (pix)	elis. (pix)	right (pix)	m	m	m	top	elispe	bottom	m	m	m
0	26	26	1314	0.000599	877	0.000586	65	125	61	0.03895	0.03655	0.037752	49	98	50	0.0287	0.0293	0.029
3	0	180	1320	0.000597	880	0.000584	141	278	137	0.08411	0.08172	0.082916	108	214	106	0.0631	0.062	0.0625
4	0	240	1324	0.000595	881	0.000584	159	307	148	0.09456	0.08802	0.091288	119	235	116	0.0695	0.0677	0.0686
22	19	1339	1321	0.000596	883	0.000583	273	540	266	0.16273	0.15855	0.160639	213	421	209	0.1241	0.1217	0.1229
23	10	1390	1319	0.000597	879	0.000585	273	544	272	0.16297	0.16238	0.162674	210	423	213	0.1229	0.1246	0.1238
24	30	1470	1319	0.000597	879	0.000585	279	557	279	0.16655	0.16655	0.166554	218	432	214	0.1276	0.1252	0.1264
25	41	1541	1315	0.000599	877	0.000586	287	566	280	0.17185	0.16766	0.169755	220	437	217	0.129	0.1273	0.1281
26	45	1605	1319	0.000597	880	0.000584	291	575	284	0.17372	0.16954	0.171628	225	443	220	0.1315	0.1286	0.13
28	0	1680	1316	0.000598	881	0.000584	293	583	289	0.17531	0.17292	0.174114	230	451	222	0.1343	0.1296	0.1319
30	3	1803	1318	0.000597	881	0.000584	302	597	296	0.18042	0.17684	0.178629	233	461	227	0.136	0.1325	0.1343

			R$_x$/R$_{xo}$	left side	right side	left side	right side
R$_{xo}$	0.003175		11.89041	559.67	5.56E+12	0.0008	23833304
del P	68975		26.11515	3769.1	3.85E+13	0.0039	1.15E+08
visc	0.195		28.75227	4727.6	5.13E+13	0.0047	1.39E+08
1-vf	0.656127		50.595	17530	2.86E+14	0.0151	4.32E+08
K$_x$	5.98E-11		51.23578	18043	2.97E+14	0.0153	4.43E+08
K$_y$	3.43E-11		52.45792	19044	3.14E+14	0.016	4.64E+08
Kx/Ky	1.74		53.46616	19892	3.3E+14	0.0164	4.82E+08
			54.0561	20397	3.43E+14	0.0169	4.93E+08
			54.83891	21079	3.59E+14	0.0174	5.07E+08
			56.261	22348	3.86E+14	0.018	5.34E+08

Table 35. Experiment SB12-1, DB120 0_{12}.

Lay-up	$[0_{12}]$							# of plys	rel. thick (cm)									
Thickness	0.46																	
Fiber Vol.	0.366						A130	0	1.74E-02									
							D155	0	2.09E-02									
							DB120	12	1.40E-02									
time		total time	x-meas	x-conv	y-meas	y-conv	x-meas dist			left half	right half	average x-radius	y-meas dist	pix		top half	bottom half	average y-radius
min	sec	(sec)	(pix)	m/pix	(pix)	m/pix	left (pix)	elis. (pix)	right (pix)	m	m	m	top	elispe	bottom	m	m	m
0	40	40	798	0.000987	536	0.00096	41	88	46	0.04046	0.04539	0.042922	36	68	33	0.0345	0.0317	0.03311
1	25	85	799	0.000985	535	0.000961	56	113	58	0.05519	0.05716	0.056172	44	89	46	0.0423	0.0442	0.04326
2	10	130	797	0.000988	535	0.000961	64	133	68	0.06323	0.06718	0.065205	51	103	52	0.049	0.05	0.04951
3	15	195	799	0.000985	536	0.00096	75	150	76	0.07391	0.0749	0.074404	59	117	58	0.0566	0.0557	0.05614
5	0	300	798	0.000987	535	0.000961	83	170	88	0.0819	0.08683	0.084364	67	133	68	0.0644	0.0654	0.06489
7	5	425	798	0.000987	535	0.000961	91	189	97	0.08979	0.09571	0.092751	74	147	74	0.0711	0.0711	0.07114
8	36	516	798	0.000987	536	0.00096	97	199	103	0.09571	0.10163	0.098672	79	155	77	0.0758	0.0739	0.07485

			R_x/R_{xo}	left side	right side	R_y^2	R_x^2/K_x
R_{xo}	0.003175		13.5188	770.07	8.86E+12	0.0011	34054279
del P	68975		17.69212	1486.6	1.88E+13	0.00187	58325050
visc	0.195		20.53701	2128.6	2.88E+13	0.00245	78590525
1-vf	0.634		23.43429	2916.2	4.32E+13	0.00315	1.02E+08
K_x	5.41E-11		26.57143	3926.4	6.64E+13	0.00421	1.32E+08
K_y	3.149E-11		29.21303	4907.4	9.41E+13	0.00506	1.59E+08
Kx/Ky	1.7181623		31.07769	5673.3	1.14E+14	0.0056	1.8E+08

Table 36. Experiment SD05-1, D155 0_5.

Lay-up	$[0_5]$							# of plys	rel. thick (cm)									
Thickness	0.315																	
Fiber Vol.	0.331429						A130	0	1.74E-02									
							D155	5	2.09E-02									
							DB120	0	1.40E-02									
time		total time	x-meas	x-conv	y-meas	y-conv	x-meas dist			left half	right half	average x-radius	y-meas dist	pix		top half	bottom half	average y-radius
min	sec	(sec)	(pix)	m/pix	(pix)	m/pix	left (pix)	elis. (pix)	right (pix)	m	m	m	top	elispe	bottom	m	m	m
0	33	33	799	0.000985	537	0.000958	98	202	105	0.09658	0.10348	0.100026	28	79	43	0.0268	0.0412	0.034
2	17	137	799	0.000985	537	0.000958	176	374	200	0.17344	0.1971	0.185271	69	139	71	0.0661	0.068	0.067
3	20	200	798	0.000987	538	0.000956	210	442	231	0.20721	0.22793	0.217571	81	162	82	0.0774	0.0784	0.0779
4	16	256	799	0.000985	536	0.00096	233	489	257	0.22962	0.25327	0.241443	90	178	89	0.0864	0.0854	0.0859
5	30	330	799	0.000985	537	0.000958	259	541	283	0.25524	0.27889	0.267066	101	196	95	0.0967	0.091	0.0939
7	0	420	799	0.000985	538	0.000956	292	609	316	0.28776	0.31141	0.299586	113	224	109	0.108	0.1042	0.1061
8	30	510	799	0.000985	537	0.000958	332	672	350	0.32718	0.34492	0.336049	124	241	119	0.1188	0.114	0.1164
10	11	611	799	0.000985	536	0.00096	350	726	376	0.34492	0.37054	0.35773	136	262	129	0.1305	0.1238	0.1271
11	20	680	799	0.000985	537	0.000958	368	759	391	0.36266	0.38532	0.37399	142	276	135	0.136	0.1293	0.1327
12	20	740	798	0.000987	537	0.000958	377	781	405	0.37199	0.39962	0.385806	144	282	136	0.1379	0.1303	0.1341

			R_x/R_{xo}	left side	right side	R_y^2	R_x^2/K_x
R_{xo}	0.003175		31.50438	5857.2	6.93E+12	0.0012	12047985
del P	68975		58.35294	24289	2.88E+13	0.0045	41333106
visc	0.195		68.52632	35006	4.2E+13	0.0061	57001634
1-vf	0.668571		76.04506	44313	5.37E+13	0.0074	70196347
K_x	8.3E-10		84.11514	55644	6.93E+13	0.0088	85885713
K_y	1.03E-10		94.35795	72067	8.82E+13	0.0113	1.08E+08
Kx/Ky	8.074516		105.8423	93250	1.07E+14	0.0135	1.36E+08
			112.6708	107258	1.28E+14	0.0162	1.54E+08
			117.7922	118464	1.43E+14	0.0176	1.68E+08
			121.5138	126986	1.55E+14	0.018	1.79E+08

Table 37. Experiment SD06-1, D155 0₆.

Table 37. Experiment SD06-1, D155 0_6.

Lay-up	[0₆]							rel. thick									
Thickness	0.315						# of plys	(cm)									
Fiber Vol.	0.397714					A130	0	1.74E-02									
						D155	6	2.09E-02									
						DB120	0	1.40E-02									
time		total time	x-meas	x-conv	y-meas	y-conv	x-meas dist			left half	right half	average x-radius	y-meas dist	pix		top half	bottom half	average y-radius
min	sec	(sec)	(pix)	m/pix	(pix)	m/pix	left (pix)	elis. (pix)	right (pix)	m	m	m	top	elispe	bottom	m	m	m
0	20	20	1344	0.000586	896	0.000574	139	268	132	0.08143	0.07733	0.079384	44	79	33	0.0253	0.0189	0.0221
1	32	92	1344	0.000586	899	0.000572	268	543	275	0.15701	0.16111	0.159062	83	157	70	0.0475	0.04	0.0438
3	25	205	1345	0.000585	896	0.000574	373	778	404	0.21836	0.23651	0.227439	120	224	101	0.0689	0.058	0.0634
4	14	254	1348	0.000584	901	0.000571	401	860	454	0.23423	0.26519	0.249713	134	249	112	0.0765	0.0639	0.0702
5	36	336	1347	0.000585	898	0.000573	457	973	515	0.26714	0.30105	0.284095	150	276	125	0.0859	0.0716	0.0788
6	0	360	1346	0.000585	899	0.000572	476	1000	523	0.27846	0.30595	0.292204	151	277	127	0.0864	0.0727	0.0795
7	0	420	1347	0.000585	896	0.000574	519	1070	552	0.30339	0.32268	0.313031	168	305	135	0.0964	0.0775	0.087
8	17	497	1346	0.000585	902	0.00057	567	1150	585	0.33169	0.34222	0.336956	180	326	146	0.1026	0.0833	0.0929
9	20	560	1348	0.000584	899	0.000572	580	1210	628	0.33879	0.36683	0.352811	193	347	154	0.1104	0.0881	0.0993
10	45	645	1346	0.000585	900	0.000572	620	1273	655	0.3627	0.38317	0.372933	206	365	163	0.1177	0.0932	0.1054
										14.2793	15.0854	14.68239						
				Rₓ/Rₓₒ	left side	right side	Rᵧ^2	Rₓ^2/Kₓ										
Rₓₒ	0.003175			25.00298	3400.6	6.06E+12	0.0005	10231514										
del P	89667.5			50.09821	17138	2.79E+13	0.0019	41077213										
visc	0.195			71.6342	38708	6.21E+13	0.004	83984147										
1-vf	0.602286			78.64985	47817	7.69E+13	0.0049	1.01E+08										
Kₓ	6.16E-10			89.47884	63957	1.02E+14	0.0062	1.31E+08										
Kᵧ	4.8E-11			92.03269	68136	1.09E+14	0.0063	1.39E+08										
Kx/Ky	12.84345			98.59243	79534	1.27E+14	0.0076	1.59E+08										
				106.1278	93815	1.51E+14	0.0086	1.84E+08										
				111.1217	103987	1.7E+14	0.0099	2.02E+08										
				117.4591	117717	1.95E+14	0.0111	2.26E+08										

Table 38. Experiment SD08-1, D155 0₈.

Table 38. Experiment SD08-1, D155 0_8.

Lay-up	[0₈]							rel. thick									
Thickness	0.366						# of plys	(cm)									
Fiber Vol.	0.456393					A130	0	1.74E-02									
						D155	8	2.09E-02									
						DB120	0	1.40E-02									
time		total time	x-meas	x-conv	y-meas	y-conv	x-meas dist			left half	right half	average x-radius	y-meas dist	pix		top half	bottom half	average y-radius
min	sec	(sec)	(pix)	m/pix	(pix)	m/pix	left (pix)	elis. (pix)	right (pix)	m	m	m	top	elispe	bottom	m	m	m
0	34	34	1416	0.000556	946	0.000544	145	288	146	0.08063	0.08119	0.080909	32	74	40	0.0174	0.0217	0.0196
3	50	230	1427	0.000552	953	0.00054	300	590	291	0.16554	0.16057	0.163053	79	159	80	0.0426	0.0432	0.0429
5	0	300	1430	0.000551	954	0.000539	346	685	345	0.19052	0.18997	0.190242	90	181	89	0.0485	0.048	0.0483
6	0	360	1429	0.000551	955	0.000539	367	733	365	0.20222	0.20112	0.201671	99	192	94	0.0533	0.0506	0.052
8	48	528	1466	0.000537	968	0.000531	461	906	445	0.24761	0.23901	0.24331	112	226	110	0.0595	0.0584	0.059
10	1	601	1461	0.000539	964	0.000534	474	943	468	0.25546	0.25223	0.253844	118	236	115	0.063	0.0614	0.0622
10	50	650	1468	0.000536	966	0.000532	502	975	476	0.26926	0.25531	0.262288	122	238	117	0.065	0.0623	0.0636
11	48	708	1469	0.000536	968	0.000531	520	1005	490	0.27873	0.26265	0.270686	124	244	119	0.0659	0.0632	0.0646
13	33	813	1468	0.000536	969	0.000531	554	1069	514	0.29715	0.2757	0.286425	131	255	125	0.0695	0.0664	0.0679
15	41	941	1467	0.000537	966	0.000532	579	1129	550	0.31077	0.29521	0.302991	136	267	131	0.0724	0.0698	0.0711
18	0	1080	1471	0.000535	967	0.000532	606	1188	582	0.32438	0.31153	0.317958	140	276	136	0.0745	0.0723	0.0734
										12.7709	12.2651	12.51801						
				Rₓ/Rₓₒ	left side	right side	Rᵧ^2	Rₓ^2/Kₓ										
Rₓₒ	0.003175			25.48305	3557.1	1.14E+13	0.0004	27123052										
del P	89667.5			51.35529	18140	7.72E+13	0.0018	1.1E+08										
visc	0.195			59.91888	25801	1.01E+14	0.0023	1.5E+08										
1-vf	0.543607			63.51854	29464	1.21E+14	0.0027	1.69E+08										
Kₓ	2.41E-10			76.63302	45091	1.77E+14	0.0035	2.45E+08										
Kᵧ	1.4E-11			79.95072	49622	2.02E+14	0.0039	2.67E+08										
Kx/Ky	17.22166			82.61035	53425	2.18E+14	0.004	2.85E+08										
				85.25528	57359	2.38E+14	0.0042	3.04E+08										
				90.21253	65143	2.73E+14	0.0046	3.4E+08										
				95.43013	73920	3.16E+14	0.0051	3.8E+08										
				100.1441	82370	3.63E+14	0.0054	4.19E+08										

Table 39. Experiment SD09-1, D155 0_9.

Lay-up	$[0_9]$								# of plys	rel. thick (cm)
Thickness	0.403						A130	0		1.74E-02
Fiber Vol.	0.466303						D155	9		2.09E-02
							DB120	0		1.40E-02

time min	sec	total time (sec)	x-meas (pix)	x-conv m/pix	y-meas (pix)	y-conv m/pix	x-meas dist left (pix)	elis. (pix)	right (pix)	left half m	right half m	average x-radius m	y-meas dist top	pix elispe	bottom	top half m	bottom half m	average y-radius m
0	27	27	1372	0.000574	909	0.000566	139	267	130	0.07977	0.07461	0.07719	31	60	30	0.0175	0.017	0.0173
4	0	240	1361	0.000579	905	0.000568	279	576	288	0.16141	0.16662	0.164018	67	137	71	0.0381	0.0404	0.0392
5	30	330	1369	0.000575	907	0.000567	315	627	313	0.18118	0.18003	0.180602	76	152	77	0.0431	0.0437	0.0434
7	0	420	1362	0.000578	910	0.000565	347	689	340	0.20061	0.19656	0.198584	82	165	84	0.0463	0.0475	0.0469
8	31	511	1364	0.000577	907	0.000567	371	726	358	0.21417	0.20666	0.210416	88	177	91	0.0499	0.0516	0.0508
10	5	605	1364	0.000577	909	0.000566	394	776	380	0.22745	0.21936	0.223405	92	186	96	0.0521	0.0543	0.0532
11	43	703	1365	0.000577	909	0.000566	420	819	402	0.24228	0.23189	0.237085	96	199	102	0.0543	0.0577	0.056
13	3	783	1363	0.000578	910	0.000565	428	840	418	0.24725	0.24148	0.244366	101	204	105	0.0571	0.0593	0.0582
14	45	885	1349	0.000584	910	0.000565	442	873	431	0.25799	0.25157	0.254781	104	215	110	0.0588	0.0622	0.0605
17	2	1022	1349	0.000584	910	0.000565	467	921	457	0.27258	0.26675	0.269666	111	224	114	0.0627	0.0644	0.0636

			R_x/R_{xo}	left side	right side	$R_y{}^2$	$R_x{}^2/K_x$
R_{xo}	0.003175		24.31195	3182.1	9.23E+12	0.0003	34438121
del P	89667.5		51.65907	18386	8.21E+13	0.0015	1.55E+08
visc	0.195		56.8824	22915	1.13E+14	0.0019	1.89E+08
1-vf	0.533697		62.54626	28449	1.44E+14	0.0022	2.28E+08
K_x	1.73E-10		66.27273	32448	1.75E+14	0.0026	2.56E+08
K_y	9.76E-12		70.36364	37170	2.07E+14	0.0028	2.88E+08
Kx/Ky	17.73029		74.67253	42525	2.4E+14	0.0031	3.25E+08
			76.96552	45535	2.68E+14	0.0034	3.45E+08
			80.24611	50037	3.03E+14	0.0037	3.75E+08
			84.93403	56873	3.49E+14	0.004	4.2E+08

Mixed Fabric Experiments

Table 40. Experiment MA01-1, A130 $[0/90_2/0]s$

Date: 7-27-99					rel. thick (cm)				
Lay-up: $[0/90_2/0]s$				# of plys					
Thickness	0.349		A130	8	1.74E-02				
Fiber Vol.	0.399542		D155	0	2.09E-02				
			DB120	0	1.40E-02				

time min	sec	total time (sec)	x-meas (pix)	x-conv m/pix	y-meas (pix)	y-conv m/pix	x-meas dist left (pix)	elis. (pix)	right (pix)	ex. port 2 inj. Port pix	left half m	right half m	average x-radius m	y-meas dist top	pix elispe	bottom	Gasket 2 inj port pix	top half m	bottom half m	average y-radius m
0	52	52	432	0.001823	294	0.001771	175	72	186	216	0.07473	0.054681	0.064705	126	39	131	147	0.0372	0.0283	0.0328
3	54	234	436	0.001806	297	0.001753	126	178	132	218	0.16615	0.155313	0.160731	98	98	102	148.5	0.0885	0.0815	0.085
4	54	294	435	0.00181	296	0.001759	118	200	124	217.5	0.18011	0.169246	0.174676	92	111	96	148	0.0985	0.0915	0.095
7	5	425	435	0.00181	297	0.001753	102	222	110	217.5	0.20907	0.194587	0.201828	79	136	83	148.5	0.1218	0.1148	0.1183
9	3	543	435	0.00181	296	0.001759	93	243	100	217.5	0.22536	0.212689	0.219024	71	153	73	148	0.1355	0.1319	0.1337
10	51	651	435	0.00181	296	0.001759	85	259	92	217.5	0.23984	0.227169	0.233505	62	169	65	148	0.1513	0.146	0.1486
14	15	855	434	0.001814	297	0.001753	70	287	77	217	0.2667	0.254	0.26035	50	195	53	148.5	0.1727	0.1674	0.1701
17	9	1029	434	0.001814	296	0.001759	61	307	67	217	0.28303	0.272143	0.277586	41	212	43	148	0.1882	0.1847	0.1865
18	1	1081	437	0.001802	297	0.001753	59	314	65	218.5	0.28739	0.276581	0.281986	39	218	41	148.5	0.192	0.1885	0.1902
20	5	1205	438	0.001798	298	0.001747	51	328	58	219	0.30202	0.289432	0.295724	34	232	34	149	0.2009	0.2009	0.2009
21	20	1280	437	0.001802	298	0.001747	47	336	55	218.5	0.30901	0.294599	0.301807	30	238	31	149	0.2079	0.2062	0.2071
27	9	1629	435	0.00181	295	0.001765	27	374	34	217.5	0.34483	0.332156	0.338491	12	271	12	147.5	0.2392	0.2392	0.2392

			R_x/R_{xo}	left side	right side	$R_y{}^2$	$R_x{}^2/K_x$
			20.37963	2089.7	1.46E+13	0.001074	2E+07
			50.62385	17553	6.56E+13	0.00723	1.2E+08
			55.01609	21235	8.24E+13	0.009024	1.4E+08
R_{xo}	0.003175		63.56782	29516	1.19E+14	0.014005	1.9E+08
del P	89667.5		68.98391	35538	1.52E+14	0.017874	2.3E+08
visc	0.195		73.54483	41085	1.82E+14	0.022096	2.6E+08
1-vf	0.651		82	52539	2.4E+14	0.02892	3.2E+08
K_x	2.11E-10		87.42857	60705	2.88E+14	0.03477	3.6E+08
K_y	9.54E-11		88.81465	62893	3.03E+14	0.036184	3.8E+08
Kx/Ky	2.213938		93.14155	69996	3.38E+14	0.040377	4.1E+08
			95.05721	73273	3.59E+14	0.042873	4.3E+08
			106.6115	94775	4.57E+14	0.057202	5.4E+08

Table 41. Experiment MA01-2, A130 [0/90₂/0]s

Date: 7-28-99-2						rel. thick															
Lay-up: [0/90₂/0]s				# of plys	(cm)																
Thickness	0.331		A130	8	1.74E-02																
Fiber Vol.	0.4213		D155	0	2.09E-02																
			DB120	0	1.40E-02																

time		total time	x-meas	x-conv	y-meas	y-conv	x-meas dist			calib. Dist. x	left half	right half	average x-radius	y-meas dist	pix		calib. Dist. Ytop		top half	bottom half	average y-radius
min	sec	sec	pix	m/pix	pix	m/pix	left	elispe	right	pix	pix	pix	m	top	center	bottom	pix		m	m	m
0	50	50	1432	5.50E-04	912	5.50E-04	621	169	654	716	95	62	0.0432	366	158	391	438.68	473.32	72.684	82.316	0.0426
1	30	90	1432	5.50E-04	914	5.49E-04	579	313	541	716	137	175	0.0858	345	206	366	439.65	474.35	94.646	108.35	0.0557
2	40	160			918	5.46E-04								313	266	342	441.57	476.43	128.57	134.43	0.0719
8	10	490	1437	5.48E-04	915	5.48E-04	413	652	373	718.5	305.5	345.5	0.1784	215	452	249	440.13	474.87	225.13	225.87	0.1236
10	0	600	1437	5.48E-04	948	5.49E-04	385	718	336	718.5	333.5	382.5	0.1962	227	497	228	474		247	246	0.1354
12	40	760	721	5.46E-04	949	5.49E-04	362	779	303	721	362	418	0.213	209	543	201	474.5		265.5	273.5	0.1479
16	5	965	1436	5.48E-04	949	5.49E-04	318	855	265	718	400	453	0.2339	173	610	167	474.5		301.5	307.5	0.1671
30	0	1800	723	5.45E-04	953	5.46E-04	543	1126	139	723	543	584	0.3068	69	817	68	476.5		407.5	408.5	0.2229

			Rx/Rxo	left side	right side		Ry^2	Rx^2/Kx
Rxo	0.003175		13.595	780.8433	1E+13		0.0018	1.14E+07
del P	86218.75		27.017	4083.298	2E+13		0.0031	4.50E+07
visc	0.195		56.175	22270.44	1E+14		0.0153	1.94E+08
1-vf	0.669		61.784	27666.08	2E+14		0.0183	2.35E+08
			67.074	33344.62	2E+14		0.0219	2.77E+08
Kx	1.64E-10		73.657	41227.87	3E+14		0.0279	3.34E+08
Ky	8.36E-11		96.645	76049.38	5E+14		0.0497	5.76E+08
Kx/Ky	1.96E+00							

Table 42. Experiment MA02-1, A130 [(90/0)₂]s

Date: 7-28-99-1						rel. thick															
Lay-up: [(90/0)₂]s				# of plys	(cm)																
Thickness	0.33		A130	8	1.74E-02																
Fiber Vol.	0.4225		D155	0	2.09E-02																
			DB120	0	1.40E-02																

time		total time	x-meas	x-conv	y-meas	y-conv	x-meas dist			calib. Dist. x	left half	right half	average x-radius	y-meas dist	pix		calib. Dist. Y	top half	bottom half	average y-radius
min	sec	sec	pix	m/pix	pix	m/pix	left	elispe	right						top	center	bottom			
0	15	15	450	1.75E-03	305	1.71E-03	203	34	213	225.0	22.0	12.0	0.021	134	44	129	148.8	14.8	19.8	0.0295
1	1	61	448	1.76E-03	305	1.71E-03	189	58	203	224.0	35.0	21.0	0.0369	122	61	124	148.8	26.8	24.8	0.044
2	35	155	449	1.75E-03	305	1.71E-03	176	88	187	224.5	48.5	37.5	0.0658	110	88	108	148.8	38.8	40.8	0.0679
3	30	210	449	1.75E-03	304	1.71E-03	171	99	180	224.5	53.5	44.5	0.078	104	99	103	148.3	44.3	45.3	0.0767
4	40	280	449	1.75E-03	306	1.70E-03	164	109	174	224.5	60.5	50.5	0.0886	100	109	99	149.3	49.3	50.3	0.0847
18	48	1128	432	1.82E-03	294	1.77E-03	118	184	131	216.0	98.0	85.0	0.1549	59	176	60	143.4	84.4	83.4	0.1486
20	38	1238	433	1.82E-03	295	1.77E-03	116	188	129	216.5	100.5	87.5	0.1591	55	183	56	143.9	88.9	87.9	0.156
28	1	1681	432	1.82E-03	294	1.77E-03	102	216	116	216.0	114.0	100.0	0.1823	43	207	46	143.4	100.4	97.4	0.1752
38	50	2330	433	1.82E-03	294	1.77E-03	87	244	101	216.5	129.5	115.5	0.21	27	238	30	143.4	116.4	113.4	0.2035
42	56	2576	433	1.82E-03	294	1.77E-03	83	256	97	216.5	133.5	119.5	0.2173	22	246	27	143.4	121.4	116.4	0.2106

				Rx/Rxo	left side	right side		Ry^2	Rx^2/Kx
Rxo	0.003175			6.613333	122.507	5E+12		0.0009	1E+07
del P	89667.5			11.625	528.902	2E+13		0.0019	3.1E+07
visc	0.195			20.71269	2172.46	5E+13		0.0046	9.9E+07
1-vf	0.577455			24.57906	3265.59	7E+13		0.0059	1.4E+08
				27.8931	4402.1	9E+13		0.0072	1.8E+08
Kx	4.37E-11			48.7963	16133.5	4E+14		0.0221	5.5E+08
Ky	4.09E-11			50.11547	17151.6	4E+14		0.0243	5.8E+08
Kx/Ky	1.07E+00			57.40741	23401	5E+14		0.0307	7.6E+08
				66.15242	32314.1	7E+14		0.0414	1E+09
				68.44342	34910	8E+14		0.0444	1.1E+09

Table 43. Experiment MA03-1, A130 [0/90/0/$\overline{90}$]s.

Date: 7-30-99					rel. thick (cm)													
Lay-up: [90/0/90/0/90/0/90]				# of plys														
Thickness	0.341		A130	7	1.74E-02													
Fiber Vol.	0.3578		D155	0	2.09E-02													
			DB120	0	1.40E-02													

time		total time	x-meas	x-conv	y-meas	y-conv	x-meas dist			calib. Dist. x	left half	right half	average x-radius	y-meas dist			calib. Dist. Y	top half	bottom half	average y-radius
min	sec	sec	pix	m/pix	pix	m/pix	left	elispe	right	pix	m	m	m	top	center	bottom	pix	m	m	m
0	12	12	1442	5.46E-04	951	5.48E-04	656	115	671	721.0	0.0355	0.0273	0.0314	372	220	362	475.5	0.0567	0.0621	0.0594
1	0	60	1445	5.45E-04	952	5.47E-04	631	177	639	722.5	0.0499	0.0455	0.0477	320	322	311	476.0	0.0853	0.0902	0.0878
1	30	90	1439	5.47E-04	951	5.48E-04	598	225	618	719.5	0.0665	0.0555	0.061	272	467	216	475.5	0.1114	0.1421	0.1268
2	0	120	1436	5.48E-04	952	5.47E-04	572	269	596	718.0	0.0801	0.0669	0.0735	247	522	185	476.0	0.1253	0.1592	0.1422
2	30	150	1443	5.46E-04	954	5.46E-04	570	301	573	721.5	0.0827	0.081	0.0819	222	557	175	477.0	0.1392	0.1648	0.152

			Rx/Rxo	left side	right side		Ry^2	Rx^2/Kx
R_{xo}	0.003175		9.889	351.3787	3E+12		0.0035	1.22E+07
del P	89667.5		15.017	997.4359	2E+13		0.0077	2.82E+07
visc	0.195		19.216	1814.617	3E+13		0.0161	4.62E+07
1-vf	0.642199		23.142	2830.5	3E+13		0.0202	6.70E+07
			25.78	3655.688	4E+13		0.0231	8.32E+07
K_x	8.05E-11							
K_y	2.95E-10							
Kx/Ky	3.67E+00							

Table 44. Experiment MA03-2, A130 [0/90/0/$\overline{90}$]s.

Lay-up: [0/90/0/90/0/90/0]							rel. thick (cm)											
Thickness	0.338					# of plys												
Fiber Vol.	0.360976					A130	7	1.74E-02										
						D155	0	2.09E-02										
						DB120	0	1.40E-02										

time		total time	x-meas	x-conv	y-meas	y-conv	x-meas dist			left half	right half	average x-radius	y-meas dist	pix		top half	bottom half	average y-radius
min	sec	(sec)	(pix)	m/pix	(pix)	m/pix	left (pix)	elis. (pix)	right (pix)	m	m	m	top	elispe	bottom	m	m	m
0	24	24	1346	0.000585	898	0.000573	79	141	60	0.04621	0.0351	0.040657	57	112	53	0.0326	0.0304	0.0315
0	54	54	1348	0.000584	901	0.000571	144	291	140	0.08411	0.08178	0.082946	88	179	90	0.0502	0.0514	0.0508
3	1	181	1344	0.000586	897	0.000573	279	563	285	0.16346	0.16697	0.165213	159	329	169	0.0912	0.0969	0.094
4	0	240	1345	0.000585	900	0.000572	307	625	320	0.17973	0.18734	0.183532	185	376	194	0.1057	0.1109	0.1083
5	20	320	1346	0.000585	898	0.000573	353	701	355	0.2065	0.20767	0.207087	212	436	226	0.1214	0.1294	0.1254
6	30	390	1347	0.000585	898	0.000573	383	760	378	0.22389	0.22096	0.222424	238	489	250	0.1363	0.1432	0.1398
8	0	480	1344	0.000586	896	0.000574	414	824	411	0.24255	0.24079	0.241669	263	540	279	0.151	0.1602	0.1556
9	25	565	1346	0.000585	901	0.000571	447	893	445	0.26149	0.26032	0.260907	290	593	305	0.1656	0.1741	0.1698
11	0	660	1346	0.000585	899	0.000572	481	955	475	0.28138	0.27787	0.279626	315	650	334	0.1802	0.1911	0.1857
15	0	900	1348	0.000584	901	0.000571	560	1102	543	0.32711	0.31718	0.322145	369	762	392	0.2106	0.2238	0.2172

			R_x/R_{xo}	left side	right side	R_y^2	R_x^2/K_x
R_{xo}	0.003175		12.80535	673.26	6.85E+12	0.001	5011284
del P	89667.5		26.12463	3772.3	1.54E+13	0.0026	20857701
visc	0.195		52.03571	18695	5.17E+13	0.0088	82750230
1-vf	0.639024		57.8052	23773	6.85E+13	0.0117	1.02E+08
K_x	3.3E-10		65.22437	31294	9.14E+13	0.0157	1.3E+08
K_y	1.4E-10		70.05494	36802	1.11E+14	0.0195	1.5E+08
Kx/Ky	2.347823		76.11607	44407	1.37E+14	0.0242	1.77E+08
			82.17533	52792	1.61E+14	0.0288	2.06E+08
			88.07132	61714	1.88E+14	0.0345	2.37E+08
			101.4629	84823	2.57E+14	0.0472	3.15E+08

Table 45. Experiment MA04-1, A130/DB120 [0/±45/0]s.

Date: 8-1-99					rel. thick															
Lay-up: [0/+-45₂/0]ₛ				# of plys	(cm)															
Thickness	0.34		A130	4	1.74E-02															
Fiber Vol.	0.3701		D155	0	2.09E-02															
			DB120	4	1.40E-02															
time		total time	x-meas	x-conv	y-meas	y-conv	x-meas dist			calib. Dist. x	left half	right half	average x-radius	y-meas dist	pix		calib. Dist. Y	top half	bottom half	average y-radius
min	sec	sec	pix	m/pix	pix	m/pix	left	elispe	right	pix	m	m	m	top	center	bottom	pix	m	m	m
1	25	85	1399	5.63E-04	933	5.58E-04	551	302	548	699.5	0.0836	0.08527	0.0844	339	235	335	466.5	0.0712	0.0734	0.0723
1	59	119	1396	5.64E-04	925	5.63E-04	526	343	526	698	0.097	0.09701	0.097	321	264	340	462.5	0.0797	0.069	0.0743
7	27	447	1400	5.62E-04	926	5.62E-04	407	592	401	700	0.1648	0.16817	0.1665	224	461	243	463	0.1344	0.1237	0.1291
9	20	560	1397	5.64E-04	927	5.62E-04	373	651	375	698.5	0.1835	0.18234	0.1829	201	502	226	463.5	0.1474	0.1334	0.1404
13	30	810	1397	5.64E-04	925	5.63E-04	313	766	320	698.5	0.2173	0.21334	0.2153	158	592	176	462.5	0.1714	0.1613	0.1663
15	1	901	1401	5.62E-04	928	5.61E-04	305	803	297	700.5	0.2223	0.22678	0.2245	146	618	165	464	0.1784	0.1678	0.1731
19	10	1150	1400	5.62E-04	929	5.60E-04	252	901	249	700	0.252	0.25366	0.2528	110	695	126	464.5	0.1987	0.1897	0.1942
21	31	1291	1397	5.64E-04	927	5.62E-04	224	947	228	698.5	0.2674	0.26519	0.2663	93	727	110	463.5	0.2081	0.1986	0.2033
25	23	1523	1401	5.62E-04	929	5.60E-04	183	1027	191	700.5	0.2908	0.28635	0.2886	64	783	81	464.5	0.2245	0.2149	0.2197
30	0	1800	1398	5.63E-04	927	5.62E-04	132	1113	153	699	0.3194	0.30753	0.3134	35	850	47	463.5	0.2407	0.2339	0.2373
			Rx/Rxo	left side	right side		Ry^2	Rx^2/Kx												
Rₓₒ	0.003175		26.59	3932.98	2E+13		5.22E-03	4.77E+07												
del P	89667.5		30.556	5452.755	3E+13		5.52E-03	6.30E+07												
visc	0.195		52.434	19024.12	1E+14		1.67E-02	1.85E+08												
1-vf	0.629882		57.606	23586.35	2E+14		1.97E-02	2.24E+08												
			67.814	34185.77	2E+14		2.77E-02	3.10E+08												
Kx	1.49E-10		70.718	37595.86	3E+14		3.00E-02	3.37E+08												
Ky	8.71E-11		79.626	49167.61	3E+14		3.77E-02	4.28E+08												
Kx/Ky	1.72E+00		83.88	55293.81	4E+14		4.13E-02	4.75E+08												
			90.898	66261.38	4E+14		4.83E-02	5.57E+08												
			98.721	79766.78	5E+14		5.63E-02	6.58E+08												

Table 46. Experiment MA05-1, A130/DB120 [0/±45/90]s.

Date: 8-2-99					rel. thick															
Lay-up: [0/+-45₂/90]ₛ				# of plys	(cm)															
Thickness	0.366		A130	4	1.74E-02															
Fiber Vol.	0.343825		D155	0	2.09E-02															
			DB120	4	1.40E-02															
time		total time	x-meas	x-conv	y-meas	y-conv	x-meas dist			calib. Dist. x	left half	right half	average x-radius	y-meas dist	pix		calib. Dist. Y	top half	bottom half	average y-radius
min	sec	sec	pix	m/pix	pix	m/pix	left	elispe	right	pix	m	m	m	top	center	bottom	pix	m	m	m
0	33	33	1422	5.54E-04	943	5.52E-04	586	223	615	711	0.06922	0.05316	0.0612	380	172	393	471.5	0.0505	0.0433	0.0469
1	25	85	1420	5.55E-04	944	5.52E-04	537	318	566	710	0.09593	0.07985	0.0879	348	238	359	472	0.0684	0.0623	0.0654
3	46	226	1426	5.52E-04	944	5.52E-04	417	563	447	713	0.16344	0.14688	0.1552	259	419	269	472	0.1175	0.112	0.1147
5	0	300	1424	5.53E-04	942	5.53E-04	373	639	415	712	0.18745	0.16423	0.1758	234	469	242	471	0.131	0.1266	0.1288
15	21	921	540	1.46E-03	367	1.42E-03	51	431	60	270	0.31933	0.30621	0.3128	25	312	32	183.5	0.2249	0.2149	0.2199
16	3	963	540	1.46E-03	366	1.42E-03	47	439	56	270	0.32517	0.31204	0.3186	23	317	29	183	0.2276	0.2191	0.2234
16	59	1019	540	1.46E-03	367	1.42E-03	40	452	50	270	0.33537	0.32079	0.3281	19	324	26	183.5	0.2334	0.2235	0.2284
		9																		
			Rx/Rxo	left side	right side		Ry^2	Rx^2/Kx												
			19.271	1827.21	9.18E+12		0.0022	1E+07												
Rₓₒ	0.00318		27.682	4323.98	2.36E+13		0.0043	3E+07												
del P	89667.5		48.87	16189.2	6.28E+13		0.0132	8E+07												
visc	0.195		55.382	21558.6	8.34E+13		0.0166	1E+08												
1-vf	0.65617		98.511	79386.6	2.56E+14		0.0484	3E+08												
			100.35	82747.1	2.68E+14		0.0499	3E+08												
Kx	3.08E-10		103.33	88369.4	2.83E+14		0.0522	4E+08												
Ky	1.51E-10				2.50E+12															
Kx/Ky	2.03E+00																			

Table 47. Experiment MD01-1, D155 [0/90$_2$/0]s.

Lay-up	[0/90$_2$/0]s								rel. thick				a130	db120	thick	vf	
Thickness	0.373							# of plys	(cm)			web	4	8	0.511	0.3561	
Fiber Vol.	0.4478						A130	0	1.74E-02			flange	14	16	1.33	0.3523	
							D155	8	2.09E-02			skin	4	2	0.281	0.348	
							DB120	0	1.40E-02								

time		total time	x-meas	x-conv	y-meas	y-conv	x-meas dist			calib. Dist. x	left half	right half	averag e x-radius	y-meas dist	pix		calib. Dist. Y	top half	bottom half	averag e y-radius
min	sec	sec	pix	m/pix	pix	m/pix	left	elispe	right	pix	m	m	m	top	center	bottom	pix	m	m	m
0	32	32	444	1.77E-03	301	1.73E-03	188	74	183	222	0.060296	0.0692	0.0647	105	80	117	150.5	0.0787	0.058	0.0683
1	0	60	445	1.77E-03	302	1.72E-03	177	97	172	222.5	0.080509	0.0894	0.0849	92	93	104	151	0.1017	0.081	0.0914
1	25	85	445	1.77E-03	302	1.72E-03	168	112	165	222.5	0.096434	0.1017	0.0991	86	121	96	151	0.1121	0.0948	0.1035
4	58	298	439	1.79E-03	299	1.74E-03	128	188	125	219.5	0.164116	0.1695	0.1668	49	192	59	149.5	0.175	0.1576	0.1663
6	4	364	440	1.79E-03	299	1.74E-03	119	205	117	220	0.180744	0.1843	0.1825	41	212	48	149.5	0.1889	0.1768	0.1829
7	15	435	441	1.79E-03	300	1.74E-03	110	224	108	220.5	0.197296	0.2009	0.1991	34	227	41	150	0.2013	0.1892	0.1953
8	30	510	441	1.79E-03	299	1.74E-03	101	240	101	220.5	0.213366	0.2134	0.2134	27	242	32	149.5	0.2133	0.2046	0.209

			Rx/Rxo	left side	right side		Ry^2	Rx^2/Kx												
R$_{xo}$	0.003175		20.387	2091.63	1E+13		0.0047	2.12E+07												
del P	89667.5		26.751	3989.08	2E+13		0.0084	3.65E+07												
visc	0.195		31.209	5729.5	3E+13		0.0107	4.97E+07												
1-vf	0.552172		52.538	19110	1E+14		0.0277	1.41E+08												
			57.491	23478.7	1E+14		0.0334	1.69E+08												
Kx	1.98E-10		62.703	28611	1E+14		0.0381	2.01E+08												
Ky	1.93E-10		67.202	33489.6	2E+14		0.0437	2.30E+08												
Kx/Ky	1.02E+00																			

Table 48. Experiment MD02-1, D155 [(90/0)$_2$]s.

Lay-up	[(90/0)$_2$]s								rel. thick									
Thickness	0.388							# of plys	(cm)									
Fiber Vol.	0.430515						A130	0	1.74E-02									
							D155	8	2.09E-02									
							DB120	0	1.40E-02									

time		total time	x-meas	x-conv	y-meas	y-conv	x-meas dist			left half	right half	average x-radius	y-meas dist	pix		top half	bottom half	average y-radius
min	sec	(sec)	(pix)	m/pix	(pix)	m/pix	left (pix)	elis. (pix)	right (pix)	m	m	m	top	elispe	bottom	m	m	m
0	25	25	1369	0.000575	916	0.000562	101	191	91	0.05809	0.05234	0.055216	98	215	117	0.055	0.0657	0.0604
1	2	62	1366	0.000576	917	0.000561	144	275	130	0.08301	0.07494	0.078971	143	309	163	0.0802	0.0914	0.0858
1	30	90	1366	0.000576	913	0.000563	171	322	151	0.09857	0.08704	0.092805	174	362	187	0.098	0.1053	0.1017
4	54	294	1367	0.000576	913	0.000563	269	525	257	0.15495	0.14803	0.15149	276	578	301	0.1555	0.1696	0.1625
6	0	360	1367	0.000576	916	0.000562	295	578	283	0.16992	0.16301	0.166466	304	635	330	0.1707	0.1853	0.178
9	29	569	1366	0.000576	915	0.000562	360	710	348	0.20751	0.2006	0.204055	369	766	400	0.2074	0.2249	0.2161
10	10	610	1368	0.000576	911	0.000565	382	750	366	0.21987	0.21066	0.215269	393	807	417	0.2219	0.2354	0.2287
11	26	686	1367	0.000576	916	0.000562	398	774	377	0.22925	0.21715	0.223202	399	833	435	0.224	0.2443	0.2342

			R$_x$/R$_{xo}$	left side	right side	R$_y$^2	R$_x$^2/K$_x$											
R$_{xo}$	0.003175		17.3908	1426.1	8.01E+12	0.0036	18037820											
del P	89667.5		24.87262	3358.7	1.99E+13	0.0074	36896758											
visc	0.195		29.22987	4914	2.88E+13	0.0103	50956411											
1-vf	0.569485		47.71324	15323	9.42E+13	0.0264	1.36E+08											
K$_x$	1.69E-10		52.43014	19021	1.15E+14	0.0317	1.64E+08											
K$_y$	1.9E-10		64.2694	30262	1.82E+14	0.0467	2.46E+08											
Kx/Ky	0.891193		67.80117	34171	1.95E+14	0.0523	2.74E+08											
			70.29993	37094	2.2E+14	0.0548	2.95E+08											

Table 49. Experiment MD03-2, D155 [0/90/0/$\overline{90}$]s.

Lay-up	[90/0/90/0/90/0/90]								rel. thick (cm)								
Thickness	0.352							# of plys									
Fiber Vol.	0.415227						A130	0	1.74E-02								
							D155	7	2.09E-02								
							DB120	0	1.40E-02								

time	total time	x-meas	x-conv	y-meas	y-conv	x-meas dist	elis.	right	left half	right half	average x-radius	y-meas dist	pix	bottom	top half	bottom half	average y-radius
min sec	(sec)	(pix)	m/pix	(pix)	m/pix	left (pix)	(pix)	(pix)	m	m	m	top	elispe		m	m	m
6 7	367	1359	0.000579	904	0.000569	278	557	277	0.16107	0.16049	0.160783	258	522	262	0.1468	0.1491	0.1479
6 50	410	1354	0.000582	903	0.00057	284	573	287	0.16516	0.1669	0.166029	268	534	265	0.1527	0.1509	0.1518
9 3	543	1377	0.000572	918	0.00056	328	650	324	0.18756	0.18527	0.186414	305	611	310	0.1709	0.1737	0.1723
11 10	670	1377	0.000572	922	0.000558	348	701	353	0.19899	0.20185	0.200424	330	662	332	0.1841	0.1852	0.1847
12 30	750	1378	0.000571	920	0.000559	368	733	364	0.21028	0.20799	0.209135	348	690	347	0.1946	0.194	0.1943
14 0	840	1379	0.000571	920	0.000559	378	764	380	0.21584	0.21698	0.216407	359	720	363	0.2007	0.2029	0.2018
15 0	900	1379	0.000571	921	0.000558	390	782	392	0.22269	0.22383	0.223258	369	736	368	0.2061	0.2055	0.2058
16 30	990	1381	0.00057	926	0.000555	405	807	403	0.23092	0.22978	0.230347	384	765	382	0.2133	0.2122	0.2127

			R_x/R_{xo}	left side	right side	$R_y{}^2$	$R_x{}^2/K_x$
R_{xo}	0.003175		50.64018	17566	1.15E+14	0.0219	1.91E+08
del P	89667.5		52.29247	18907	1.28E+14	0.023	2.04E+08
visc	0.195		58.71314	24633	1.69E+14	0.0297	2.57E+08
1-vf	0.584773		63.12564	29052	2.09E+14	0.0341	2.98E+08
K_x	1.35E-10		65.86938	32001	2.34E+14	0.0377	3.24E+08
K_y	1.15E-10		68.15954	34582	2.62E+14	0.0407	3.47E+08
Kx/Ky	1.169826		70.31762	37115	2.81E+14	0.0424	3.69E+08
			72.55033	39838	3.09E+14	0.0453	3.93E+08

Table 50. Experiment MD04-1, D155/DB120 [0/±45$_2$/0]s.

Lay-up	[0/+-45$_2$/0]$_s$								rel. thick (cm)								
Thickness	0.354							# of plys									
Fiber Vol.	0.394463						A130	0	1.74E-02								
							D155	4	2.09E-02								
							DB120	4	1.40E-02								

time	total time	x-meas	x-conv	y-meas	y-conv	x-meas dist	elis.	right	left half	right half	average x-radius	y-meas dist	pix	bottom	top half	bottom half	average y-radius
min sec	(sec)	(pix)	m/pix	(pix)	m/pix	left (pix)	(pix)	(pix)	m	m	m	top	elispe		m	m	m
0 44	44	1358	0.00058	925	0.000556	169	342	173	0.09799	0.10031	0.09915	69	142	72	0.0384	0.04	0.0392
3 5	185	1390	0.000566	928	0.000554	290	595	302	0.16428	0.17108	0.167677	125	248	124	0.0693	0.0687	0.069
4 23	263	1386	0.000568	925	0.000556	336	681	344	0.19088	0.19543	0.193157	143	279	138	0.0795	0.0767	0.0781
5 16	316	1394	0.000565	933	0.000551	355	721	365	0.20052	0.20617	0.203346	151	301	150	0.0832	0.0827	0.083
6 15	375	1390	0.000566	926	0.000555	382	770	389	0.21639	0.22036	0.218376	162	316	156	0.09	0.0867	0.0883
7 31	451	1395	0.000564	933	0.000551	406	817	410	0.22916	0.23142	0.230293	176	343	167	0.097	0.0921	0.0945
8 45	525	1389	0.000567	928	0.000554	429	861	434	0.24319	0.24603	0.24461	183	359	179	0.1014	0.0992	0.1003
10 0	600	1395	0.000564	932	0.000552	446	898	452	0.25174	0.25513	0.253436	192	378	187	0.106	0.1032	0.1046
12 0	720	1387	0.000568	925	0.000556	479	962	480	0.27193	0.2725	0.272212	205	404	199	0.114	0.1107	0.1123
15 0	900	1394	0.000565	930	0.000553	508	1022	512	0.28694	0.2892	0.288073	221	439	220	0.1222	0.1217	0.122

			R_x/R_{xo}	left side	right side	$R_y{}^2$	$R_x{}^2/K_x$
R_{xo}	0.003175		31.22828	5737.8	1.33E+13	0.0015	36073381
del P	89667.5		52.81151	19339	5.57E+13	0.0048	1.03E+08
visc	0 195		60.83694	26710	7.92E+13	0.0061	1.37E+08
1-vf	0.605537		64.04591	30023	9.52E+13	0.0069	1.52E+08
K_x	2.73E-10		68.77986	35300	1.13E+14	0.0078	1.75E+08
K_y	4.66E-11		72.53333	39817	1.36E+14	0.0089	1.95E+08
Kx/Ky	5.853887		77.04248	45638	1.58E+14	0.0101	2.2E+08
			79.82222	49442	1.81E+14	0.0109	2.36E+08
			85.73612	58090	2.17E+14	0.0126	2.72E+08
			90.73171	65989	2.71E+14	0.0149	3.05E+08

173

Table 51. Experiment MD04-1, D155/DB120 [0/±45$_2$/90]s.

Lay-up	[0/+-45$_2$/90]$_s$							# of plys	rel. thick (cm)
Thickness	0.38								
Fiber Vol.	0.367474						A130	0	1.74E-02
							D155	4	2.09E-02
							DB120	4	1.40E-02

time		total time	x-meas	x-conv	y-meas	y-conv	x-meas dist			left half	right half	average x-radius	y-meas dist	pix		top half	bottom half	average y-radius
min	sec	(sec)	(pix)	m/pix	(pix)	m/pix	left (pix)	elis. (pix)	right (pix)	m	m	m	top	elispe	bottom	m	m	m
5	18	318	1320	0.000597	879	0.000585	282	547	263	0.16822	0.15688	0.16255	237	489	252	0.1387	0.1475	0.1431
6	21	381	1320	0.000597	876	0.000587	303	586	281	0.18074	0.16762	0.174182	255	531	277	0.1497	0.1626	0.1562
9	10	550	1320	0.000597	878	0.000586	351	682	328	0.20938	0.19566	0.202517	299	614	316	0.1752	0.1851	0.1801
9	50	590	1325	0.000594	881	0.000584	368	703	342	0.21869	0.20324	0.210964	305	636	329	0.1781	0.1921	0.1851
10	50	650	1322	0.000596	878	0.000586	381	732	346	0.22693	0.20608	0.216505	317	650	335	0.1857	0.1962	0.191
11	30	690	1325	0.000594	880	0.000584	390	749	360	0.23176	0.21394	0.222849	326	668	346	0.1905	0.2022	0.1964
12	20	740	1323	0.000595	877	0.000586	399	770	368	0.23747	0.21902	0.228245	331	679	350	0.1941	0.2053	0.1997
13	33	813	1316	0.000598	878	0.000586	404	795	386	0.24172	0.23095	0.23634	345	704	358	0.2021	0.2097	0.2059
15	0	900	1306	0.000603	878	0.000586	426	826	404	0.25684	0.24358	0.250208	360	732	372	0.2109	0.2179	0.2144
16	56	1016	1307	0.000602	882	0.000583	455	875	421	0.27411	0.25363	0.263872	381	773	392	0.2222	0.2286	0.2254

				R$_x$/R$_{xo}$	left side	right side	R$_y$^2	R$_x$^2/K$_x$			
R$_{xo}$	0.003175			51.19697	18012	9.17E+13	0.0205	1.43E+08			
del P	89667.5			54.86061	21098	1.1E+14	0.0244	1.64E+08			
visc	0.195			63.78485	29746	1.59E+14	0.0325	2.22E+08			
1-vf	0.632526			66.44528	32640	1.7E+14	0.0343	2.4E+08			
K$_x$	**1.85E-10**			68.19062	34618	1.88E+14	0.0365	2.53E+08			
K$_y$	**1.4E-10**			70.18868	36961	1.99E+14	0.0386	2.68E+08			
Kx/Ky	1.318102			71.88813	39020	2.13E+14	0.0399	2.81E+08			
				74.43769	42223	2.35E+14	0.0424	3.02E+08			
				78.80551	48031	2.6E+14	0.046	3.38E+08			
				83.10941	54155	2.93E+14	0.0508	3.76E+08			

APPENDIX B

SAMPLE PERMEABILITY CALCULATION

This section details clamping pressure calculations for experiment MD04-1. The parameters needed for calculations are part thickness (0.354 cm), number of D155 and DB120 plies (4 each) and the relative thicknesses for the D155 and DB120 fabrics ($2.09 \cdot 10^{-2}$ cm and 1.40e-2 cm).

Relative Thickness Example Calculation

First, the thickness of the glass in the D155 and DB120 layers needs to be calculated.

D155:	$4 \cdot (2.09 \cdot 10^{-2}) = 0.836$ cm
DB120	$4 \cdot (1.40 \cdot 10^{-2}) = 0.560$ cm
total glass	0.1396 cm
D155 fraction	0.599
DB120 fraction	0.401

Next the fiber volume fraction of the lay-up is calculated by dividing the glass thickness by the thickness of the part.

v_f $0.1396/.354 = 0.394$

This fiber volume is then used in the relations given in Table 14 to find the permeabilities of each fabric.

D155 K_x	$4.30 \cdot 10^{-8} \cdot e^{-11.4 \cdot (0.394)} = 4.82 \cdot 10^{-10}$ m^2
D155 K_y	$3.59 \cdot 10^{-8} \cdot e^{-17.3 \cdot (0.394)} = 3.93 \cdot 10^{-11}$ m^2
DB120 K_x	$6.39 \cdot 10^{-9} \cdot e^{-13.2 \cdot (0.394)} = 3.52 \cdot 10^{-11}$ m^2
DB120 K_y	$6.44 \cdot 10^{-9} \cdot e^{-14.7 \cdot (0.394)} = 1.97 \cdot 10^{-11}$ m^2

Finally the permeabilities are summed according to their fraction of the lay-up.

K_x	$0.599 \cdot 4.82 \cdot 10^{-10} + 0.401 \cdot 3.52 \cdot 10^{-11} = 3.03 \cdot 10^{-10}$ m^2
K_y	$0.599 \cdot 3.93 \cdot 10^{-11} + 0.401 \cdot 1.97 \cdot 10^{-10} = 3.14 \cdot 10^{-10}$ m^2

Clamping Pressure Example Calculation

The first step for the clamping pressure method is to find a clamping pressure that will give the proper thickness for a lay-up using the relations in Table 15.

D155	$-4.06 \cdot 10^{-3} \ln(16.733 \text{ (kPa)}) + 5.66 \cdot 10^{-2} = 0.0452$
DB120	$-4.21 \cdot 10^{-3} \ln(16.733 \text{ (kPa)}) + 5.52 \cdot 10^{-2} = 0.0433$

D155 lay-up frac.   0.505
DB120 lay-up frac.   0.495

Next the fiber volume fraction of each layer is figured by dividing the relative thickness of a layer by its total thickness.

D155 v_f $2.09 \cdot 10^{-2}/0.0452 = 0.462$

DB120 v_f $1.40 \cdot 10^{-2}/0.0433 = 0.323$

This fiber volume is then used in the relations given in Table 14 to find the permeabilities of each layer.

D155 K_x $4.30 \cdot 10^{-8} \cdot e^{-11.4 \cdot (0.462)} = 2.22 \cdot 10^{-10} \, m^2$

D155 K_y $3.59 \cdot 10^{-8} \cdot e^{-17.3 \cdot (0.462)} = 1.21 \cdot 10^{-11} \, m^2$

DB120 K_x $6.39 \cdot 10^{-9} \cdot e^{-13.2 \cdot (0.323)} = 8.99 \cdot 10^{-11} \, m^2$

DB120 K_y $6.44 \cdot 10^{-9} \cdot e^{-14.7 \cdot (0.323)} = 5.58 \cdot 10^{-11} \, m^2$

Finally the permeabilities are summed according to their fraction of the lay-up.

K_x $0.505 \cdot 2.22 \cdot 10^{-10} + 0.495 \cdot 8.99 \cdot 10^{-11} = 1.57 \cdot 10^{-10} \, m^2$

$K_{y\cdot}$ $0.505 \cdot 1.21 \cdot 10^{-11} + 0.495 \cdot 5.58 \cdot 10^{-11} = 3.37 \cdot 10^{-11} \, m^2$

APPENDIX C

BLADE MODEL INFORMATION

Key-points along Blade

The blade was divided into 10 cross-sections. The key-points used in each of the cross-sections are given in Table 52. Cross-sections were numbered in order from the root end of the blade to the tip.

Table 52. Key-points for blade model.

Cross Section	x (m)	y (m)	z (m)	Cross Section	x (m)	y (m)	z (m)	Cross Section	x (m)	y (m)	z (m)
1	0.0000	0.3000	0.0000	4	0.0000	0.3000	1.7363	7	0.0000	0.3000	4.1133
1	0.1677	0.4264	0.0000	4	0.1273	0.3803	1.7363	7	0.1097	0.3537	4.1133
1	0.2258	0.4353	0.0000	4	0.2272	0.3997	1.7363	7	0.1800	0.3645	4.1133
1	0.4498	0.4176	0.0000	4	0.3212	0.4033	1.7363	7	0.2098	0.3680	4.1133
1	0.5501	0.3564	0.0000	4	0.5552	0.3858	1.7363	7	0.3141	0.3664	4.1133
1	0.3411	0.2251	0.0000	4	0.7493	0.3517	1.7363	7	0.4576	0.3418	4.1133
1	0.2258	0.1917	0.0000	4	0.6221	0.3391	1.7363	7	0.6071	0.3213	4.1133
1	0.1954	0.1871	0.0000	4	0.3177	0.2374	1.7363	7	0.4946	0.3099	4.1133
1	0.1354	0.1803	0.0000	4	0.2272	0.2065	1.7363	7	0.3128	0.2578	4.1133
2	0.0000	0.3000	0.3983	4	0.1962	0.1992	1.7363	7	0.2078	0.2404	4.1133
2	0.1317	0.3991	0.3983	4	0.1263	0.2031	1.7363	7	0.1773	0.2421	4.1133
2	0.1982	0.4130	0.3983	5	0.0000	0.3000	2.4103	7	0.1078	0.2542	4.1133
2	0.2264	0.4177	0.3983	5	1.2230	0.3690	2.4103	8	0.0000	0.3000	4.4263
2	0.3178	0.4180	0.3983	5	0.1892	0.3837	2.4103	8	0.1035	0.3458	4.4263
2	0.4989	0.4057	0.3983	5	0.3215	0.3902	2.4103	8	0.1707	0.3564	4.4263
2	0.6477	0.3514	0.3983	5	0.5281	0.3701	2.4103	8	0.2017	0.3598	4.4263
2	0.5429	0.3143	0.3983	5	0.7173	0.3417	2.4103	8	0.3074	0.3579	4.4263
2	0.3142	0.2244	0.3983	5	0.5254	0.3206	2.4103	8	0.4464	0.3328	4.4263
2	0.2264	0.1971	0.3983	5	0.3228	0.2531	2.4103	8	0.5537	0.3134	4.4263
2	0.1954	0.1905	0.3983	5	0.2204	0.2209	2.4103	8	0.4725	0.3056	4.4263
2	0.1305	0.1849	0.3983	5	0.1897	0.2158	2.4103	8	0.3060	0.2660	4.4263
3	0.0000	0.3000	1.0633	5	0.1230	0.2217	2.4103	8	0.2013	0.2514	4.4263
3	0.1281	0.3882	1.0633	6	0.0000	0.3000	3.0439	8	0.1697	0.2542	4.4263
3	0.1960	0.4050	1.0633	6	0.1162	0.3605	3.0439	8	0.1037	0.2640	4.4263
3	0.2265	0.4091	1.0633	6	0.1855	0.3745	3.0439	9	0.0000	0.3000	5.0923
3	0.3279	0.4112	1.0633	6	0.2151	0.3779	3.0439	9	0.0918	0.3399	5.0923
3	0.5989	0.3858	1.0633	6	0.3047	0.3801	3.0439	9	0.1659	0.3477	5.0923
3	0.3266	0.2411	1.0633	6	0.4685	0.3593	3.0439	9	0.1959	0.3503	5.0923
3	0.2254	0.2035	1.0633	6	0.6579	0.3304	3.0439	9	0.2991	0.3471	5.0923
3	0.1953	0.1978	1.0633	6	0.5530	0.3233	3.0439	9	0.3931	0.3263	5.0923
3	0.1271	0.1942	1.0633	6	0.3035	0.2504	3.0439	9	0.5004	0.3059	5.0923
3	0.7214	0.3205	1.0633	6	0.2144	0.2309	3.0439	9	0.3904	0.2927	5.0923
3	0.5907	0.2767	1.0633	6	0.1851	0.2273	3.0439	9	0.2960	0.2737	5.0923
				6	0.1145	0.2387	3.0439	9	0.1954	0.2619	5.0923
								9	0.1648	0.2637	5.0923
								9	0.0910	0.2715	5.0923
								10	0.0000	0.3000	5.7573
								10	0.0899	0.3345	5.7573
								10	0.1583	0.3412	5.7573
								10	0.1899	0.3414	5.7573
								10	0.2921	0.3354	5.7573
								10	0.3643	0.3198	5.7573
								10	0.4445	0.3046	5.7573
								10	0.3741	0.2983	5.7573
								10	0.2915	0.2847	5.7573
								10	0.1893	0.2758	5.7573
								10	0.1584	0.2746	5.7573
								10	0.0892	0.2768	5.7573

Lay-up Information and Permeabilities for Blade Model

The lay-up schedule as well as the permeabilities used in the blade model are listed in Table 53. A schematic showing the different sections of a the blade is given in Figure 71.

Table 53. Permeabilities along blade section.

section	region	lay-up	0° fabric	±45° fabric	thickness (cm)	v_f	K_x	K_y	A130 thick	a130 vf	DB thick	DB120 vf	clamping p	total thick
root	1	$[\pm45/0_4/\pm45/0_4/\pm45]_s$	16	6	1.118	0.325	2.32E-10	7.05E-11	0.820	0.340	0.298	0.283	3.75	1.12
web	2-9	$[\pm45/0_2/\pm45]_s$	4	4	0.401	0.314	2.02E-10	7.79E-11	0.204	0.342	0.197	0.284	4.00	0.40
spar cap 1	2	$[\pm45/0_4/\pm45/0_4/\pm45]_s$	16	6	1.118	0.325	2.32E-10	7.05E-11	0.820	0.340	0.298	0.283	3.75	1.12
spar cap 2	3-4	$[\pm45/0_3/\pm45/0_3/\pm45]_s$	12	6	0.889	0.330	1.97E-10	6.64E-11	0.599	0.349	0.290	0.291	5.16	0.89
spar cap 3	5-7	$[\pm45/0_2/\pm45/0_2/\pm45]_s$	8	6	0.660	0.339	1.52E-10	5.90E-11	0.383	0.364	0.277	0.304	8.50	0.66
spar cap 4	8-9	$[\pm45/0/\pm45/0/\pm45]_s$	4	6	0.432	0.356	9.31E-11	4.46E-11	0.177	0.394	0.255	0.331	20.73	0.43
flange 1	2	$[\pm45/0_2/\pm45]_s$ & $[\pm45/0_4/\pm45/0_4/\pm45]_s$	20	10	1.499	0.326	2.09E-10	6.92E-11	1.010	0.345	0.489	0.287	4.50	1.50
flange 2	3-4	$[\pm45/0_2/\pm45]_s$ & $[\pm45/0_3/\pm45/0_3/\pm45]_s$	16	10	1.270	0.330	1.84E-10	6.57E-11	0.792	0.352	0.478	0.293	5.77	1.27
flange 3	5-7	$[\pm45/0_2/\pm45]_s$ & $[\pm45/0_2/\pm45/0_2/\pm45]_s$	12	10	1.041	0.336	1.54E-10	6.07E-11	0.577	0.362	0.464	0.302	8.08	1.04
flange 4	8-9	$[\pm45/0_2/\pm45]_s$ & $[\pm45/0/\pm45/0/\pm45]_s$	8	10	0.813	0.344	1.18E-10	5.29E-11	0.369	0.378	0.444	0.316	13.12	0.81
leading edge1	2	$[\pm45/0_2/\pm45]_s$	4	4	0.391	0.322	1.78E-10	7.06E-11	0.199	0.351	0.192	0.292	5.44	0.39
leading edge2	3-9	$[\pm45/0/\pm45]_s$	2	4	0.277	0.329	1.28E-10	6.13E-11	0.095	0.368	0.182	0.308	9.87	0.28
trailing edge1	2-8	$[\pm45/0_2/\pm45]_s$	4	4	0.391	0.322	1.78E-10	7.06E-11	0.199	0.351	0.192	0.292	5.44	0.39
trailing edge2	9	$[\pm45/0]_s$	2	2	0.196	0.322	1.78E-10	7.06E-11	0.099	0.351	0.096	0.292	5.44	0.20

DISTRIBUTION

J. Ahlgrimm
Office of Wind and Hydro Technology
EE-12
U.S. Department of Energy
1000 Independence Avenue SW
Washington, DC 20585

J. Cadogan
Office of Wind and Hydro Technology
EE-12
U.S. Department of Energy
1000 Independence Avenue SW
Washington, DC 20585

D. Cairns (5)
Montana State University
Mechanical & Industrial Engineering Dept.
220 Roberts Hall
Bozeman, MT 59717

S. Calvert
Office of Wind and Hydro Technology
EE-12
U.S. Department of Energy
1000 Independence Avenue SW
Washington, DC 20585

S. Finn
GE Global Research
One Research Circle
Niskayuna, NY 12309

P. Finnegan
GE Global Research
One Research Circle
Niskayuna, NY 12309

P. R. Goldman
Director
Office of Wind and Hydro Technology
EE-12
U.S. Department of Energy
1000 Independence Avenue SW
Washington, DC 20585

D. Griffin
GEC
5729 Lakeview Drive NE, Ste. 100
Kirkland, WA 98033

T. Hermann
Wetzel Engineering, Inc.
P.O. Box 4153
Lawrence, KS 66046-1153

W. Lin
GE Global Research
One Research Circle
Niskayuna, NY 12309

J. Locke, Associate Professor
Wichita State University
207 Wallace Hall, Box 44
Wichita, KS 67620-0044

J. F. Mandell
Montana State University
302 Cableigh Hall
Bozeman, MT 59717

L. McKittrick
Montana State University
Mechanical & Industrial Engineering Dept.
220 Roberts Hall
Bozeman, MT 59717

NWTC Library (5)
NREL
1617 Cole Boulevard
Golden, CO 80401

D. Sanchez
U.S. Dept. of Energy
Albuquerque Operations Office
P.O. Box 5400
Albuquerque, NM 87185

K. Wetzel
Wetzel Engineering, Inc.
PO Box 4153
4108 Spring Hill Drive
Lawrence, KS 66046-1153

M. Zuteck
MDZ Consulting
601 Clear Lake Road
Clear Lake Shores, TX 77565